UNIVERSITY OF CALIFORNIA SAN DIEGO

Towards a circuit-based understanding of neuropsychiatric disorders: circuit-specific contributions to major depressive disorder and addiction

A dissertation submitted in partial satisfaction of the requirements for the degree
Doctor of Philosophy

in

Neurosciences

by

Daniel Adam Knowland

Committee in charge:

Professor Byungkook Lim, Chair
Professor Brenda L. Bloodgood
Professor Christina M. Gremel
Professor Roberto Malinow
Professor Nicholas C. Spitzer

2018

The Dissertation of Daniel Adam Knowland is approved, and it is acceptable in quality and form for publication on microfilm and electronically:

_____

_____

_____

_____

_____

Chair

University of California San Diego

2018

DEDICATION

For Dad, Mom, Amy, Katie, and Grandma

TABLE OF CONTENTS

LIST OF FIGURES

Chapter I:

Chapter II:

Appendix A:

ACKNOWLEDGEMENTS

It is profoundly unfair that my name is the only one on the title page of this dissertation. The following individuals (and many more I have likely overlooked, my apologies!) were instrumental helping me get to this point. I am filled with immense gratitude that I have so many supportive people in my life, and count myself extremely lucky that I've had this team of individuals help me get here.

First, I would like to acknowledge my thesis advisor Dr. Byungkook Lim. For being unwaveringly supportive in your mentorship on a scientific, mental health, and personal level. From the talks about my project, random science ideas, to just talking about sports you fostered a comfortable and creative environment that I appreciate and am thankful for beyond words. With your support I feel I've improved as both a scientist and person. I would also like to thank my doctoral committee members – Drs. Brenda Bloodgood, Tina Gremel, Roberto Malinow, and Nicholas Spitzer. For your scientific support and insight that has helped shape my project into the form it's in today. I would also like to thank my previous mentors Dr. Hongwei Dong and Dr. Dritan Agalliu for taking a chance on someone who had little scientific background and inspired me to pursue science.

To the members of the Lim lab – thank you for your collaboration and making the lab environment a fun and welcoming place to work. In particular, I am extremely indebted to the direct help and support of Varoth, Cindy (and Bentley!), Sora, Chris, MJ, and Xiao-yun. These projects would quite literally not be possible without all your guys help and work. To Eric – for your neurophilosophical discussions, always sunny in Philadelphia impressions, and keeping the lab a fun (and weird) place to work. To Amanda for your fun run 3 prowess

and introducing Eric to healthy food. Finally, to Varoth. We were BK's first grad students together and have come a long way since the beginning. This entire dissertation would not be possible without your help. FedEx is lucky to have such a hard worker as you in the future.

A massive thanks to everyone, past and present in the UCSD neurograd program (to Linh and Erin, I don't think the program would exist without you two). In particular, my classmates who are always inspiring, and often intimidating how passionate, intelligent, and all around great people you are. To Steph, finding someone who also recognizes the unequalled excellence of Punjab Tandoori and Radiohead. Thanks to the other members of the Campus house – Katie, Jess, Joao, and Kerin.

A massive thank you to my friends outside the program – Art, Sophia, Matt, Athena, Chris, Billy, etc. for the greasy outdoor adventures that kept me sane, you guys are the most loyal. Eric and Elena, cheers to the mates across the pond and for all the fun times we had in SD. And to all my Irvine and UCLA friends, particularly my fantasy football league providing the ever-needed outlet to trash talk and talk sports.

I cannot begin to express how thankful I am for my family – Mom, Dad, Amy, Katie, and Grandma. Thank you for all being role models on how to be a good person and live life. Mom and Dad, thank you for providing me the supportive environment, resources, and freedom to pursue my interests. You guys inspire me how to be a better person and exemplify the kind of relationship I hope to have in the future. I love you all so much. Finally – to my beautiful and wonderful girlfriend Amy. Sharing these milestones with you are what makes them truly worthwhile. I love you so much, and can't wait to embark on the next chapter in my life with you.

Chapter I, in full, is a reprint of the material as it appears in Knowland D, Lilascharoen V, Pacia CP, Shin S, Wang EHJ, Lim BK. *Distinct Ventral Pallidal Neural Populations Mediate Separate Symptoms of Depression*. Cell, 170.2 (2017): 284-297. The dissertation author was the primary investigator and author of this paper.

Chapter II, in full, is a reprint of Barrientos C, Knowland D, Wu MJ, Lilascharoen V, Huang KW, Malenka, RC, Lim BK. *Cocaine induced structural plasticity in input regions to distinct cell types in nucleus accumbens*. Biological Psychiatry (2018): in press. The dissertation author was the primary investigator and author of this paper with equal contribution from Cindy Barrientos.

Appendix A, Circuit-based Frameworks of Depressive Behaviors: The Role of Reward Circuitry and Beyond, is a reprint of Knowland D, Lim BK. *The Neural Basis of Depressive Behaviors: The Role of Reward Circuitry and Beyond*. Pharmacology Biochemistry and Behavior (2018) DOI: 10.1016/j.pbb.2017.12.010. The dissertation author was the primary researcher and author of this review paper.

VITA

2011	Bachelor of Science in Neuroscience
	University of California Los Angeles
2011-2013	Junior Research Associate
	University of California Irvine
2018	Doctor of Philosophy in Neurosciences
	University of California San Diego

PUBLICATIONS

Barrientos C*, **Knowland D***, Wu MJ, Lilascharoen V, Huang KW, Malenka, RC, Lim BK. Cocaine induced structural plasticity in input regions to distinct cell types in nucleus accumbens. *Biological Psychiatry* (2018): *in press*.

Knowland D, Lim BK. The Neural Basis of Depressive Behaviors: The Role of Reward Circuitry and Beyond. *Pharmacology Biochemistry and Behavior* (2018): *in press*.

Shin S, Pribiag H, Lilascharoen V, **Knowland D**, Wang XY, Lim BK. Drd3 Signaling in the Lateral Septum Mediates Early Life Stress-induced Social Dysfunction. *Neuron* 97.1 (2018): 195-208.

Knowland, D, Lilascharoen, V, Pacia, CP, Shin, S, Wang, EHJ and Lim, BK. Distinct Ventral Pallidal Neural Populations Mediate Separate Symptoms of Depression. *Cell*, 170.2 (2017): 284-297.

Dileepan T*, E Smith*, **Knowland D**, Hsu M, Platt M, Bittner-Eddy P, Cohen B, Southern P, Latimer E, Harley E, Agalliu D, Cleary P. Group A Streptococcus-specific Th17 cells enter the brain after multiple intranasal infections and are accompanied by neurovascular damage and IgG deposition. *The Journal of Clinical Investigation* 126.1 (2016): 303.

Knowland D*, Arac A*, Sekiguchi KJ, Hsu M, Lutz SE, Perrino J, Steinberg GK, Barres BA, Nimmerjahn A, Agalliu D. Stepwise Recruitment of Transcellular and Paracellular Pathways Underlines Blood-Brain Barrier Breakdown in Stroke. *Neuron* 82.3 (2014): 603-617.

ABSTRACT OF THE DISSERTATION

Towards a circuit-based understanding of neuropsychiatric disorders: circuit-specific contributions to major depressive disorder and addiction

by

Daniel Adam Knowland

Doctor of Philosophy in Neurosciences

University of California San Diego, 2018

Professor Dr. Byungkook Lim, Chair

Motivation directs and guides an organisms interaction with their environment and is profoundly influenced by internal brain states in conjunction with external environmental stimuli. Motivated behaviors can range from survival-based actions such as foraging for food

or avoiding potentially deadly conflict to pursuit of pleasure or sex. Proper maintenance of every day motivation is essential for guiding behavior to preserve homeostatic balance and stable functioning.

However, states of pathological motivation result when proper motivational control is lost. Instances of hyper-motivation misdirected towards harmful or negative stimuli can manifest as addiction, and conversely loss of motivation and extreme apathy is a hallmark of major depressive disorder (MDD). How then, does the brain regulate motivation and what kind of adaptations lead to conditions such as addiction and depression?

Components of the reward circuitry in the brain such as the nucleus accumbens (NAc) has been heavily studied in the context of addiction and MDD. As a central node in the reward circuitry, the NAc receives dopaminergic input from the ventral tegmental area (VTA) in the midbrain and sends its primary output to the ventral pallidum (VP) and back to the VTA. While structural and electrophysiological changes in neurons within the NAc have been well described in addiction and MDD, much less is known how the NAc interacts with the reward circuitry as a whole. In particular, how do the various interconnections within the reward circuit relate to the complex behaviors characteristic of neuropsychiatric conditions such as MDD and addiction? This dissertation aims to shed light on how discrete aspects of circuits involving the NAc and VP contribute to discrete behavioral aspects of addiction and MDD. Chapter I illustrates that discrete components of the ventral pallidal circuit mediates separate depressive-like behaviors in a mouse model of depression. In chapter II, we outline discrete structural changes in separate input structures of the NAc at different stages of

addiction. In all, this dissertation hopes to illuminate the circuit-specific changes governing neuropsychiatric disorders that may provide a platform for more specific treatments.

INTRODUCTION

Towards circuit-specific manipulations in the brain, a brief history

It is well-accepted that different areas of the brain govern different functions. Today, it is hard to imagine thinking otherwise. With its capacity to selectively manipulate discrete neural pathways in awake, behaving animals while simultaneously monitoring cellular activity, modern neuroscience has helped to tease apart how interconnections within the brain give rise to different behaviors and how these connections can be disrupted in pathological brain states. However, the enormous complexity of the brain and how function was distributed amongst brain regions was not always appreciated. It took many years and advances in both philosophy and technology that allowed us to arrive where we are today in the circuit-based neuroscience field.

In biblical times, the heart was considered the seat of thought and perception. Even ancient Greek philosophers such as Aristotle propounded the cardio-centric view of intelligence while the brain was thought to function as a mere cooling system for the blood. Thankfully, Aristotle's legacy is not for his idea of a cerebral air conditioner. One of the earliest figures to recognize the brain as the epicenter of thought and cognitive control was Hippocrates (Finger, 2000). However, his understanding of the brain was severely limited based on the Greek idea at the time that the soul was contained within the body and that performing autopsies or dissections after death would disrupt the soul. Later, figures such as Galen obtained a better yet crude understanding of the brain through dissections of non-human mammals. These dissections that elucidated basic ideas of speech and movement did much to depart thinking from the cardiocentric view of the body. Aided by dissections of

human cadavers, Andreas Vesalius began to describe the landscape of the brain and its finer anatomical features (Finger, 2000). With his description of the cerebellum, cerebral hemispheres, and brainstem, Vesalius laid out the crude foundation for neuroanatomy and the possibility that the brain wasn't a globular mass – certainly not a mere blood refrigerator – but that it had regionalized parts to it that could give rise to separate functions.

The idea that discrete areas of the brain could have separate functions was championed by the father of phrenology, Franz Joseph Gall in the early 19th century. In his view, certain skills and personality traits were localized to certain regions of the brain which he referred to as modules. This idea was advanced to suggest that measuring the size and curvature of the skull could allow scientists to gain insight into the personalities and predilections of patients (Fodor, 1983). In all, phrenology was much more pseudoscience than anything concrete, but the core idea of "localization of mental functions [in] the brain" had merit.

Phrenology calipers aside, Gall's work gave way to the central figure of truly establishing the localization of functions in the brain, Paul Broca. Broca's work showed that disruption to a precise part of the brain, now known as Broca's area, was essential for proper speech in humans (Broca, 1961). With Broca's work as a catalyst, future work began to uncover how localized areas of the brain governed different behaviors in humans such as iconic work in patient H.M. showing that the hippocampus was central to memory (Squire, 2009).

While the localization of function in the brain was widely accepted, how neurons were able to communicate with each other, and consequently how different brain regions could relay information to and from one another via electrical and chemical signals were being

discovered in parallel by a series of landmark experiments (del Castillo and Katz, 1952; Fatt and Katz, 1952; Hodgkin and Huxley, 1952a, 1952b, 1952c, 1952d, 1952e; Katz and Miledi, 1964). In spite of this knowledge, the ability to dissect how and whether different regions of the brain communicated with each other to generate and modify specific behaviors was still intractable. Electric stimulation of brain areas were too crude a tool and did not allow for the level of specificity required to tackle these circuit-based questions. In 1979 Francis Crick, the Nobel Prize winner famed for his part in the discovery of the structure of DNA, presciently challenged the neuroscience community in an opinion article for Scientific American that development of tools to selectively label and manipulate neural circuits would be necessary to drive the field forward. In this article, he championed circuit-based neuroscience as necessary because "the basic problem is that almost any process we can study by observing overall behavior involves the complex interaction of many different regions of the brain, each with its own way of handling information. … Moreover, we seldom know what operation each region is performing, that is, what relates the outputs to the inputs, and in some instances we do not have the faintest idea of what is going on (Crick, 1979)." Up to this point, the brain had been treated relatively like a black box with more emphasis placed on studying inputs (environmental/external effects on an individual) and outputs (the response of the individual, how the inputs affect behavior) rather than changes in neural processes within the brain. In fact, this strategy had been relatively successful in other fields such as genetics. For example, simply studying breeding patterns had yielded considerable insight into inheritance and genes. For something as complex as the brain, however, this approach is insufficient. In order to shed light on this black box, Crick argued that scientists should study neural circuits since "different regions of the brain do different jobs." Ultimately, to achieve this scientists would

need to develop “a method that would make it possible to inject one neuron with a substance that would then clearly stain all the neurons connected to it, and no others, would be invaluable. So would a method by which all neurons of just one type could be inactivated, leaving the others more of less unaltered (Crick, 1979).” This challenge would go unanswered for almost 25 years, but would foreshadow the advent of one of the most important technologies in circuit-based neuroscience – optogenetics.

In 2003, the first evidence demonstrating use of an opsin to depolarize cells was published (Nagel et al., 2003). The idea of opsins – light gated ion channels derived from algae that exploit all-*trans*-retinal to transduce light into a conformational change to drive the flow of ions across a membrane – had been described for some time (Schobert and Lanyi, 1986). Nagel et. al described a particular opsin, channelrhodopsin-2 (ChR2), which they were able to express in oocytes and human embryonic kidney cells. Soon after, the first evidence of driving action potential firing in neurons via blue light activation of ChR2 was published in a now seminal paper (Boyden et al., 2005). Theory and speculation had turned into the reality Crick predicted in 1979. By carefully selecting the location where an optical fiber was implanted in the brain, nerve afferents in one brain area originating from a different area could be stimulated to the exclusion of other afferents. Shortly thereafter, viral vectors conditionally expressing ChR2 were combined with mouse genetics to restrict ChR2 (and NpHR for inhibition of neurons) expression to subsets of neurons (Atasoy et al., 2008; Petreanu et al., 2007; Tsai et al., 2009; Wang et al., 2007). At last, precise subpopulations of neurons as defined by their anatomical location *and* molecular identity could be excited or inhibited to the exclusion of other cells or circuits they were embedded in. By stimulating or inhibiting a particular circuit, scientists were now able to understand if a specific populations

of neurons was sufficient or necessary to generate a particular behavior. Furthermore, could a behavior only be elicited by stimulating particular brain area, or was it dispersed throughout many regions of the brain? Understanding how discrete regions and connections in the brain could underlie aspects of neuropsychiatric disorders were suddenly tractable problems.

The work contained within this dissertation leverages these technical advances in an attempt to understand the complex circuits of the brain and how discrete pathways can generate and modify motivational behavior. In particular, the following chapters utilize viral-genetic techniques in an attempt to uncover how circuits adapt and change in conditions of pathological motivation such as addiction and depression.

Circuits contributing to major depressive disorder

Major depressive disorder (MDD) is a prevalent affliction that affects about 7% of Americans while an additional 20% experience a less severe, more acute depressive episode at some point throughout their lives (Substance Abuse and Mental Health Services Administration, 2017). This high prevalence corresponds with a profound economic burden with estimates as high as $210 billion including both direct medical costs and indirect costs such as loss of productivity at work (Greenberg et al., 2015). This significant economic cost to society has translated into significant efforts to finding an effective treatment for MDD, however available antidepressants have a nearly 50% unresponsive rate and a high placebo rate (Hillhouse and Porter, 2015). These figures demonstrate that currently prescribed therapeutics are inadequate, and suggests that we have a tenuous understanding of the true neural basis underlying MDD.

The prevailing hypothesis on the etiology of MDD is the monoamine hypothesis suggested over 50 years ago. In short, human patients with MDD were seen to have diminished levels of monoamine neurotransmitters such as serotonin, norepinephrine, and dopamine (Bunney and Davis, 1965; Schildkraut, 1965). This hypothesis was initially brought about by clinical evidence by which patients who had taken reserpine (a monoamine transporter inhibitor) precipitated acute depressive episodes (Muller et al., 1953). Later, imipramine was approved in 1958 as the first compound in what would be a new class of antidepressants, tricyclics (Hillhouse and Porter, 2015). Deriving their name from their chemical structure, tricyclic antidepressants have a broad pharmacologic profile, affecting both receptors and transporters from the serotonergic, adrenergic, noradrenergic, and histaminergic systems. While tricyclic antidepressants were being prescribed, postmortem evidence revealed a significant reduction in serotonin levels in MDD patients (Shaw et al., 1967). As such, efforts to selectively target the serotonin system were undertaken which culminated in the FDA approval of fluoxetine in 1987, the first selective serotonin reuptake inhibitor (SSRI) synthesized by Eli Lilly (brand name: Prozac). Since the fluoxetines approval in 1987, most new therapeutics are slight derivations of existing drugs and belong to the same SSRI or tricyclic class of compounds. The economic (and variable clinical) success of tricyclics and SSRIs which all to some degree targeted the monoaminergic system further ingrained the monoamine hypothesis into medical canon. Why then, despite all the economic investment, research, and time since these antidepressants were founded is MDD still poorly understood? Clearly, a different approach is needed when considering the neurobiology of depression.

A significant barrier to effectively treat MDD is the wide and often variable set of behavioral symptoms patient often present. Symptoms of MDD can range from loss of appetite, anhedonia, social withdrawal, feelings of worthlessness, to loss of energy. Separate patients often express different combinations of symptoms and differing levels of severity of each. In fact, the DSM-V list ten separate symptoms of MDD, five of which need to be present in order to meet the diagnostic criteria (Hillhouse and Porter, 2015).

With the variable behavioral symptoms that patients present, it is possible that discrete circuits within the brain may underlie distinct depressive symptoms in patients. While monoamine dysregulation likely contributes to the depressive behaviors, a comprehensive circuit-based approach may provide new insights and possible new treatments for MDD. How then might we approach studying MDD through the lens of neural circuits?

Patients with MDD often have other comorbid conditions, with some numbers estimating nearly 11% of MDD patients abused an illicit substance and others going as high as 20% (NSDUH 2016, Russo and Nestler, 2013). Conversely, nearly 40% of individuals meeting the criteria for addiction have a comorbid mood or anxiety disorder. This large degree of behaviral overlap between addiction and mood disorders suggests that the neural circuits that mediate these conditions might be similar as well. The mesolimbic dopaminergic system including the ventral tegmental area (VTA) and the nucleus accumbens (NAc) have been heavily studied in the context of addiction (for detailed background, please see 'Nucleus accumbens connectivity and addiction' section and Chapter II of dissertation). In addition to these reward-promoting regions, the lateral habenula (LHb) has also been thought to be the 'anti-reward' nucleus of the brain with increases in activity in the LHb shown to signal

aversion (Proulx et al., 2014). Not surprisingly, the NAc, VTA, and LHb are also well represented in MDD literature.

Many studies have shown that increases in VTA dopaminergic neuron activity is characteristic of animals exhibiting depressive-like behaviors (Cao et al., 2010; Chaudhury et al., 2013; Friedman et al., 2014). However, this was specific to VTA dopaminergic neurons projecting to the NAc, not the mPFC (Chaudhury et al., 2013). This may explain the discrepancy in other studies reporting a reduction in VTA firing rate in animal models of depression (Chang and Grace, 2014). Artificially silencing VTA dopaminergic neurons projecting to the NAc, but not mPFC is sufficient to block social defeat stress-induced social withdrawal and anhedonia (Chaudhury et al., 2013). These results point to precise cell type- and projection-specific circuit mechanisms that underlie depressive-like behaviors.

In addition to the VTA, the NAc has also received considerable attention in animal models of depression. Social defeat stress (SDS), a commonly used animal model that induces several depressive-like behaviors in rodents, separates experimental groups into those that display depressive-like behaviors (susceptible) and those that do not (resilient). The resilient group is thought to mimic an active coping mechanism in response to aversive external stimuli in order to maintain normal physiological functioning often found in humans, giving the model robust face validity (Golden et al., 2011). D1-MSNs exhibit a decrease in excitatory synaptic input in susceptible, but not resilient animals while D2-MSNs show a selective increase in excitatory synaptic input (Francis et al., 2015). Somewhat surprisingly, D1-MSNs in susceptible animals are hyperexcitable compared to their control and resilient counterparts when examining the number of action potentials elicited by a given current injection (Francis

et al., 2015). Interestingly, artificial stimulation of D2-MSNs before SDS increases the propensity that animals develop a susceptible phenotype (Francis et al., 2015). In line with these results, animals displaying anhedonic-like behaviors show long-term synaptic depression at D1-MSN, but not D2-MSN synapses (Lim et al., 2012). Studies monitoring *in vivo* cellular activity using fiber photometry reported increased activity in D1-MSNs during SDS that was predictive of developing resilience (Muir et al., 2017). Together, these results indicate that increased D2-MSN firing in the NAc may be a pathological hallmark of susceptible animals, while increased D1-MSN activity promotes resilience.

Reports also indicate that distinct afferents to the NAc have separate roles mediating depressive-like behaviors. In particular, glutamatergic afferents originating from the basolateral amygdala (BLA), medial prefrontal cortex (mPFC), and ventral hippocampus (vHPC) have been implicated in promoting resilience or susceptibility to SDS-induced depressive behaviors. Stimulation of mPFC cell bodies as well as nerve terminals in the NAc promoted resilience to SDS (Bagot et al., 2015; Covington et al., 2010). Stimulation of the BLA had the same pro-resilient effect, while vHPC terminal stimulation in the NAc enhanced SDS-induced social withdrawal behavior in mice (Bagot et al., 2015). Furthermore, induction of long-term depression at vHPC-to-NAc synapses was sufficient to induce resilience to SDS, indicating that enhanced or reduced activity could drive the propensity to become susceptible or resilient, respectively (Bagot et al., 2015).

In contrast to the NAc and VTA which are primarily thought to function as reward-promoting regions, the lateral habenula (LHb) is considered the “anti-reward” nucleus of the brain. Artificial stimulation of the LHb is aversive and promotes active avoidance in rodents

(Proulx et al., 2014; Shabel et al., 2012). Not surprisingly, then, the LHb has received considerable attention in both basic science and clinical realms concerning its role in MDD. In the chronic learned helplessness (cLH) model of depression, animals have blunted inhibitory input to the LHb suggesting, that heightened activity within the LHb may be a hallmark of depressive-like behaviors (Shabel et al., 2010). Chronic SSRI treatment not only reversed the behavioral cLH deficits, but also restored GABAergic transmission to the LHb to normal levels indicating that reduced activity may be important to maintain stable physiologic functioning in animals (Shabel et al., 2010). While this study found reduced GABAergic transmission in the LHb as a primary driver of cLH, another study reported increased excitatory activity in VTA-projecting LHb neurons in cLH governed by increases in presynaptic release probability of glutamate (Li et al., 2011). Although different mechanisms, the end result converges on increased activity of the LHb correlated with heightened expression of depressive-like symptoms. In line with this reasoning, silencing of the LHb with either muscimol injection or inhibitory DREADDs reverses depression-related behaviors in rodents (Sachs et al., 2015; Winter et al., 2011). These pre-clinical work in rodents has laid a strong foundation implicating the LHb in depression, and studies have begun to target LHb for deep brain stimulation in humans to alleviate treatment-resistant depression with considerable success (Kiening and Sartorius, 2013; Sartorius et al., 2010).

Despite this large body of work implicating these separate regions in MDD, much less is known on a circuit-level how these regions interact and how alterations across these regions may relate to the symptom diversity characteristic of MDD patients. The ventral pallidum (VP) is a lesser-known region in the basal ganglia that is anatomically poised to confer information across the NAc, VTA, and LHb. The VP projects to all three brain regions and

receives reciprocal input from the NAc and VTA (Beier et al., 2015; Faget et al., 2016; Root et al., 2015). The VP also mediates a variety of motivational-related behaviors including reward and aversion (Root et al., 2015; Smith et al., 2009). PET imaging studies in human MDD patients show a selective reduction in serotonin receptor binding in the VP, suggesting that the VP may play a critical role contributing to the maintenance or development of MDD (Murrough et al., 2011). Furthermore, 5-HT1B receptors in the VP are essential for conferring the antidepressant-like effects of ketamine in monkeys (Yamanaka et al., 2014). Taken together, the VP is a likely region that can convey depression-related signals across the brain to areas such as the LHb, VTA, and NAc, yet it remains a largely overlooked brain region in MDD research,

Chapter I provides a thorough dissection of parvalbumin-positive (PV) ventral pallidal neuronal circuitry and how distinct components of the VP circuit mediates distinct depressive-like behaviors. We find that two distinct subpopulations of VP PV neurons project to either the lateral habenula (LHb) or ventral tegmental area (VTA), but not both. These subpopulations receive distinct inputs, and over the course of social defeat stress display related but distinct electrophysiological adaptations. These cellular changes result in hyperactivity of both populations of VP PV neurons in susceptible animals and are reversed by chronic fluoxetine treatment, indicating that VP PV neuronal activity contributes to the expression of depressive-like behaviors. Finally, we find that manipulation of LHb-projecting VP PV neurons modulate expression of behavioral despair-like phenotypes, while VTA-projecting VP PV neurons mediate social withdrawal. These findings are critical in that it may provide a foundation for symptom-specific treatment of MDD. In addition, it could provide a framework for how to study notoriously heterogeneous and complex neuropsychiatric

disorders on a circuit-level basis, and understanding how precise pathways in the brain may underlie discrete facets of the larger condition.

Nucleus accumbens connectivity and addiction

The use of psychoactive drugs, substances that induce a state of altered consciousness, dates back to ancient cultures nearly 8,000 years ago in the form of chewing coca leaves (Dillehay et al., 2010). Since then, psychoactive drug use has become a prevalent part of society ranging from plant-based substances such as marijuana and psilocybin-containing mushrooms to synthetic compounds synthesized in laboratories such as cocaine and LSD. While psychoactive substance use is often recreational, prolonged and habitual use can lead to substance abuse disorder and result in severe health decline and even death. Addiction initially develops during a period of acute, non-compulsory use followed by periods of abstinence. Protracted and continual use, however, eventually results in habitual drug-seeking and use whereby environmental cues associated with the drug elicit similar responses comparable to drug use itself. This can be followed by periods of withdrawal and abstinence whereby alterations in the brain persist despite the absence of drug. These persistent maladapted changes in the brain often lead to relapse, and the cycle continues (Ostlund and Halbout, 2017).

Derived from the coca plant, cocaine is a highly addictive substance resulting in feelings of euphoria, increased attention, and enhanced energy. Nearly 5 million Americans were reported to have used cocaine in the past year, second to only marijuana in illicit drug use (NSDUH, 2016). Acute usage of cocaine often leads to compulsory use, with nearly 1

million American's meeting the criteria for substance abuse disorder to cocaine (NSDUH, 2016).

Like most drugs of abuse, the rewarding properties of cocaine are primarily derived from its ability to cross the blood-brain barrier and subsequently enhance the level of the neurotransmitter dopamine (DA) in the brain. Early experiments where rats could press a lever to deliver an electrical stimulation in certain areas of the brain provided the first evidence that discrete areas of the brain could induce positive reinforcement, while others could either be neutral or aversive. When a stimulating electrode was placed in the nucleus accumbens (NAc), rats repeatedly lever pressed to stimulate this area to the exclusion of food, water, and even normal levels of sleep (Olds and Milner, 1954) highlighting this area as a reward hub in the brain.

As expected, most addictive drugs modulate activity of the NAc. In particular, psychoactive, addictive drugs tend to converge on the mesolimbic dopaminergic pathway in the brain by which DA neurons in the ventral tegmental area (VTA) release DA within the NAc (Kuhar et al., 1991). Even in the absence of drugs, selectively stimulating VTA DA neurons is sufficient to induce positive reinforcement similar to that seen of Olds and Milner (1954) (Adamantidis et al., 2011; Tsai et al., 2009). The drive to self-stimulate VTA DA neurons is so robust that it persists even when animals need to endure a mild foot shock to receive stimulation (Pascoli et al., 2015). More direct evidence via microdialysis experiments measured increases in DA levels in the NAc directly following an injection of cocaine (Pettit and Justice, 1989).

DA release in the NAc also occurs in response to natural rewards such as water consumption and orgasm. However, DA release has been shown to occur at higher levels in response to cocaine use which may in part explain the dramatic compulsory drive to seek cocaine characteristic of addicted individuals (Nestler, 2005). Overall, this $VTA^{dopamine}$-NAc pathway has received heavy attention and is thought to be a primary mechanism by which cocaine and other addictive drugs exert their addictive properties. Supporting this idea, self-stimulation of VTA DA neurons induced potentiation at VTA DA-NAc synapses, indicating that this particular output of the VTA was important to drive this contingent seeking behavior (Pascoli et al., 2015). Non-contingent VTA DA stimulation also produced positive reinforcement and a concomitant increase in NAc DA levels (Tsai et al., 2009). Finally, selectively stimulating VTA DA terminals within the NAc was sufficient to drive positive reinforcement which could be blocked by dopamine receptor antagonists (Steinberg et al., 2014). Together, this non-exhaustive collection of studies underlines VTA released dopamine within the NAc as both necessary and sufficient to drive reward-like behaviors.

Since being identified as a reward hub in the brain, further work characterizing the anatomy and chemical makeup of the NAc have been undertaken. The NAc is primarily comprised of two non-overlapping cell-types, dopamine type-1 and dopamine type-2 medium spiny neurons (D1-MSNs and D2-MSNs, respectively) (Le Moine and Bloch, 1995). Classically, these populations were thought to belong to distinct anatomical pathways similar to the basal ganglia with D1-MSNs being part of a ‘direct pathway’ through their projections to the VTA and D2-MSNs belonging to the ‘indirect pathway’ via their projections to the ventral pallidum (VP) (Bock et al., 2013; MacAskill et al., 2012). In addition to their distinct anatomical projections, studies have indicated that they have opposing functions with D1-

MSNs driving positive reinforcement and D2-MSNs signaling aversion (Ferguson et al., 2011; Hikida et al., 2010; Kim et al., 2011; Lobo et al., 2010). Cocaine and animal models of depression have also been shown to induce separate electrophysiological adaptations in D1- or D2-MSNs (Francis et al., 2015; Kim et al., 2011). However, recent reports have challenged this idea and shown that both D1- and D2-MSNs project to the VP (Kupchik et al., 2015). Further studies have shown that although they both project to the VP, they undergo separate electrophysiological adaptations at the D1- or D2-MSN-to-VP synapse in response to acute cocaine administration and withdrawal (Creed et al., 2016).

Pharmacological studies have attempted to parse out the contributions of D1- and D2-MSNs to separate stages of cocaine addiction. On one hand, antagonism of both D1- and D2-MSNs block escalation of DA release in the NAc (Steinberg et al., 2014), however other studies indicate that blockade of only D1-receptors in the NAc is sufficient to abolish cocaine self-administration (Maldonado et al., 1993). Furthermore, D1-MSN antagonism attenuates reinstatement of cocaine-seeking after a period of withdrawal, suggesting that D1-MSN activity is critical both for the transition from acute to chronic cocaine use, but also for relapse after prolonged abstinence (Anderson et al., 2003). Interestingly, D2-receptor antagonism specifically in the shell subregion of the NAc, but not the core, had the same effect on reinstatement of cocaine seeking (Anderson et al., 2006) while optogenetic stimulation of D2-MSNs blocked cocaine administration (Bock et al., 2013). This points to the potential that specific anatomical subdivisions within the nucleus accumbens (classically separate as core vs. medial or lateral shell) may add another layer of specificity when considering the NAc contributions to cocaine-seeking behavior. On a structural level, increases in spine density

were observed selectively in D1-MSNs after cocaine administration and maintained after a period of withdrawal (Lee et al., 2006).

Despite the established importance of dopamine release on D1- and D2-MSNs in the NAc, it has become increasingly evident that the influence of VTA-derived dopamine on NAc activity is not sufficient to fully capture the complex stages of addiction. While many studies show that stimulation of VTA DA neurons and DA release in the NAc is sufficient for reward and cocaine seeking (Adamantidis et al., 2011; Kuhar et al., 1991; Pascoli et al., 2015; Tsai et al., 2009), other studies show that animals in which dopamine synthesis has been abolished will continue to self-administer cocaine indicating that dopamine release is not the only player driving cocaine seeking (Hnasko et al., 2007; Pettit et al., 1984). Revelations that VTA dopaminergic neurons could co-release glutamate in the NAc provided insight that glutamatergic transmission originating from the VTA may contribute to reward seeking in parallel with dopamine (Stuber et al., 2010), supporting previous studies that abolished reinstatement of cocaine seeking behavior by intra-NAc infusion of glutamatergic antagonists (Cornish and Kalivas, 2000).

In addition to glutamatergic co-release from the VTA, the main sources of glutamatergic input in the NAc are supplied by the basolateral amygdala (BLA), prelimbic prefrontal cortex (PrL), ventral hippocampus (vHPC), and paraventricular thalamus (PVT) (Grueter et al., 2012; Lüscher and Malenka, 2011; Ma et al., 2014; MacAskill et al., 2012; Neumann et al., 2016; Russo and Nestler, 2013). These separate inputs have been hypothesized to support discrete stages of addiction and have been shown to be modulated by cocaine exposure. In particular, the BLA is thought to represent emotional value of the drug,

vHPC encodes environmental context associated with drug, and the PrL top-down operational drive for the drug (Russo and Nestler, 2013).

Indeed, studies have found separate cocaine-induced structural and electrophysiological adaptations dependent on the afferent brain region to the NAc, and whether these projections synapse on D1- or D2-MSNs. When inputs to the NAc are electrically stimulated in a non-input specific manner, no changes in synaptic strength were observed in either D1-MSNs or $D1^-$ neurons after cocaine administration and withdrawal (Joffe and Grueter, 2016). However, when inputs from the medial prefrontal cortex (mPFC, including the PrL) or midline thalamus (mThal, a component of the PVT) were selectively stimulated a selective increase in AMPA/NMDA ratio was measured after cocaine administration in PFC-to-D1-MSN synapses, but not mThal-to-D1-MSN synapses. Furthermore, putative D2-MSNs as defined by their lack of dopamine receptor 1 expression exhibited a reduction in AMPA-NMDA ratio when inputs from the mThal were stimulated, but not from the mPFC (Joffe and Grueter, 2016). Cocaine's effect at the mThal-to-D2-MSN synapse appears not to be selective for cocaine, as repeated morphine administration also potentiated this pathway, but had no effect on D1-MSNs (Zhu et al., 2016).

Again using AMPA/NMDA receptor ratio as a proxy for synaptic plasticity, no change was found in the BLA-to-D1-MSN pathway after withdrawal from cocaine self-administration (Pascoli et al., 2014). In contrast, an increase in AMPA/NMDA ratio was observed at vHPC-to-D1-MSN synapses while a decrease was observed at mPFC-to-D1-MSN synapses (Pascoli et al., 2014). Other work has shown that this input-specific plasticity in response to cocaine withdrawal is specific to D1-MSNs, as no change in excitatory

postsynaptic current amplitude (EPSC) was seen in D2-MSNs when projections from both BLA and vHPC were stimulated (MacAskill et al., 2014). In contrast, an increase in EPSC amplitude was observed at BLA-to-D1-MSN synapses while a concomitant decrease in EPSC amplitude was measured at vHPC-to-D1-MSN synapses (MacAskill et al., 2014). This study measured synaptic strength only 3 days after the last cocaine administration, as opposed to a 30 day withdrawal period in Pascoli et al., 2014 which could explain the differences in their results.

Taken together, these studies emphasize the high degree of complexity when studying the neural adaptations in addiction. In particular, when trying to parse the separate contributions of the NAc to addiction at a circuit-level perspective it is critical to consider three aspects: 1) input region specificity (e.g. BLA, vHPC, PrL, etc.), 2) cell-type specificity within the NAc (e.g. D1- or D2-MSN), 3) stage specificity (e.g. initial acute stages of drug intake, chronic intake, after withdrawal, after relapse/reinstatement). Simultaneously taking into account all these factors can provide a more thorough framework when considering questions such as do separate brain regions contribute to discrete aspects of cocaine use, and do distinct cell-types within the NAc differentially contribute to separate stages of drug intake?

In Chapter II, we begin to address these questions by measuring spine density changes as a structural proxy for synaptic strength. In this manner, we can leverage the advantages of the transsynaptic labeling capacity of rabies virus in order to measure changes in input regions upstream of the NAc. While most studies have focused on changes occurring within D1- or D2-MSNs, or at synapses within the NAc, much less is known about the cocaine-induced

alterations occurring in neurons in the PrL cortex, BLA, and vHPC. Chapter II, which is currently in review for publication at *Biological Psychiatry*, examines the changes in spine density of these neurons projecting to either D1- or D2-MSNs at separate stages of cocaine addiction. There, we discovered profound structural plasticity that was stage-, input-, and cell-type specific that we believe extends our knowledge of cocaine-induced plasticity beyond the NAc and into upstream regions.

References

Adamantidis, A.R., Tsai, H.-C., Boutrel, B., Zhang, F., Stuber, G.D., Budygin, E.A., Tourino, C., Bonci, A., Deisseroth, K., and de Lecea, L. (2011). Optogenetic Interrogation of Dopaminergic Modulation of the Multiple Phases of Reward-Seeking Behavior. J. Neurosci. *31*, 10829–10835.

Anderson, S.M., Bari, A.A., and Pierce, R.C. (2003). Administration of the D1-like dopamine receptor antagonist SCH-23390 into the medial nucleus accumbens shell attenuates cocaine priming-induced reinstatement of drug-seeking behavior in rats. Psychopharmacology (Berl). *168*, 132–138.

Anderson, S.M., Schmidt, H.D., and Pierce, R.C. (2006). Administration of the D2 dopamine receptor antagonist sulpiride into the shell, but not the core, of the nucleus accumbens attenuates cocaine priming-induced reinstatement of drug seeking. Neuropsychopharmacology *31*, 1452–1461.

Atasoy, D., Aponte, Y., Su, H.H., and Sternson, S.M. (2008). A FLEX Switch Targets Channelrhodopsin-2 to Multiple Cell Types for Imaging and Long-Range Circuit Mapping. J. Neurosci. *28*, 7025–7030.

Bagot, R.C., Parise, E.M., Peña, C.J., Zhang, H.-X., Maze, I., Chaudhury, D., Persaud, B., Cachope, R., Bolaños-Guzmán, C. a., Cheer, J., et al. (2015). Ventral hippocampal afferents to the nucleus accumbens regulate susceptibility to depression. Nat. Commun. *6*, 7062.

Beier, K.T., Steinberg, E.E., DeLoach, K.E., Xie, S., Miyamichi, K., Schwarz, L., Gao, X.J., Kremer, E.J., Malenka, R.C., and Luo, L. (2015). Circuit Architecture of VTA Dopamine Neurons Revealed by Systematic Input-Output Mapping. Cell *162*, 622–634.

Bock, R., Shin, J.H., Kaplan, A.R., Dobi, A., Markey, E., Kramer, P.F., Gremel, C.M., Christensen, C.H., Adrover, M.F., and Alvarez, V. a (2013). Strengthening the accumbal indirect pathway promotes resilience to compulsive cocaine use. Nat. Neurosci. *16*, 632–638.

Boyden, E.S., Zhang, F., Bamberg, E., Nagel, G., and Deisseroth, K. (2005). Millisecond-timescale, genetically targeted optical control of neural activity. Nat. Neurosci. *8*, 1263–1268.

Broca, P. (1961). Remarques sur le siège de la faculté du langage articulé, suivies d'une observation d'aphémie (perte de la parole). Bull. La Société Anat. *6*, 330–357.

Bunney, W.E., and Davis, J.M. (1965). Norepinephrine in Depressive Reactions. Arch. Gen. Psychiatry *13*, 483–494.

Cao, J.-L., Covington, H.E., Friedman, a. K., Wilkinson, M.B., Walsh, J.J., Cooper, D.C., Nestler, E.J., and Han, M.-H. (2010). Mesolimbic Dopamine Neurons in the Brain Reward Circuit Mediate Susceptibility to Social Defeat and Antidepressant Action. J. Neurosci. *30*, 16453–16458.

del Castillo, J., and Katz, B. (1952). Quantal components of the end-plate potential. J. Physiol. *124*, 560–573.

Chang, C.H., and Grace, A. a. (2014). Amygdala-ventral pallidum pathway decreases dopamine activity after chronic mild stress in rats. Biol. Psychiatry *76*, 223–230.

Chaudhury, D., Walsh, J.J., Friedman, A.K., Juarez, B., Ku, S.M., Koo, J.W., Ferguson, D., Tsai, H.-C., Pomeranz, L., Christoffel, D.J., et al. (2013). Rapid regulation of depression-related behaviours by control of midbrain dopamine neurons. Nature *493*, 532–536.

Cornish, J.L., and Kalivas, P.W. (2000). Glutamate transmission in the nucleus accumbens mediates relapse in cocaine addiction. J. Neurosci. *20*, RC89.

Covington, H.E., Lobo, M.K., Maze, I., Vialou, V., Hyman, J.M., Zaman, S., LaPlant, Q., Mouzon, E., Ghose, S., Tamminga, C. a, et al. (2010). Antidepressant effect of optogenetic stimulation of the medial prefrontal cortex. J. Neurosci. *30*, 16082–16090.

Creed, M., Ntamati, N.R., Chandra, R., Lobo, M.K., and Lüscher, C. (2016). Convergence of Reinforcing and Anhedonic Cocaine Effects in the Ventral Pallidum. Neuron 214–226.

Crick, F.H. (1979). Thinking about the brain. Sci. Am. *241*, 219–232.

Dillehay, T., Rossen, J., Ugent, D., Karathanasis, A., Vásquez, V., and Netherly, P. (2010). Early Holocene coca chewing in norhern Paru. Antiquity *84*, 939–953.

Faget, L., Osakada, F., Duan, J., Ressler, R., Johnson, A.B., Proudfoot, J.A., Yoo, J.H., Callaway, E.M., and Hnasko, T.S. (2016). Afferent Inputs to Neurotransmitter-Defined Cell Types in the Ventral Tegmental Area. Cell Rep. *15*, 2796–2808.

Fatt, P., and Katz, B. (1952). Spontaneous subthreshold activity at motor nerve endings. J. Physiol. *117*, 109–128.

Ferguson, S.M., Eskenazi, D., Ishikawa, M., Wanat, M.J., Phillips, P.E.M., Dong, Y., Roth, B.L., and Neumaier, J.F. (2011). Transient neuronal inhibition reveals opposing roles of indirect and direct pathways in sensitization. Nat. Neurosci. *14*, 22–24.

Finger, S. (2000). Minds behind the brain: A history of the pioneers and their discoveries. Oxford University Press.

Fodor, J.A. (1983). The Modularity of Mind.

Francis, T.C., Chandra, R., Friend, D.M., Finkel, E., Dayrit, G., Miranda, J., Brooks, J.M., Iñiguez, S.D., O'Donnell, P., Kravitz, A., et al. (2015). Nucleus Accumbens Medium Spiny Neuron Subtypes Mediate Depression-Related Outcomes to Social Defeat Stress. Biol. Psychiatry *77*, 212–222.

Friedman, A.K., Walsh, J.J., Juarez, B., Ku, S.M., Chaudhury, D., Wang, J., Li, X., Dietz, D.M., Pan, N., Vialou, V.F., et al. (2014). Enhancing Depression Mechanisms in Midbrain Dopamine Neurons Achieves Homeostatic Resilience. Science *344*, 313–

319.

Golden, S. a, Covington, H.E., Berton, O., and Russo, S.J. (2011). A standardized protocol for repeated social defeat stress in mice. Nat. Protoc. *6*, 1183–1191.

Greenberg, P.E., Fournier, A.-A., Sisitsky, T., Pike, C.T., and Kessler, R.C. (2015). The Economic Burden of Adults With Major Depressive Disorder in the United States (2005 and 2010). J. Clin. Psychiatry *76*, 155–162.

Grueter, B. a, Rothwell, P.E., and Malenka, R.C. (2012). Integrating synaptic plasticity and striatal circuit function in addiction. Curr. Opin. Neurobiol. *22*, 545–551.

Hikida, T., Kimura, K., Wada, N., Funabiki, K., and Nakanishi Shigetada, S. (2010). Distinct Roles of Synaptic Transmission in Direct and Indirect Striatal Pathways to Reward and Aversive Behavior. Neuron *66*, 896–907.

Hillhouse, T.M., and Porter, J.H. (2015). A brief history of the development of antidepressant durgs: From monamines to glutamate. Exp. Clin. Psychopharmacol. *23*, 1–21.

Hnasko, T.S., Sotak, B.N., and Palmiter, R.D. (2007). Cocaine-Conditioned Place Preference by Dopamine-Deficient Mice Is Mediated by Serotonin. J. Neurosci. *27*, 12484–12488.

Hodgkin, A., and Huxley, A. (1952a). The components of membrane conductance in the giant axon of loligo. J. Physiol. *116*, 473–496.

Hodgkin, A., and Huxley, A. (1952b). A quantitative description of membrane current and its application to conduction and excitation in nerve. J. Physiol. *117*, 500–544.

Hodgkin, A., and Huxley, A. (1952c). The dual effect of membrane potential on sodium conductance in the giant axon of loligo. J. Physiol. *116*, 497–506.

Hodgkin, A., and Huxley, A. (1952d). Measurement of Current-Voltage Relations in the Membrane of the Giant Axon of Loligo. J. Physiol. *116*, 424–448.

Hodgkin, A., and Huxley, A. (1952e). Currents carried by sodium and potassium ions through the membrane of the giant axon of loligo. J. Physiol. *116*, 449–472.

Joffe, M.E., and Grueter, B.A. (2016). Cocaine Experience Enhances Thalamo-Accumbens N-Methyl-D-Aspartate Receptor Function. Biol. Psychiatry *80*, 671–681.

Katz, B., and Miledi, R. (1964). The measurement of synaptic delay, and the time course of acetylcholine release at the neuromuscular junction. J. Physiol. *161*, 483–495.

Kiening, K., and Sartorius, A. (2013). A new translational target for deep brain stimulation to treat depression. EMBO Mol. Med. *5*, 1151–1153.

Kim, J., Park, B.H., Lee, J.H., Park, S.K., and Kim, J.H. (2011). Cell type-specific alterations in the nucleus accumbens by repeated exposures to cocaine. Biol. Psychiatry *69*, 1026–1034.

Kuhar, M.J., Ritz, M.C., and Boja, J.W. (1991). The dopamine hypothesis of the reinforcing

properties of cocaine. Trends Neurosci. *14*, 299–302.

Kupchik, Y.M., Brown, R.M., Heinsbroek, J. a, Lobo, M.K., Schwartz, D.J., and Kalivas, P.W. (2015). Coding the direct/indirect pathways by D1 and D2 receptors is not valid for accumbens projections. Nat. Neurosci. *18*, 1230–1232.

Lee, K.-W., Kim, Y., Kim, A.M., Helmin, K., Nairn, A.C., and Greengard, P. (2006). Cocaine-induced dendritic spine formation in D1 and D2 dopamine receptor-containing medium spiny neurons in nucleus accumbens. Proc. Natl. Acad. Sci. U. S. A. *103*, 3399–3404.

Li, B., Piriz, J., Mirrione, M., Chung, C., Proulx, C.D., Schulz, D., Henn, F., and Malinow, R. (2011). Synaptic potentiation onto habenula neurons in the learned helplessness model of depression. Nature *470*, 535–539.

Lim, B.K., Huang, K.W., Grueter, B. a, Rothwell, P.E., and Malenka, R.C. (2012). Anhedonia requires MC4R-mediated synaptic adaptations in nucleus accumbens. Nature *487*, 183–189.

Lobo, M.K., Covington, H.E., Chaudhury, D., Friedman, A.K., Sun, H., Damez-Werno, D., Dietz, D.M., Zaman, S., Koo, J.W., Kennedy, P.J., et al. (2010). Cell Type-Specific Loss of BDNF Signaling Mimics Optogenetic Control of Cocaine Reward. Science (80-.). *327*, 385–391.

Lüscher, C., and Malenka, R.C. (2011). Drug-Evoked Synaptic Plasticity in Addiction: From Molecular Changes to Circuit Remodeling. Neuron *69*, 650–663.

Ma, Y., Lee, B.R., Wang, X., Guo, C., Liu, L., Cui, R., Lan, Y., Balcita-pedicino, J.J., Wolf, M.E., Sesack, S.R., et al. (2014). Article Bidirectional Modulation of Incubation of Cocaine Craving by Silent Synapse-Based Remodeling of Prefrontal Cortex to Accumbens Projections. 1453–1467.

MacAskill, A.F., Little, J.P., Cassel, J.M., and Carter, A.G. (2012). Subcellular connectivity underlies pathway-specific signaling in the nucleus accumbens. Nat. Neurosci. *15*, 1624–1626.

MacAskill, A.F., Cassel, J.M., and Carter, A.G. (2014). Cocaine exposure reorganizes cell type– and input-specific connectivity in the nucleus accumbens. Nat. Neurosci. *17*, 1198–1207.

Maldonado, R., Robledo, P., Chover, A.J., Caine, S.B., and Koob, G.F. (1993). D1 dopamine receptors in the nucleus accumbens modulate cocaine self-administration in the rat. Pharmacol. Biochem. Behav. *45*, 239–242.

Le Moine, C., and Bloch, B. (1995). D1 and D2 dopamine receptor gene expression in the rat striatum: Sensitive cRNA probes demonstrate prominent segregation of D1 and D2 mRNAS in distinct neuronal populations of the dorsal and ventral striatum. J. Comp. Neurol. *355*, 418–426.

Muir, J., Lorsch, Z.S., Ramakrishnan, C., Deisseroth, K., Nestler, E.J., Calipari, E.S., and

Bagot, R.C. (2017). In Vivo Fiber Photometry Reveals Signature of Future Stress Susceptibility in Nucleus Accumbens. Neuropsychopharmacol. Adv. Online Publ. *doi*.

Muller, J.C., Pryor, W.W., Gibbons, J.E., and Orgain, E.S. (1953). Depression and Anxiety Occuring During Rauwolfia Therapy. J. Am. Med. Assoc. *159*, 836–839.

Murrough, J.W., Henry, S., Hu, J., Gallezot, J.D., Planeta-Wilson, B., Neumaier, J.F., and Neumeister, A. (2011). Reduced ventral striatal/ventral pallidal serotonin1B receptor binding potential in major depressive disorder. Psychopharmacology (Berl). *213*, 547–553.

Nagel, G., Szellas, T., Huhn, W., Kateriya, S., Adeishvili, N., Berthold, P., Ollig, D., Hegemann, P., and Bamberg, E. (2003). Channelrhodopsin-2, a directly light-gated cation-selective membrane channel. Proc. Natl. Acad. Sci. *100*, 13940–13945.

Nestler, E. (2005). The Neurobiology of Cocaine Addiction. Sci. Pract. Perspect. *3*, 4–10.

Neumann, P.A., Wang, Y., Yan, Y., Wang, Y., Ishikawa, M., Cui, R., Huang, Y.H., Sesack, S.R., Schlüter, O.M., and Dong, Y. (2016). Cocaine-Induced Synaptic Alterations in Thalamus to Nucleus Accumbens Projection. Neuropsychopharmacology *41*, 2399–2410.

Olds, J., and Milner, P. (1954). Positive reinforcement produced by electrical stimulation of septal area and other regions of rat brain. J. Comp. Physiol. Psychol. 419–427.

Ostlund, S.B., and Halbout, B. (2017). Mesolimbic Dopamine Signaling in Cocaine Addiction (Elsevier Inc.).

Pascoli, V., Terrier, J., Espallergues, J., Valjent, E., O'Connor, E.C., and Lüscher, C. (2014). Contrasting forms of cocaine-evoked plasticity control components of relapse. Nature *509*, 459–464.

Pascoli, V., Terrier, J., Hiver, A., and Lüscher, C. (2015). Sufficiency of Mesolimbic Dopamine Neuron Stimulation for the Progression to Addiction. Neuron *88*, 1054–1066.

Petreanu, L., Huber, D., Sobczyk, A., and Svoboda, K. (2007). Channelrhodopsin-2-assisted circuit mapping of long-range callosal projections. Nat. Neurosci. *10*, 663–668.

Pettit, H.O., and Justice, J.B. (1989). Dopamine in the nucleus accumbens during cocaine self-administration as studied by in vivo microdialysis. Pharmacol. Biochem. Behav. *34*, 899–904.

Pettit, H.O., Ettenberg, A., Bloom, F.E., and Koob, G.F. (1984). Destruction of dopamine in the nucleus accumbens selectively attenuates cocaine but not heroin self-administration in rats. Psychopharmacology (Berl). *84*, 167–173.

Proulx, C.D., Hikosaka, O., and Malinow, R. (2014). Reward processing by the lateral habenula in normal and depressive behaviors. Nat. Neurosci. *17*, 1146–1152.

Root, D.H., Melendez, R.I., Zaborszky, L., and Napier, T.C. (2015). The ventral pallidum:

Subregion-specific functional anatomy and roles in motivated behaviors. Prog. Neurobiol.

Russo, S.J., and Nestler, E.J. (2013). The brain reward circuitry in mood disorders. Nat. Rev. Neurosci. *14*, 609–625.

Sachs, B.D., Ni, J.R., Caron, M.G., and Mcewen, B.S. (2015). Brain 5-HT deficiency increases stress vulnerability and impairs antidepressant responses following psychosocial stress. Proc. Natl. Acad. Sci. *112*, 2557–2562.

Sartorius, A., Kiening, K.L., Kirsch, P., von Gall, C.C., Haberkorn, U., Unterberg, A.W., Henn, F.A., and Meyer-Lindenberg, A. (2010). Remission of Major Depression Under Deep Brain Stimulation of the Lateral Habenula in a Therapy-Refractory Patient. Biol. Psychiatry *67*, e9–e11.

Schildkraut, J.J. (1965). The Catecholamine Hypothesis of Affective Disorders : A Review of Supporting Evidence. Am. J. Psychiatry *122*, 509–522.

Schobert, B., and Lanyi, J.K. (1986). Halorhodopsin: a light-driven chloride ion pump. Annu. Rev. Biophys. Biophys. Chem. *15*, 11–28.

Shabel, S.J., Proulx, C.D., Trias, A., Murphy, R.T., and Malinow, R. (2010). GABA/glutamate co-release controls habenula output and is modified by antidepressant treatment. Science *17*, 1.

Shabel, S.J., Proulx, C.D., Trias, A., Murphy, R.T., and Malinow, R. (2012). Input to the lateral habenula from the basal ganglia is excitatory, aversive, and suppressed by serotonin. Neuron *74*, 475–481.

Shaw, D.M., Camps, F.E., and Eccleston, E.G. (1967). 5-Hydroxytryptamine in the Hind-Brain of Depressive Suicides. Br. J. Psychiatry *113*, 1407–1411.

Smith, K.S., Tindell, A.J., Aldridge, J.W., and Berridge, K.C. (2009). Ventral pallidum roles in reward and motivation. Behav. Brain Res. *196*, 155–167.

Squire, L.R. (2009). The Legacy of Patient H.M. for Neuroscience. Neuron *61*, 6–9.

Steinberg, E.E., Boivin, J.R., Saunders, B.T., Witten, I.B., Deisseroth, K., and Janak, P.H. (2014). Positive reinforcement mediated by midbrain dopamine neurons requires D1 and D2 receptor activation in the nucleus accumbens. PLoS One *9*.

Stuber, G.D., Hnasko, T.S., Britt, J.P., Edwards, R.H., and Bonci, A. (2010). Dopaminergic Terminals in the Nucleus Accumbens But Not the Dorsal Striatum Corelease Glutamate. J. Neurosci. *30*, 8229–8233.

Substance Abuse and Mental Health Services Administration (2017) Key Substance Use and Mental Health Indicators in the United States: Results from the 2016 National Survey on Drug Use and Health.

Tsai, H.-C., Zhang, F., Adamantidis, A., Stuber, G.D., Bonci, A., de Lecea, L., and Deisseroth, K. (2009). Phasic Firing in Dopaminergic Neurons Is Sufficient for

Behavioral Conditioning. Science (80-.). *324*, 1080–1084.

Wang, H., Peca, J., Matsuzaki, M., Matsuzaki, K., Noguchi, J., Qiu, L., Wang, D., Zhang, F., Boyden, E., Deisseroth, K., et al. (2007). High-speed mapping of synaptic connectivity using photostimulation in Channelrhodopsin-2 transgenic mice. Proc. Natl. Acad. Sci. *104*, 8143–8148.

Winter, C., Vollmayr, B., Djodari-Irani, A., Klein, J., and Sartorius, A. (2011). Pharmacological inhibition of the lateral habenula improves depressive-like behavior in an animal model of treatment resistant depression. Behav. Brain Res. *216*, 463–465.

Yamanaka, H., Yokoyama, C., Mizuma, H., Kurai, S., Finnema, S.J., Halldin, C., Doi, H., and Onoe, H. (2014). A possible mechanism of the nucleus accumbens and ventral pallidum 5-HT1B receptors underlying the antidepressant action of ketamine: a PET study with macaques. Transl. Psychiatry *4*, e342.

Zhu, Y., Wienecke, C.F.R., Nachtrab, G., and Chen, X. (2016). A thalamic input to the nucleus accumbens mediates opiate dependence. Nature *530*.

CHAPTER I:

Distinct Ventral Pallidal Neural Populations Mediate Separate Symptoms of Depression

Daniel Knowland, Varoth Lilascharoen, Christopher Pham Pacia, Sora Shin, Eric Hou-Jen Wang, Byung Kook Lim

Article

Cell

Distinct Ventral Pallidal Neural Populations Mediate Separate Symptoms of Depression

Graphical Abstract

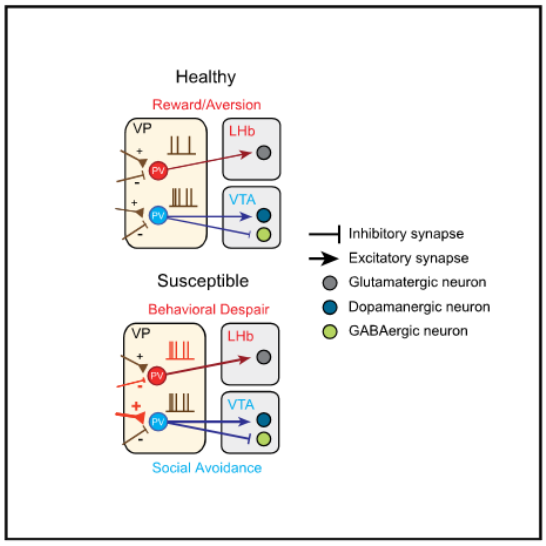

Authors

Daniel Knowland, Varoth Lilascharoen, Christopher Pham Pacia, Sora Shin, Eric Hou-Jen Wang, Byung Kook Lim

Correspondence

bklim@ucsd.edu

In Brief

Distinct symptoms of depression are encoded in discrete circuits of the ventral pallidum that project to separate brain regions contributing to depression.

Highlights

- VP PV neurons project to the LHb and VTA and release different transmitters
- Elevated VP PV neuronal activity is a hallmark of depressed animals
- VP PV neurons mediate distinct depressive-like symptoms based on projection target

Knowland et al., 2017, Cell *170*, 1–14
July 13, 2017 Published by Elsevier Inc.
http://dx.doi.org/10.1016/j.cell.2017.06.015

CellPress

Please cite this article in press as: Knowland et al., Distinct Ventral Pallidal Neural Populations Mediate Separate Symptoms of Depression, Cell (2017), http://dx.doi.org/10.1016/j.cell.2017.06.015

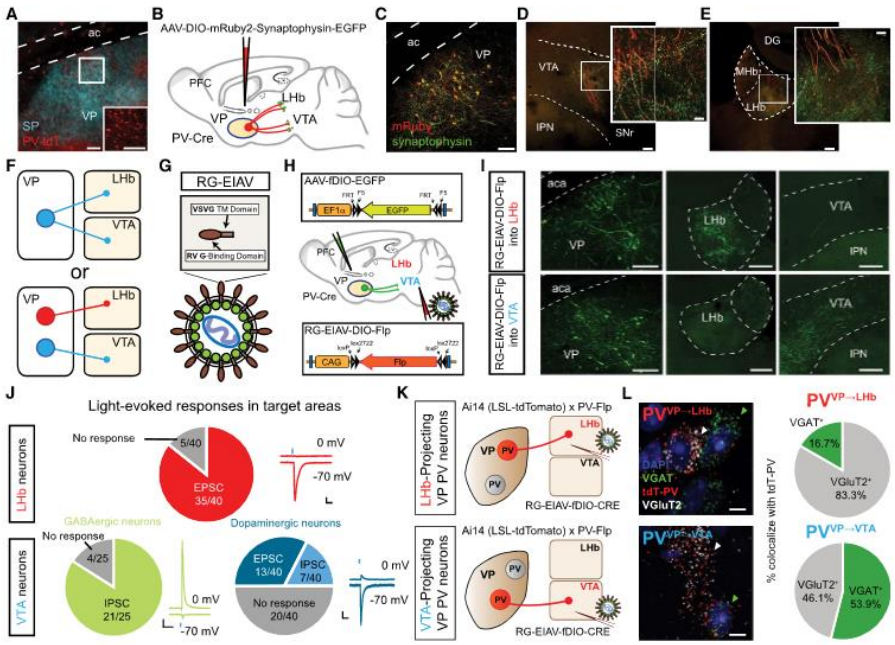

Figure 1. Distinct Subpopulations of VP PV Neurons Project to the LHb and VTA

(A) PV neuronal localization in VP. Substance P (SP) immunostaining denotes boundaries of VP. Scale bars, 100 μm; inset, 50 μm.

(B) Schematic of tracing strategy. Cell bodies and efferent fibers are in red and presynaptic sites are in green using AAV-DIO-mRuby2-T2A-Synaptophysin-eGFP.

(C) Representative image of injection site in VP. Scale bar, 80 μm.

(D and E) Fibers and synaptic puncta in LHb (D) and VTA (E) from VP PV neurons. Scale, 200 μm; inset, 20 μm.

(F) Two possible projection patterns: VP PV neurons send collateralized axons to both the LHb and VTA (top) or independent subpopulations send axons exclusively to either LHb or VTA (bottom).

(G and H) Schematic of viral strategy. EIAV is pseudotyped with a fusion protein containing rabies virus glycoprotein and VSVG transmembrane (RG-EIAV; G). Injection of RG-EIAV-DIO-Flp into target area and AAV-fDIO-eGFP into VP of PV-Cre mice is shown.

(I) Images of injection site and target areas showing cell-type and projection-specific labeling. VP PV neurons selectively project to either the LHb or VTA, respectively, but not to both. Scale, 200 μm.

(J) Light-evoked synaptic responses in LHb or VTA. EPSCs measured at −70 mV and IPSCs at 0 mV. Pie charts indicate whether absolute amplitude was greater for evoked EPSC, IPSC, or no response (individual responses in Figure S4). Top row, LHb neurons; bottom row, VTA neurons distinguished as either GABAergic or dopaminergic. Scales, 50 pA, 100 ms.

(K) Strategy using PV-Flp × Ai14 mouse for labeling VP PV neurons in projection-specific manner. RG-EIAV-fDIO-Cre is injected into either LHb (top) or VTA (bottom).

(L) mRNA labeling of $PV^{VP\rightarrow LHb}$ neurons (top panel) and $PV^{VP\rightarrow VTA}$ neurons (bottom panel). Green arrowheads show $VGAT^+$ cells, and white arrowheads show $VGluT2^+$ cells. Scale, 10 μm. Pie charts indicate percentage of tdTomato-$mRNA^+$ neurons projecting to LHb or VTA colocalizing with probes to VGAT or VGluT2 (n = 154 tdT^+ cells for VTA-projecting, n = 24 cells for LHb-projecting).

EIAV, equine infectious anemia virus; RV G, rabies virus glycoprotein; ac, anterior commissure; SNr, substantia nigra reticulata; MHb, medial habenula; CPu caudate putamen.

See also Figures S1, S2, S3, and S4.

RESULTS

VP PV Neurons Projecting to the LHb or VTA Represent Independent Subpopulations

Consistent with previous reports, we find a substantial population of PV neurons in the VP (Brauer et al., 1993; Zahm et al., 1996) using a Cre-dependent tdTomato (tdT) reporter line (Ai14-LSL-tdT) crossed with a PV-Cre mouse (Figure 1A; Figures S1A and S1B). To identify projection targets of VP PV neurons, we labeled VP PV axons and presynaptic terminals by injecting adeno-associated virus (AAV)-DIO-mRuby-T2A-Synaptophysin-eGFP (green fluorescent protein) into the VP of PV-Cre

mice (Figure 1B). Unlike their cortical and striatal local-projecting counterparts, VP PV neurons are long-range projection neurons demonstrated by dense innervation in several brain areas including the LHb, VTA (lateral part), and others (Figures 1C–1E and S1D).

The VTA is primarily thought to mediate reward while the LHb encodes aversive signals (Pascoli et al., 2015; Shabel et al., 2012). These opposing functions led us to distinguish between two possible circuit organizations: (1) do individual VP PV neurons send collateralized axons to target structures and coordinately regulate activity, or (2) do LHb- and VTA-projecting VP PV neurons represent distinct subpopulations capable of independently regulating target activity (Figure 1F)? To define neurons by both their cell type and projection target, we developed and adapted a novel viral vector capable of neuron-specific retrograde infection by pseudotyping equine infectious anemia lentivirus (EIAV) with a fusion protein (FuG-B2) carrying extracellular and transmembrane domains of the rabies glycoprotein connected to the cytoplasmic domain of vesicular stomatitis virus glycoprotein (RG-EIAV, Figure 1G) (Cetin and Callaway, 2014; Kato et al., 2011). RG-EIAV confers stable, retrograde expression of transgene suitable for long-term studies without cytotoxicity.

In PV-Cre mice, we injected RG-EIAV inducing Flp recombinase in a Cre-recombinase-dependent manner (RG-EIAV-DIO-Flp) into either the LHb or VTA concurrently with an adeno-associated virus expressing eGFP in a Flp-dependent manner (AAV-fDIO-eGFP) into the VP (Figure 1H). In this manner, only PV neurons that project to the injection site of RG-EIAV-DIO-Flp (VTA or LHb) will be labeled. Examination of axonal fibers originating from LHb- or VTA-projecting VP PV neurons ($PV^{VP\rightarrow LHb}$, $PV^{VP\rightarrow VTA}$, respectively) revealed that cells projected primarily to the LHb or VTA, but not both (Figures 1I and S1E–S1G).

We also injected Cholera toxin subunit B conjugated to Alexa Fluor 488 or 647 into the LHb and VTA of transgenic PV-Cre x Ai14-tdT mice (Figures S1H and S1I) and quantitated double-labeled PV-tdT^+ and CTb-positive neurons. We again found largely non-overlapping populations of neurons projecting to the LHb and VTA (Figure S1J); however, they did not localize to specific anatomical regions within the VP (Figure S2).

VP PV Neurons Transmit Both Excitatory and Inhibitory Signals

To investigate the transmitter identity of $PV^{VP\rightarrow LHb}$ and $PV^{VP\rightarrow VTA}$ neurons, we injected AAV-DIO-ChR2-eYFP into the VP of PV-Cre animals and obtained whole-cell patch-clamp recordings from neurons in the LHb or VTA. Surprisingly, blue light stimulation of VP PV terminals in the LHb evoked excitatory postsynaptic currents (eEPSCs) in nearly all LHb neurons, with smaller to no inhibitory postsynaptic currents (eIPSCs, Figure 1J, top; Figures S3A–S3D).

Since the lateral VTA is known to contain GABAergic and dopaminergic (DAergic) neurons (Tan et al., 2012; van Zessen et al., 2012), we sought to determine whether VP PV neurons specifically innervated one population or the other. To label GABAergic and DAergic neurons in slice, we crossed GAD67-GFP or TH-GFP mice with PV-Flp mice, a mouse line that expresses Flp-recombinase under control of the endogenous PV promoter (GAD67-GFP × PV-Flp, TH-GFP × PV-Flp, respectively) and injected AAV-fDIO-ChR2-tdT into the VP.

Interestingly, unlike $PV^{VP\rightarrow LHb}$ neurons, we found that VP PV neurons send exclusively inhibitory projections to GABAergic VTA neurons. Despite being less synaptically connected than GABAergic neurons, DAergic neurons received mixed, but more excitatory inputs (Figure 1J, bottom; Figures S3E–S3J). In total, we see that VP PV neurons transmit exclusively inhibitory signals to GABAergic neurons and predominantly excitatory input to DAergic neurons.

Because PV neurons have long been considered to be GABAergic, we looked to further confirm our electrophysiological results. To precisely label $PV^{VP\rightarrow LHb}$ or $PV^{VP\rightarrow VTA}$ neurons, we used a new intersectional approach by crossing PV-Flp mice with Ai14-LSL-tdT reporter animals (PV-Flp × Ai14 hereafter). We then injected RG-EIAV expressing Cre-recombinase in a Flp-dependent manner (RG-EIAV-fDIO-Cre) into either the LHb or VTA such that only $PV^{VP\rightarrow LHb}$ or $PV^{VP\rightarrow VTA}$ neurons, respectively, would be selectively labeled with tdT (Figure 1K).

To validate whether RG-EIAV virus expression using this strategy was specific, we employed a multiplexing fluorescent *in situ* hybridization (FISH) assay to visualize mRNA expression of endogenous PV with tdT from RG-EIAV virus. Quantitation revealed the majority of virally labeled tdT^+ neurons co-localized with PV mRNA (Figures S4A and S4B). Furthermore, employing the same labeling strategy we collected mRNA from individual tdT^+ neurons from acute brain slices and performed RT-PCR; Figure S4C). RT-PCR results revealed that all tdT^+ neurons collected expressed PV mRNA (Figures S4D–S4F).

Again injecting RG-EIAV-fDIO-Cre into the LHb or VTA of PV-Flp × Ai14 mice, we used FISH to probe mRNA expression of VGAT and VGluT2, markers for GABAergic and glutamatergic neurons, respectively. In line with our physiological recordings, we found extensive colocalization of tdT and VGluT2 mRNA in $PV^{VP\rightarrow LHb}$ neurons and mixed VGluT2 and VGAT colocalization for $PV^{VP\rightarrow VTA}$ neurons (Figure 1L). Cells that co-expressed VGAT and VGluT2 were not found. In contrast, quantitation of all VP PV neurons (non-projection specific) with probes to VGAT and VGluT2 revealed that majority of VP PV neurons are GABAergic (Figures S4G and S4H) (Gaykema and Zaborszky, 1997).

Finally, we crossed PV-Flp animals with mice expressing Cre-recombinase in glutamatergic neurons (PV-Flp × VGluT2-Cre). We then injected a mixture of AAV-fDIO-tdT and AAV-DIO-eGFP into the VP. Colocalization of viral labeling in fixed tissue again revealed a population of VP PV neurons that were glutamatergic (Figure S4I). Immunohistochemistry with synaptic markers in the VTA and LHb also revealed similar trends (Figure S4J).

Upstream and Downstream Connectivity of $PV^{VP\rightarrow LHb}$ and $PV^{VP\rightarrow VTA}$ Neurons

Since $PV^{VP\rightarrow LHb}$ and $PV^{VP\rightarrow VTA}$ neurons can be distinguished based on their efferent target, we hypothesized that they may receive distinct inputs as well. To test this, we probed the input-output organization of VP PV neurons by cell-type and projection-specific *trans*-synaptic tracing (Schwarz et al., 2015). First, we injected RG-EIAV-DIO-Flp into either the LHb or VTA, then Flp-dependent AAVs expressing TVA receptor and an

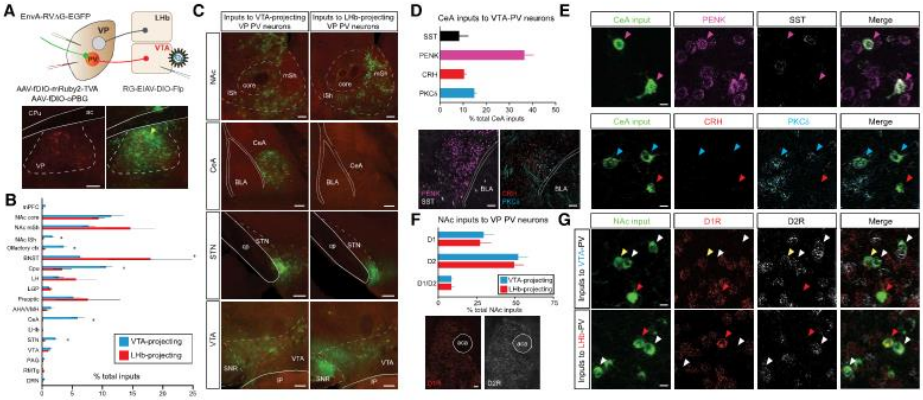

Figure 2. Input-Output Mapping Reveals Anatomically and Molecularly Distinct Inputs of $PV^{VP\rightarrow LHb}$ and $PV^{VP\rightarrow VTA}$ Neurons

(A) Injection regiment to map pseudotype rabies-mediated monosynaptic inputs to either LHb-projecting or VTA-projecting VP PV neurons (top). Starter cell localization of AAV-fDIO-mRuby2-TVA, AAV-fDIO-oPBG, and EnvA-RVΔG-eGFP (bottom, yellow arrows). Scale, 200 μm.

(B) Whole-brain quantitation of inputs to $PV^{VP\rightarrow LHb}$ and $PV^{VP\rightarrow VTA}$ neurons. Data are presented as mean ± SEM, percentage of total cells in a given brain area relative to total number of brain-wide inputs. Unpaired t tests were used for individual brain regions, $^{*}p < 0.05$, $^{**}p < 0.01$, n = 4 for each condition.

(C) Representative images of inputs in select brain areas. Scale bars, 200 μm.

(D) Molecular characterization of CeA inputs to $PV^{VP\rightarrow VTA}$ neurons via FISH assay. Quantitation (top) and representative images of mRNA labeling (bottom). n = 257 cells from two animals. Scale, 100 μm.

(E) Images of CeA neurons sending input to $PV^{VP\rightarrow VTA}$ neurons with cell-type-specific markers. Colored arrows represent colocalization between rabies^{+} input cells and mRNA for specified probe. Scale, 10 μm.

(F) Quantitation of NAc D1R- and D2R-expressing MSN inputs to $PV^{VP\rightarrow LHb}$ and $PV^{VP\rightarrow VTA}$ neurons. Scale, 100 μm.

(G) Representative images in NAc showing colocalization of D1R or D2R in neurons projecting to $PV^{VP\rightarrow LHb}$ and $PV^{VP\rightarrow VTA}$ neurons. Red arrows denote D1R colocalization, white arrows denote D2R, yellow arrows co-express D1R and D2R. n = 1,505 cells from two animals each. Scale, 10 μm.

mPFC, medial prefrontal cortex; BNST, bed nucleus stria terminalis; LH, lateral hypothalamus; LGP, lateral globus pallidus; AHA/VMH, anterior hypothalamic area/ventromedial hypothalamus; PAG, periaqueductal gray; RMTg, rostromedial tegmental nucleus; DRN, dorsal raphe nucleus. SST, somatostatin; PENK, preproenkephalin; CRH, corticotropin releasing hormone; PKCδ, protein kinase C delta.

All data are presented as mean + SEM. See also Figure S5.

optimized rabies glycoprotein into the VP (AAV-fDIO-mRuby-TVA, AAV-fDIO-oPBG, respectively) (Kim et al., 2016). We then delivered EnvA-pseudotyped, glycoprotein-deleted rabies virus (EnvA-RVΔG-eGFP) into the VP to map monosynaptic inputs to these two populations (Figure 2A) (Wickersham et al., 2007).

Whole-brain quantitation of eGFP-labeled neurons revealed significant differences in inputs to $PV^{VP\rightarrow LHb}$ and $PV^{VP\rightarrow VTA}$ neuronal populations. In particular, while $PV^{VP\rightarrow LHb}$ neurons receive proportionally more input from the bed nucleus of the stria terminalis (BNST) and medial shell of NAc, $PV^{VP\rightarrow VTA}$ cells receive significantly more input from areas such as the NAc lateral shell (NAc lSh), subthalamic nucleus (STN), and central amygdala (CeA) (Figures 2B and 2C).

Since the CeA to VP connection has been poorly defined, we combined input-output viral tracing with FISH to investigate the molecular identity of CeA input neurons. Among the major cell types in the CeA (Haubensak et al., 2010), we found the most extensive colocalization of rabies-eGFP^{+} CeA neurons with preproenkephalin (PENK) (Figures 2D and 2E).

Finally, recent work has shown that contrary to canonical direct-indirect pathway notions of accumbal projections to the VP, both D1- and D2-receptor (D1R and D2R) expressing medium spiny neurons (MSNs) project to the VP (Creed et al., 2016; Kupchik et al., 2015). As such, we investigated whether $PV^{VP\rightarrow LHb}$ and $PV^{VP\rightarrow VTA}$ received preferential input from D1R or D2R MSNs. Quantitation revealed that both $PV^{VP\rightarrow LHb}$ and $PV^{VP\rightarrow VTA}$ neurons receive proportionally more input from D2R-expressing MSNs than D1R-expressing MSNs, with a smaller fraction of input neurons co-expressing D1R and D2R (Figures 2F and 2G).

We next sought to determine the downstream connectivity of LHb and VTA neurons receiving input from VP PV neurons. We used a multi-virus strategy by injecting AAV-DIO-Synaptophysin-eGFP into the VP of PV-Cre mice and glycoprotein-deleted rabies viruses encoding different fluorescent markers (RVΔG-tdT, RVΔG-mTagBFP2, RVΔG-iRFP670) into common output regions of the VTA and LHb (Figure S5A). This approach revealed that LHb neurons receiving inputs from VP PV neurons project to the RMTg, while VTA neurons project predominantly to the NAc lSh (Figures S5B–S5D).

Since we were limited by modest expression of RV-iRFP670 and RV-mTagBFP, we leveraged the development of rabies virus

expressing spaghetti monster fluorescent proteins (RV-smFPs), which combines the advantages of epitope tagging and traditional fluorescence to robustly label LHb and VTA outputs (Figure S5E; Viswanathan et al., 2015). Somatic and dendritic quantitation of smFP-synaptophysin^{+} synaptic contacts again revealed that VTA neurons receiving input from VP PV neurons primarily projected to NAc lSh while LHb neurons preferentially project to the RMTg (Figures S5F–S5I).

$PV^{VP \rightarrow LHb}$ Neurons Mediate Reward and Aversion

Since our tracing data suggest that $PV^{VP \rightarrow LHb}$ and $PV^{VP \rightarrow VTA}$ neurons represent discrete subpopulations, we hypothesized that they may have different roles in reward-related behaviors. To this end, we used optogenetics to test whether $PV^{VP \rightarrow LHb}$ and $PV^{VP \rightarrow VTA}$ neurons mediate reward and aversion by subjecting mice to a 3-day context dependent conditioned place preference/aversion (CPP/CPA) protocol (Figures S6A–S6C) (Lammel et al., 2012).

In line with previous studies indicating that increases in LHb activity are aversive (Shabel et al., 2012), silencing $PV^{VP \rightarrow LHb}$ glutamatergic projections induced a robust preference on day 3 of testing while stimulation of this projection induced aversion and even blocked cocaine-induced preference (Figures S6D–S6H). Surprisingly, we observed no change in preference or aversion after $PV^{VP \rightarrow VTA}$ pathway manipulation, suggesting that $PV^{VP \rightarrow LHb}$ and $PV^{VP \rightarrow VTA}$ neurons have differential effects on reward and can mediate separate behaviors.

Stress-Induced Hyperactivity of $PV^{VP \rightarrow LHb}$ Neurons

The differential effects of projection-specific manipulation observed in CPP/CPA in conjunction with our tracing data strongly suggest that these populations are separately involved in motivation-related behaviors. Since elevated activity in the LHb and VTA have been previously described in maladapted behavioral states such as depression (Cao et al., 2010; Li et al., 2011), we next reasoned that $PV^{VP \rightarrow LHb}$ and $PV^{VP \rightarrow VTA}$ may exhibit aberrant physiological adaptations in depression as well.

To mimic depression in mice, we used the chronic social defeat stress (SDS) model of depression (Figures 3A and 3B) (Golden et al., 2011). SDS reliably induces an array of depressive-like phenotypes that parallel those seen in humans. Additionally, SDS exhibits robust predictive validity; chronic but not acute antidepressant treatment reverses its behavioral effects (Berton et al., 2006, Figure 3C). After 10 days of SDS, mice can be separated into those that develop depressive-like behaviors (susceptible) and those that actively respond and cope with stress and do not display depressive-like symptoms (resilient) (Franklin et al., 2012).

To label only $PV^{VP \rightarrow LHb}$ or $PV^{VP \rightarrow VTA}$ neurons for electrophysiological recordings, we again employed the intersectional strategy using PV-Flp × Ai14 mice injected with RG-EIAV-fDIO-Cre into the LHb or VTA (Figures 3D and 3J). *Ex vivo* acute brain slices were prepared and whole-cell patch-clamp recordings were obtained from either healthy animals, or a separate cohort that was subjected to SDS and subsequently separated into resilient or susceptible animals. We also treated a cohort of susceptible animals to 2 weeks of daily antidepressant treatment (fluoxetine [FLX]; Figure 3B).

Interestingly, we observed an increase in intrinsic excitability of $PV^{VP \rightarrow LHb}$ neurons in both susceptible and resilient animals following SDS, yet animals that were previously susceptible but received chronic treatment of FLX exhibited excitability levels similar to controls (Figures 3E, 3F, and S7A). We also examined changes in synaptic inputs by measuring the ratio of evoked EPSCs and IPSCs (E/I ratio). We observed that susceptible animals had significantly greater E/I ratios compared to resilient and FLX-treated animals (Figures 3G–3I), suggesting that FLX-treated animals have an afferent profile that closely resembles resilient and healthy animals. This maintained, reduced E/I ratio observed in resilient animals may serve to counteract the increase in SDS-induced excitability.

To understand whether the increase in E/I ratio observed in susceptible animals was due to an increase in excitatory input, a reduction in inhibitory input, or both; we measured the frequency and amplitude of spontaneous IPSCs and EPSCs (sIPSCs and sEPSCs, respectively). We found a decrease in the frequency and amplitude of sIPSCs in $PV^{VP \rightarrow LHb}$ neurons in susceptible animals, yet no changes in sEPSCs. The reduction in sIPSC frequency persisted in animals treated with FLX, but the amplitude of sIPSCs returned to the level of control group (Figures S7F–S7I). Taken together, the increase in intrinsic excitability coupled with the decrease in inhibitory drive onto susceptible $PV^{VP \rightarrow LHb}$ neurons has a net increase in glutamatergic $PV^{VP \rightarrow LHb}$ activity.

It is possible that stress-induced alterations in synaptic input may cause the observed excitability changes. To isolate excitability measures from synaptic input, we measured intrinsic excitability in the presence of blockers for excitatory and inhibitory synaptic currents, 2,3-dihydroxy-6-nitro-7-sulfamoyl-benzo[f]quinoxaline-2,3-dione (NBQX) and picrotoxin (PTX), respectively. We also quantified membrane and action potential (a.p.) properties to gain an in-depth understanding of how excitability changes may arise (Figure S8A). We again find increased excitability in both resilient and susceptible animals, suggesting that changes in intrinsic excitability are not a secondary effect of synaptic alterations (Figure S8B). Furthermore, we find that the rheobase, the minimum current required to elicit an a.p., as well as the a.p. threshold and half-width, is significantly reduced in susceptible $PV^{VP \rightarrow LHb}$ neurons relative to healthy controls (Figures S8C–S8L).

Related, but Distinct, SDS-Driven Cellular Changes in $PV^{VP \rightarrow VTA}$ Neurons

We next examined whether $PV^{VP \rightarrow VTA}$ neurons also displayed SDS-driven physiological changes. In contrast to $PV^{VP \rightarrow LHb}$ neurons, $PV^{VP \rightarrow VTA}$ neurons in susceptible animals displayed no changes in intrinsic excitability compared to healthy controls. However, a significant decrease in excitability was observed in both resilient and FLX-treated groups (Figures 3K, 3L, and S8B), representing possible compensatory changes functioning to maintain low levels of activity in these cells.

Blunted excitability of $PV^{VP \rightarrow VTA}$ neurons in resilient animals was also accompanied by a significant increase in rheobase and a.p. half-width (Figures S8N and S8Q). We also observed significant stress-induced changes in membrane properties. Namely, neurons from resilient animals displayed increases in

Please cite this article in press as: Knowland et al., Distinct Ventral Pallidal Neural Populations Mediate Separate Symptoms of Depression, Cell (2017), http://dx.doi.org/10.1016/j.cell.2017.06.015

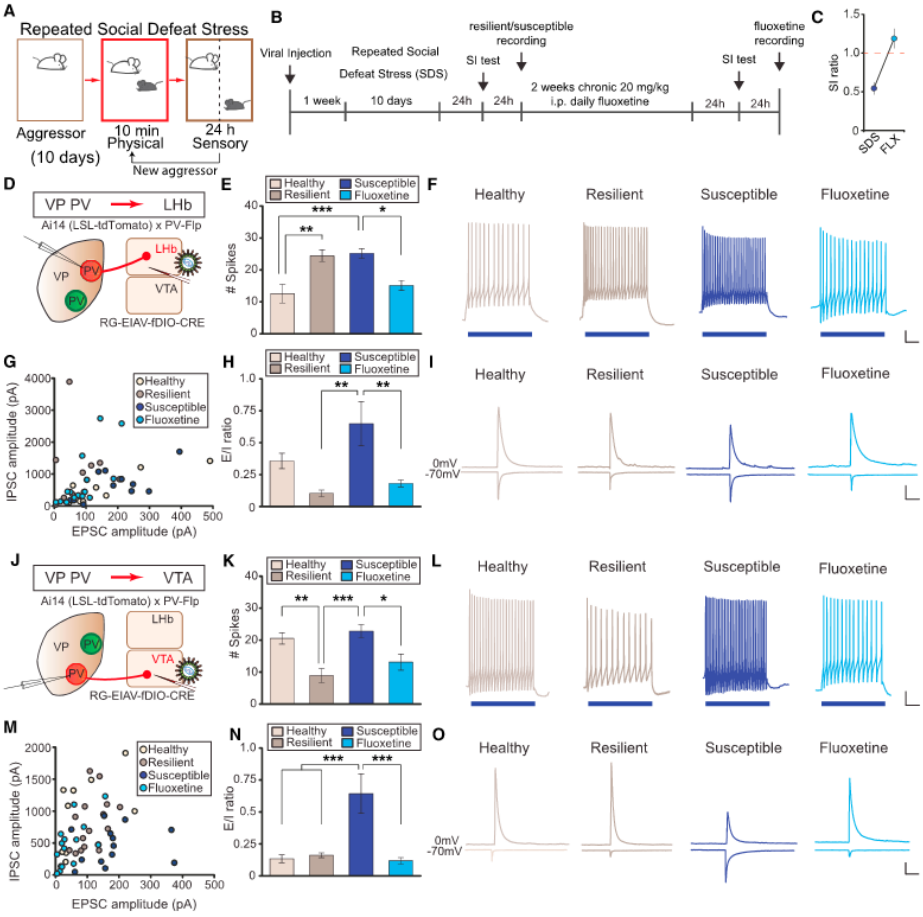

Figure 3. $PV^{VP \rightarrow LHb}$ and $PV^{VP \rightarrow VTA}$ Neurons from Susceptible Animals Exhibit Distinct Electrophysiological Adaptations to SDS and Can Be Reversed by Chronic Fluoxetine

(A and B) Behavioral paradigm (A) and experimental timeline (B) of repeated chronic social defeat stress (SDS) experiments.

(C) Chronic fluoxetine (FLX) treatment ameliorates SDS-induced social withdrawal. Red line indicates bound between susceptible (<1) and resilient animals (>1).

(D) Schematic for labeling $PV^{VP \rightarrow LHb}$ neurons in acute slices.

(E and F) Spikes elicited after 100 pA current injection in $PV^{VP \rightarrow LHb}$ neurons. One-way ANOVA $F_{3,34} = 9.088$, $p < 0.001$. Tukey post-test; ***$p < 0.001$, **$p < 0.01$, *$p < 0.05$; n = 9, 11, 10, and 8 cells from four animals each in control, resilient, susceptible, and FLX groups, respectively. Example traces are in (F); blue bars represent duration of current injection (500 ms). For full responses, see Figure S7A.

(G–I) Evoked excitatory and inhibitory inputs (E/I) onto $PV^{VP \rightarrow LHb}$ neurons in healthy and SDS groups. Absolute amplitudes (G), ratio of E/I inputs (E/I ratio; H), and example traces (I) of cells recorded. One-way ANOVA $F_{3,42} = 5.499$, $p < 0.01$; Tukey post-test: **$p < 0.01$; n = 8, 9, 13, and 16 cells from five animals each in control, resilient, susceptible, FLX groups, respectively.

(J) Schematic for labeling $PV^{VP \rightarrow VTA}$ neurons in acute slices.

(K and L) Same as in (E and F), but $PV^{VP \rightarrow VTA}$ neurons. One-way ANOVA $F_{3,36} = 8.770$, $p < 0.001$. Tukey post-test; ***$p < 0.001$, **$p < 0.01$, *$p < 0.05$; n = 12, 10, 10, and 8 cells from seven, four, four, and three animals in control, resilient, susceptible, and FLX groups, respectively. For full responses, see Figure S7B.

(legend continued on next page)

capacitance and corresponding reductions in membrane resistance (Figures S8U and S8V).

Similar to the $PV^{VP \rightarrow LHb}$ population, $PV^{VP \rightarrow VTA}$ neurons in susceptible animals displayed a significant increase in E/I ratio relative to healthy and resilient animals that was reversed by FLX treatment (Figures 3M–3O). This reversal was not due to passive recovery during the 2-week FLX treatment period post-SDS, as the E/I ratio remained elevated after chronic saline injections (Figures S7C–S7E) (Krishnan et al., 2007).

We additionally found an increase in both frequency and amplitude of sEPSCs, but not sIPSCs, in $PV^{VP \rightarrow VTA}$ neurons in susceptible groups relative to healthy controls, which was reversed by FLX (Figures S7J–S7M). The increase in excitatory synaptic input to VP PV neurons via enhanced E/I ratio and sEPSC frequency and amplitude selectively observed in susceptible animals suggests that, similar to $PV^{VP \rightarrow LHb}$ neurons, increased $PV^{VP \rightarrow VTA}$ activity is a hallmark of depressed mice. Interestingly, although both populations exhibit enhanced activity, the cellular adaptations by which this altered susceptible state is achieved are different.

Overall, we find that enhanced VP PV neuronal activity is a salient characteristic of susceptible animals, which can be normalized by an antidepressant commonly prescribed to human patients with MDD. Furthermore, animals that have undergone SDS but are resilient exhibit neither the social avoidance behavioral phenotypes nor the physiological changes seen in susceptible animals.

Silencing of VP PV Neurons Induces Resilience to SDS

Our physiological results strongly suggest that cellular hyperactivity of $PV^{VP \rightarrow VTA}$ and $PV^{VP \rightarrow LHb}$ neurons is a hallmark of animals susceptible to SDS. If heightened activity of VP PV neurons is characteristic of susceptibility to SDS, we hypothesized that reducing VP PV activity may promote resilience to SDS. To achieve this, we expressed $Kir_{2.1}$, an inward-rectifying potassium channel that reduces cellular activity by hyperpolarizing cells (Rothwell et al., 2014), in VP PV neurons and subsequently subjected mice to SDS (Figure 4A).

Silencing of VP PV neuronal activity did not induce changes in baseline measures of locomotion, anxiety, or sociability (Figures 4B–4D). Interestingly, after 10 days of SDS we observed that reduced VP PV neuronal activity significantly attenuated the acquisition of a subset of depressive-like behaviors; behavioral despair/helplessness as measured by the tail suspension test (TST) and social avoidance in social interaction test (SI) (Steru et al., 1985).

On the other hand, no difference was seen in the sucrose preference test (SPT), a measure of anhedonia (Figures 4E–4G). These differences indicate that reducing VP PV neuronal activity promotes a pro-resilient-like phenotype in a subset of depressive-like behaviors: social withdrawal and behavioral despair but not anhedonia.

Distinct VP PV Neuronal Circuitries Are Involved in Different Subsets of Depressive Behaviors

Given that increased activity of VP PV neurons is characteristic of susceptible animals and that silencing of these neurons attenuates the acquisition of behavioral despair and social withdrawal phenotypes, we hypothesized that silencing of VP PV neurons in susceptible animals would acutely reverse depressive-like behaviors.

To specifically manipulate each population in vivo, PV-Cre animals were injected with AAV-DIO-ChR2-eYFP (yellow fluorescent protein), AAV-DIO-NpHR3.0-eYFP, or AAV-DIO-eYFP into the VP and optic cannulae implanted over the LHb or VTA (Figures 5A and 5B). In SDS-naive mice, silencing or activating VP PV neuronal terminals in both LHb and VTA showed no difference in baseline social interaction compared to eYFP controls (Figures S5I and S5J). After SDS, we again observed that $PV^{VP \rightarrow LHb}$ neuronal terminal manipulation had no effect on social interaction. However, NpHR-mediated inhibition of the $PV^{VP \rightarrow VTA}$ pathway reversed social withdrawal behavior as indicated by a robust increase in social interaction (Figures 5C–5F).

Conversely, on measures of behavioral despair/helplessness in the TST we found that manipulation of $PV^{VP \rightarrow VTA}$ neuronal terminals had no effect on time spent immobile, yet manipulation of $PV^{VP \rightarrow LHb}$ neuronal terminals induced a strong bidirectional effect. Inhibition and stimulation caused significant decreases and increases, respectively, in time spent immobile compared to healthy controls (Figures 5G and 5H).

Taken together with the electrophysiological results, it is likely that NpHR-mediated silencing mitigates the elevated activity seen in susceptible $PV^{VP \rightarrow LHb}$ and $PV^{VP \rightarrow VTA}$ populations resulting in acute reversal of SDS-induced behavior.

Chemogenetic Manipulation Recapitulates Optogenetic Behavior

Recent studies have challenged the efficacy of optogenetic terminal inhibition (Mahn et al., 2016). To circumvent this potential constraint, we utilized chemogenetics by using designer receptors exclusively activated by designer drugs (DREADDS) (Armbruster et al., 2007). We expressed the G_i-coupled inhibitory DREADD (hM4Di) in $PV^{VP \rightarrow LHb}$ or $PV^{VP \rightarrow VTA}$ neurons by bilaterally injecting RG-EIAV-DIO-Flp into the LHb or VTA in PV-Cre mice and AAV-fDIO-hM4Di-mCherry or AAV-fDIO-mCherry into the VP (Figures 6A and 6B). Thus, we achieved selective inhibition of $PV^{VP \rightarrow LHb}$ or $PV^{VP \rightarrow VTA}$ neurons by injecting clozapine-N-oxide (CNO), an inert ligand specific to hM4Di receptors.

Consistent with optogenetic data, CNO-mediated inhibition of $PV^{VP \rightarrow VTA}$, but not $PV^{VP \rightarrow LHb}$, neurons increased social interaction in susceptible animals with no effects on locomotion (Figures 6C–6E; data not shown). Additionally, CNO-mediated inhibition of $PV^{VP \rightarrow LHb}$, but not $PV^{VP \rightarrow VTA}$, reduced the amount of

(M–O) $PV^{VP \rightarrow VTA}$ neurons have a significant increase in E/I ratio in susceptible animals that is normalized by FLX. Absolute amplitudes (M), E/I ratio quantitation (N), and example traces (N). One-way ANOVA $F_{3,50} = 9.585$, $p < 0.001$; n = 11, 15, 13, 15 cells from five animals each in control, resilient, susceptible, FLX groups, respectively. Tukey post-test: ***$p < 0.001$.

Scale for (F) and (L), 100 ms, 10 mV, and for (I) and (O), 200 pA, 100 ms. Data are presented as average mean ± SEM. See also Figures S6, S7, and S8.

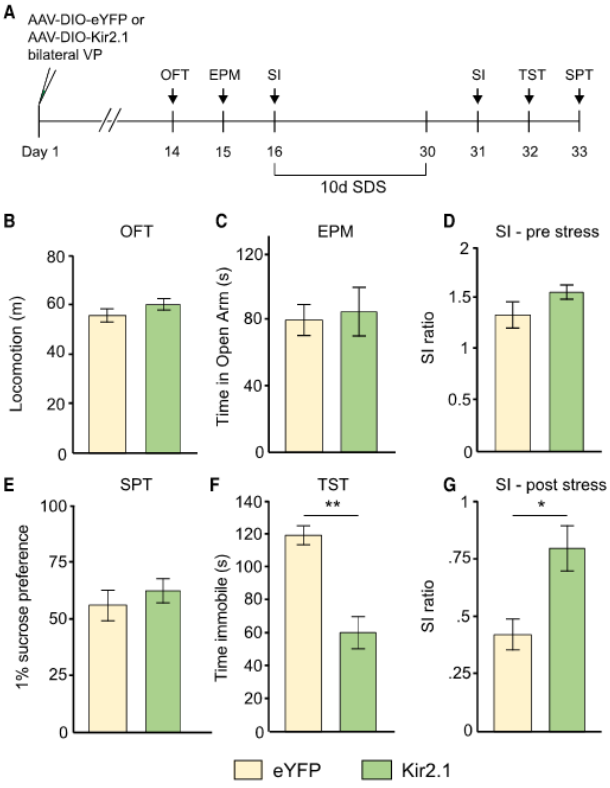

Figure 4. Silencing VP PV Activity Promotes Resilience to a Subset of Depressive-like Phenotypes

(A) Experimental timeline of $Kir_{2.1}$-mediated silencing.

(B–D) No changes in pre-stress measures of locomotion in open field test (OFT, B), anxiety on elevated plus maze (EPM, C), or social interaction (SI, D). n = 6, 11 for eYFP, $Kir_{2.1}$, respectively.

(E) No significant difference in measures of anhedonia on sucrose preference test (SPT) after SDS.

(F) $Kir_{2.1}$ animals show significantly reduced time spent immobile on measure of behavioral despair, the tail suspension test (TST) after SDS. U = 69, $p < 0.001$; n = 8, 9 for eYFP and $Kir_{2.1}$, respectively.

(G) $Kir_{2.1}$ animals display increased social interaction ratios relative to controls after SDS. U = 13, $p < 0.05$; n = 8, 8 for eYFP and $Kir_{2.1}$, respectively. All data were tested on Mann-Whitney U test and presented as mean ± SEM. $^*p < 0.05$, $^{**}p < 0.01$. See also Figure S8.

time spent immobile on the TST (Figures 6F–6H). Overall, we show that both chemogenetic and optogenetic silencing of $PV^{VP \rightarrow LHb}$ and $PV^{VP \rightarrow VTA}$ activity induces symptom-specific anti-depressive effects in susceptible mice.

$PV^{VP \rightarrow VTA}$ Stimulation Is Sufficient to Induce Social Withdrawal

If a decrease in VP PV activity can promote resilience ($Kir_{2.1}$ experiments) and both optogenetic and chemogenetic inhibition of $PV^{VP \rightarrow LHb}$ and $PV^{VP \rightarrow VTA}$ activity in susceptible mice attenuates depressive-like behaviors, we hypothesized that artificially driving $PV^{VP \rightarrow LHb}$ or $PV^{VP \rightarrow VTA}$ activity may be sufficient to recapitulate phenotypes seen in SDS-exposed animals.

To test this, we injected AAV-DIO-ChR2-eYFP into the VP and implanted optic fiber cannula over the LHb and VTA. Twice a day for 10 days, animals were subjected to 10 min light stimulation in their home cage (Figure 7A). Surprisingly, 10 days of $PV^{VP \rightarrow VTA}$ terminal stimulation without any previous exposure to aggressive CD1 mice was sufficient to induce a social avoidance phenotype similar to susceptible animals (Figure 7B). In line with our previous results demonstrating behavioral specificity, $PV^{VP \rightarrow VTA}$ stimulation did not induce an effect in the TST or SPT (Figures 7C and 7D). On the contrary, $PV^{VP \rightarrow LHb}$ terminal stimulation had no effect (Figures 7E–7G).

We then reasoned that mice may require acute subthreshold environmental exposure to CD1 aggressors as a primer in order for $PV^{VP \rightarrow LHb}$ stimulation to affect changes (Christoffel et al., 2015; Walsh et al., 2014). Again, $PV^{VP \rightarrow LHb}$ terminal stimulation in conjunction with subthreshold exposure to aggressive CD1 mice was not sufficient to induce differences in SI, SPT, or TST, suggesting that $PV^{VP \rightarrow LHb}$ terminal activation is necessary but not sufficient to elicit depressive-like behaviors (Figures 7H–7J).

DISCUSSION

Uncovering Neural Circuitries for Specific Depressive Symptoms

The DSM-V lists several core symptoms present in patients with MDD and requires that at least five be present for official diagnosis. Inherent in this diagnostic guideline is the wide patient to patient variability of behavioral symptoms, yet few studies have taken a systematic approach to understand how different circuits may underlie the behavioral heterogeneity seen in MDD.

We find that silencing distinct VP PV neuronal outputs ameliorates separate depressive-like behaviors. In particular, silencing $PV^{VP \rightarrow LHb}$ neurons attenuates helplessness on the TST, while

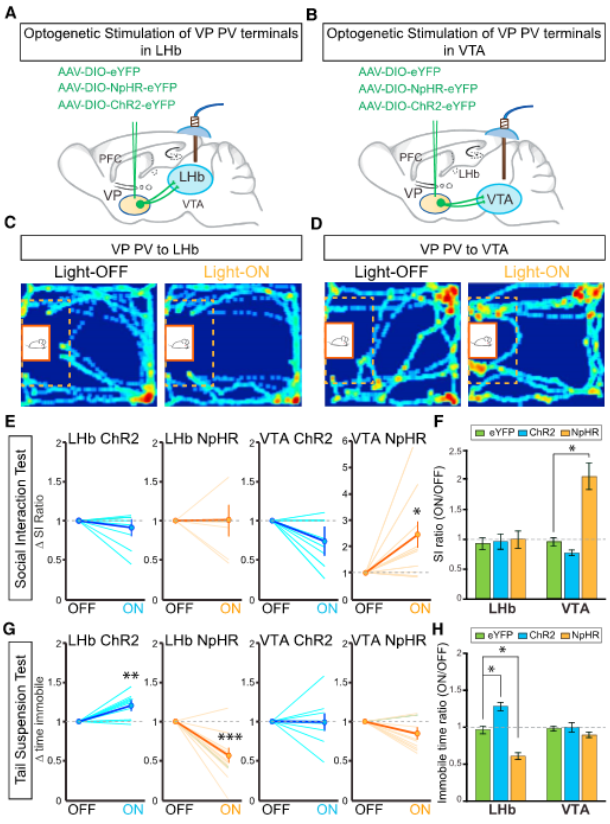

Figure 5. $PV^{VP \rightarrow LHb}$ and $PV^{VP \rightarrow VTA}$ Neurons Mediate Discrete Symptoms of Depression

(A and B) Schematic of viral injections and optic fiber implantations in LHb (A) or VTA (B) for optogenetic manipulation in stressed animals.

(C and D) Representative traces of animals expressing NpHR in VP PV neurons in social interaction (SI) test in susceptible animals during light stimulation of LHb (C) or VTA (D) terminals: off (left panels) and light on (589 nm; right panels). Red rectangle indicates cage in which aggressive CD1 animal was placed, yellow dashed lines outline the "interaction zone." Warmer colors indicate increased time spent.

(E and F) Silencing terminals of VP PV neurons in VTA, but not in LHb, alleviates social withdrawal symptoms in SI test. SI ratio = time interaction zone light ON/light OFF. Dashed line indicates no change. Each line in (E) represents single animal; bolded line indicates average ± SEM. Mann-Whitney U test U = 80, $p < 0.05$. (F) shows population means of data in (E). VTA SI: one-way ANOVA $F_{2,21} = 6.132$, $p < 0.01$. Tukey post-test: *$p < 0.05$; n = 5, 9, and 10 and n = 6, 7, and 9 animals for eYFP, ChR2, NpHR groups in VTA and LHb conditions, respectively.

(G and H) Modulation of VP PV neuronal terminals in LHb, but not in VTA, induces bidirectional effects on the tail suspension test (TST). For (G), LHb-ChR2: Mann-Whitney U test U = 56, **$p < 0.01$; LHb-NpHR U = 15, ***$p < 0.001$. For (H), LHb TST: one-way ANOVA $F_{2,25} = 24.49$ $p < 0.001$. Tukey post-test: *$p < 0.05$; n = 5, 8, 11 and 6, 8, 14 for eYFP, ChR2, and NpHR in VTA and LHb groups, respectively. All data are reported as mean ± SEM.

reduction of $PV^{VP \rightarrow VTA}$ neuronal activity increases social interaction in animals susceptible to SDS. Furthermore, chronically reducing VP PV neuronal activity before animals undergo SDS promotes a pro-resilient phenotype in a subset of depressive-like behaviors: social withdrawal and behavioral despair/helplessness but not anhedonia.

In addition to increased activity of VP PV neurons being necessary for the development and expression of SDS-induced helplessness and social withdrawal behaviors, we also show that prolonged artificial stimulation of $PV^{VP \rightarrow VTA}$ neuronal terminals in VTA is sufficient to induce social withdrawal but not behavioral despair phenotypes (Figure 7). Surprisingly, this suggests that the $PV^{VP \rightarrow VTA}$ circuit specifically encodes social withdrawal phenotypes independent of environmental primers such as acute subthreshold exposure to aggressive CD1 mice.

On the other hand, artificially driving $PV^{VP \rightarrow LHb}$ terminal activity in an animal's home cage or during subthreshold SDS is insufficient to induce any behavioral abnormalities, suggesting that this circuit may either not be sufficient to induce depressive behaviors or that it partakes in different forms of neural adaptations that may require more long-term exposure to adverse environmental stimuli.

Enhanced $PV^{VP \rightarrow LHb}$ and $PV^{VP \rightarrow VTA}$ Activity Defines Susceptibility to SDS

Previous studies report increased cellular activity in the LHb and dopaminergic neurons in the VTA in animal models of depression (Chaudhury et al., 2013; Li et al., 2011).

Using ex vivo whole-cell patch-clamp electrophysiology, we find that susceptible, but not resilient, animals are characterized by increased activity in both $PV^{VP \rightarrow LHb}$ and $PV^{VP \rightarrow VTA}$ populations via altered synaptic input, but by different mechanisms. Increased activity of $PV^{VP \rightarrow LHb}$ and $PV^{VP \rightarrow VTA}$ neurons observed in susceptible animals would thus have a net effect of enhanced postsynaptic activity in the LHb and VTA, in line with previous reports. It may be the case that aberrant ventral pallidal activity is

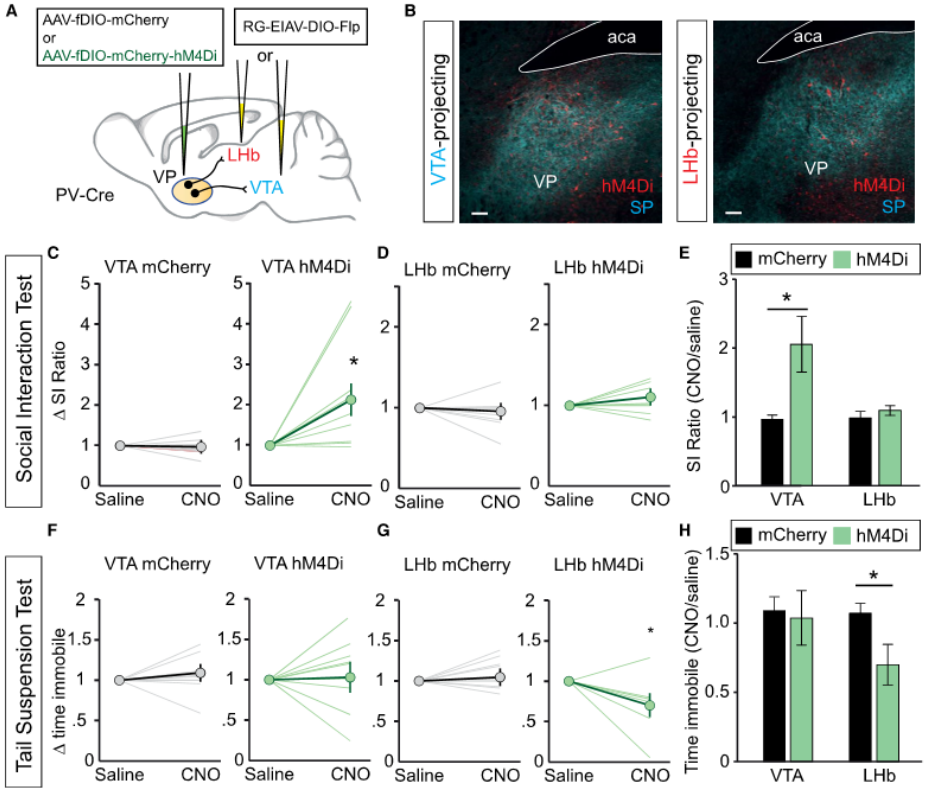

Figure 6. Cell-Type- and Projection-Specific Inhibitory DREADDs Recapitulate Optogenetic Behavior

(A) Experimental setup for expression of inhibitory DREADD (hM4Di) or control virus (mCherry) in $PV^{VP \rightarrow LHb}$ or $PV^{VP \rightarrow VTA}$ neurons.

(B) Representative images of injection site. hM4Di expression is in red, and Substance P (SP) is in blue to delineate VP.

(C) Inhibition of $PV^{VP \rightarrow VTA}$ neurons expressing hM4Di by CNO injection promotes increased social interaction in susceptible animals. Mann-Whitney U test U = 6, *p < 0.05. Individual lines represent individual animals. n = 8, 9 for mCherry, hM4Di, respectively.

(D) Inhibition of $PV^{VP \rightarrow LHb}$ neurons expressing hM4Di by CNO injection has no effect on social interaction in susceptible animals.

(E) Changes in SI ratio in response to i.p. CNO injection. Mann-Whitney U test U = 5, *p < 0.05.

(F) No effect of CNO injection in animals expressing hM4Di in $PV^{VP \rightarrow VTA}$ neurons on behavioral helplessness as measured by change in time immobile with respect to saline injections.

(G) The inhibition of $PV^{VP \rightarrow LHb}$ neurons expressing hM4Di by CNO injection reduces time spent immobile relative to saline injections in susceptible animals. Mann-Whitney U test U = 40, *p < 0.05. n = 8, 7 for mCherry, hM4Di, respectively.

(H) hM4Di expression in $PV^{VP \rightarrow LHb}$, but not $PV^{VP \rightarrow VTA}$, neurons, reduces time spent immobile in response to CNO injection. Mann-Whitney U test U = 42, *p < 0.05. n = 8, 7 for mCherry, hM4Di, respectively.

All data are presented as mean + SEM.

upstream of the stress-induced increases in firing previously observed in the LHb and VTA.

The different synaptic adaptations between $PV^{VP \rightarrow LHb}$ and $PV^{VP \rightarrow VTA}$ populations may in part be explained by the distinct input patterns observed on to each population (Figure 2).

Our mapping study of the input-output relationship of VP PV neurons demonstrates that $PV^{VP \rightarrow VTA}$ and $PV^{VP \rightarrow LHb}$ neurons

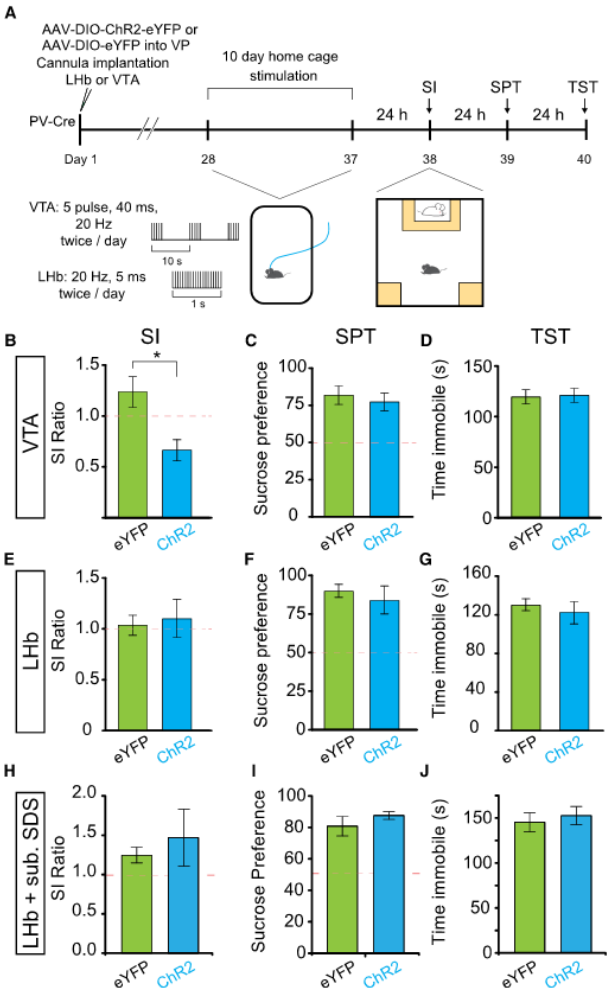

Figure 7. Repeated, Chronic Stimulation of $PV^{VP \rightarrow VTA}$ Terminals Is Sufficient to Induce Social Interaction Deficits

(A) Experimental timeline for (B)–(G).

(B–D) Repeated stimulation of VP PV terminals in VTA is sufficient to induce social avoidance (B) but has no effect on SPT (C) or TST (D). Mann-Whitney test; U = 162, *p < 0.05; n = 15, 14 for eGFP and ChR2 groups, respectively for SI and TST test, n = 7 for SPT).

(E–G) No effect of repeated stimulation of VP PV terminals in LHb in SI (E), SPT (F), or TST (G); n = 5 each condition.

(H–J) No change in depressive-like phenotypes in SI (H), SPT (I), or TST (J) after subthreshold defeat stress with VP PV terminal stimulation in LHb (n = 5 each). All data were tested on Mann-Whitney U test and presented as mean ± SEM. Red dashed lines indicate levels separating resilient and susceptible animals (SI ratio of 1 and 50% sucrose preference for SI, SPT, respectively).

receive excitatory or inhibitory inputs from distinct brain areas. Thus, it is possible that projections from different areas preferentially targeting specific VP PV neuronal populations, such as the CeA, which preferentially targets $PV^{VP \rightarrow VTA}$, may induce selective synaptic changes of individual populations in susceptible animals, which in turn elicits specific depressive behaviors. Future studies will need to parse the contributions of area-specific synaptic inputs onto VP PV neurons to understand which precise upstream pathways drive SDS-induced changes within the VP.

We also show that chronic FLX, an FDA-approved antidepressant prescribed in humans, reverses the SDS-induced cellular adaptations in $PV^{VP \rightarrow LHb}$ and $PV^{VP \rightarrow VTA}$ neurons to healthy levels by modulating intrinsic properties and synaptic balance (Figure 3).

However, it is important to emphasize that, while chronic FLX treatment induces changes in VP PV neurons, it remains unclear whether this is a direct effect or whether FLX engages a larger circuit of which VP PV neurons are a part of. Many studies have underscored serotonergic neurons in the dorsal raphe nucleus (DRN) as a critical mediator of FLX actions (Adachi et al., 2017; Neumaier et al., 1996). Our tracing data reveal that VP PV neurons receive input from the DRN (Figure 2), which could alternatively explain how FLX treatment affects VP PV activity rather than direct effects on VP PV neurons themselves. Further studies are required to parse this possibility, yet for now it is sufficient to say that VP PV neuronal activity is modulated—directly or indirectly—by chronic FLX treatment and correlates with the presentation of SDS-induced depressive-like symptoms.

Engagement of Distinct Downstream Midbrain Circuitry

How might different components of a related circuit mediate separate behaviors? One manner in which this may be possible

is the engagement of separate downstream midbrain circuitries by $PV^{VP \rightarrow LHb}$ and $PV^{VP \rightarrow VTA}$ neurons. We show that $PV^{VP \rightarrow LHb}$ neurons preferentially synapse onto LHb neurons projecting to the RMTg and cortex-projecting medial VTA neurons (Figure S5D; Lammel et al., 2012). Both the LHb→RMTg→VTA and LHb→medial VTA→cortex connections have been reported to encode aversive signals (Lammel et al., 2012), consistent with our results showing that the activation of glutamatergic $PV^{VP \rightarrow LHb}$ fibers induces aversion (Figures S6A–S6H).

It also follows that increased activity of $PV^{VP \rightarrow LHb}$ neurons in susceptible animals would increase LHb excitatory inputs to the cortex-projecting medial VTA neurons and to RMTg neurons, which are mainly GABAergic, that have been reported to inhibit VTA DA neurons (Beier et al., 2015; Lammel et al., 2012). Consequently, it may be the combined downstream effect of increased medial cortex-projecting VTA DA neuronal activity (via excitatory LHb projections) with decreased other VTA DA neuronal activity (via inhibitory RMTg projections) that engages changes in helplessness/behavioral despair in susceptible animals.

$PV^{VP \rightarrow VTA}$ neurons preferentially project to the lateral portion of the VTA which contains largely non-overlapping populations of GABAergic and DAergic neurons. Previous studies indicate that lateral VTA neurons preferentially project to the lateral shell of the NAc, a finding supported by our own tracing data (Lammel et al., 2008; Figure S5). VP PV neurons synapse on both cell types, yet to separate degrees and strength. VP PV neurons send strong inhibitory projections to GABA neurons, while DA neurons receive mixed, but stronger excitatory projections.

It follows then that increased $PV^{VP \rightarrow VTA}$ neuronal activity seen in susceptible animals would drive a reduction in GABA VTA activity and net increase in monosynaptic DA VTA activity. Previous studies have shown that GABA VTA neurons send local inhibitory projections to DA neurons (van Zessen et al., 2012). Thus, in addition to direct DA excitation, the net reduction in GABAergic VTA activity would relieve its inhibition onto DAergic neurons and further drive increased VTA DA activity—a hallmark previously described in susceptible animals (Cao et al., 2010; Chaudhury et al., 2013).

Together, we see that the same manipulation at VP PV neuronal projections in different target structures may have distinct changes in neuronal activity within different populations of VTA neurons. Ultimately, the separate effects on specific downstream midbrain areas and different combinations of activity across regions may account for the discrete effects of $PV^{VP \rightarrow LHb}$ and $PV^{VP \rightarrow VTA}$ pathway in different depressive behaviors.

Of note, we surprisingly find no effect on social interaction silencing the $PV^{VP \rightarrow VTA}$ pathway in healthy animals, yet after stress the same manipulation induces a robust attenuation of social withdrawal. This suggests that the synaptic connection between VP PV neurons and VTA neurons is weak in non-stressed animals but may get selectively stronger in susceptible animals, which is required to induce behavioral effects on social interaction. One possible explanation for the post-stress synaptic enhancement of this pathway is increased activity of $PV^{VP \rightarrow VTA}$ neurons. In line with this reasoning, we show that $PV^{VP \rightarrow VTA}$ neurons receive increased excitatory synaptic input in susceptible, but not resilient, mice that persists up to 2 weeks after SDS (Figures 3J–3O). In effect, it is this increase in activity of $PV^{VP \rightarrow VTA}$ neurons that is required for the expression of social avoidance behaviors and explains why we see only effects of silencing $PV^{VP \rightarrow VTA}$ neurons in susceptible, but not healthy, animals. This also explains why silencing VP PV neuronal activity before SDS with $Kir_{2.1}$ would reduce the development of social withdrawal symptoms in response to stress, and why reduction of $PV^{VP \rightarrow VTA}$ neuronal activity with FLX ameliorates social avoidance in susceptible animals as well.

However, since $PV^{VP \rightarrow VTA}$ neurons synapse onto two distinct cell types, there may be either: (1) a selective enhancement of one pathway over the other (GABA versus DA), or (2) an altered balance of synaptic drive onto DA neurons, in particular, an increase in excitatory drive. Future interrogation into the downstream circuitries and midbrain cell types engaged by VP PV neurons and their neural adaptations in response to SDS will be required.

In sum, we delineate and describe two distinct PV-positive VP circuits that underlie separate depressive-like behaviors. We believe these results highlight the need for more circuit-based studies in neuropsychiatric disorders to parse the neural underpinnings of distinct behavioral symptoms in patients to move toward symptom-based treatments in the future.

STAR★METHODS

Detailed methods are provided in the online version of this paper and include the following:

- KEY RESOURCES TABLE
- CONTACT FOR REAGENT AND RESOURCE SHARING
- EXPERIMENTAL MODEL AND SUBJECT DETAILS
  - Mice
- METHOD DETAILS
  - Virus generation
  - Stereotaxic injections and optic fiber/cannula implantations
  - *Ex vivo* electrophysiology
  - Immunohistochemistry
  - Circuit mapping quantitation
  - FISH assay
  - Behavioral Assays
- QUANTIFICATION AND STASTISTICAL ANALYSIS

SUPPLEMENTAL INFORMATION

Supplemental Information includes eight figures and can be found with this article online at http://dx.doi.org/10.1016/j.cell.2017.06.015.

AUTHOR CONTRIBUTIONS

Conceptualization, D.K. and B.K.L.; Investigation, D.K., V.L., and C.P.P.; Resources, V.L. and S.S.; Software, E.H.-J.W.; Writing – Original Draft, D.K.; Writing – Review & Editing, D.K., V.L., E.H.-J.W., and B.K.L.; Funding Acquisition, B.K.L.; Supervision, B.K.L.

ACKNOWLEDGMENTS

We thank X. Wang for technical assistance and H. Pribiag and the Lim laboratory for comments on manuscript. This work was supported by the Klingenstein foundation, Searle scholar program (Kinship foundation; Searle

15-SSP-229), the Whitehall foundation (2014-08-63), NARSAD young investigator grant (24094), and grants from NIH (MH107742 and MH108594). V.L. is also supported by Anandamahidol Foundation Fellowship.

Received: January 3, 2017
Revised: April 28, 2017
Accepted: June 8, 2017
Published: July 6, 2017

REFERENCES

Adachi, M., Autry, A.E., Mahgoub, M., Suzuki, K., and Monteggia, L.M. (2017). TrkB signaling in dorsal raphe nucleus is essential for antidepressant efficacy and normal aggression behavior. Neuropsychopharmacology *42*, 886–894.

Armbruster, B.N., Li, X., Pausch, M.H., Herlitze, S., and Roth, B.L. (2007). Evolving the lock to fit the key to create a family of G protein-coupled receptors potently activated by an inert ligand. Proc. Natl. Acad. Sci. USA *104*, 5163–5168.

Bagot, R.C., Parise, E.M., Peña, C.J., Zhang, H.-X., Maze, I., Chaudhury, D., Persaud, B., Cachope, R., Bolaños-Guzmán, C.A., Cheer, J.F., et al. (2015). Ventral hippocampal afferents to the nucleus accumbens regulate susceptibility to depression. Nat. Commun. *6*, 7062.

Beier, K.T., Steinberg, E.E., DeLoach, K.E., Xie, S., Miyamichi, K., Schwarz, L., Gao, X.J., Kremer, E.J., Malenka, R.C., and Luo, L. (2015). Circuit architecture of VTA dopamine neurons revealed by systematic input-output mapping. Cell *162*, 622–634.

Berton, O., McClung, C.A., Dileone, R.J., Krishnan, V., Renthal, W., Russo, S.J., Graham, D., Tsankova, N.M., Bolanos, C.A., Rios, M., et al. (2006). Essential role of BDNF in the mesolimbic dopamine pathway in social defeat stress. Science *311*, 864–868.

Brauer, K., Härtig, W., Bigl, V., and Brückner, G. (1993). Distribution of parvalbumin-containing neurons and lectin-binding perineuronal nets in the rat basal forebrain. Brain Res. *631*, 167–170.

Cao, J.-L., Covington, H.E., 3rd, Friedman, A.K., Wilkinson, M.B., Walsh, J.J., Cooper, D.C., Nestler, E.J., and Han, M.-H. (2010). Mesolimbic dopamine neurons in the brain reward circuit mediate susceptibility to social defeat and antidepressant action. J. Neurosci. *30*, 16453–16458.

Cetin, A., and Callaway, E.M. (2014). Optical control of retrogradely infected neurons using drug-regulated "TLoop" lentiviral vectors. J. Neurophysiol. *111*, 2150–2159.

Chaudhury, D., Walsh, J.J., Friedman, A.K., Juarez, B., Ku, S.M., Koo, J.W., Ferguson, D., Tsai, H.-C., Pomeranz, L., Christoffel, D.J., et al. (2013). Rapid regulation of depression-related behaviours by control of midbrain dopamine neurons. Nature *493*, 532–536.

Christoffel, D.J., Golden, S.A., Walsh, J.J., Guise, K.G., Heshmati, M., Friedman, A.K., Dey, A., Smith, M., Rebusi, N., Pfau, M., et al. (2015). Excitatory transmission at thalamo-striatal synapses mediates susceptibility to social stress. Nat. Neurosci. *18*, 962–964.

Creed, M., Ntamati, N.R., Chandra, R., Lobo, M.K., and Lüscher, C. (2016). Convergence of reinforcing and anhedonic cocaine effects in the ventral pallidum. Neuron *92*, 214–226.

Donato, F., Rompani, S.B., and Caroni, P. (2013). Parvalbumin-expressing basket-cell network plasticity induced by experience regulates adult learning. Nature *504*, 272–276.

Franklin, T.B., Saab, B.J., and Mansuy, I.M. (2012). Neural mechanisms of stress resilience and vulnerability. Neuron *75*, 747–761.

Friedman, A.K., Walsh, J.J., Juarez, B., Ku, S.M., Chaudhury, D., Wang, J., Li, X., Dietz, D.M., Pan, N., Vialou, V.F., et al. (2014). Enhancing depression mechanisms in midbrain dopamine neurons achieves homeostatic resilience. Science *344*, 313–319.

Gaykema, R.P.A., and Zaborszky, L. (1997). Parvalbumin-containing neurons in the basal forebrain receive direct input from the substantia nigra-ventral tegmental area. Brain Res. *747*, 173–179.

Golden, S.A., Covington, H.E., 3rd, Berton, O., and Russo, S.J. (2011). A standardized protocol for repeated social defeat stress in mice. Nat. Protoc. *6*, 1183–1191.

Haber, S.N., Groenewegen, H.J., Grove, E.A., and Nauta, W.J. (1985). Efferent connections of the ventral pallidum: Evidence of a dual striato pallidofugal pathway. J. Comp. Neurol. *235*, 322–335.

Haubensak, W., Kunwar, P.S., Cai, H., Ciocchi, S., Wall, N.R., Ponnusamy, R., Biag, J., Dong, H.-W., Deisseroth, K., Callaway, E.M., et al. (2010). Genetic dissection of an amygdala microcircuit that gates conditioned fear. Nature *468*, 270–276.

Heimer, L., Switzer, R.D., and Van Hoesen, G.W. (1982). Ventral striatum and ventral pallidum. Components of the motor system? Trends Neurosci. *5*, 83–87.

Kato, S., Kobayashi, K., Inoue, K., Kuramochi, M., Okada, T., Yaginuma, H., Morimoto, K., Shimada, T., Takada, M., and Kobayashi, K. (2011). A lentiviral strategy for highly efficient retrograde gene transfer by pseudotyping with fusion envelope glycoprotein. Hum. Gene Ther. *22*, 197–206.

Kim, E.J., Jacobs, M.W., Ito-Cole, T., and Callaway, E.M. (2016). Improved monosynaptic neural circuit tracing using engineered rabies virus glycoproteins. Cell Rep. *15*, 692–699.

Krishnan, V., Han, M.H., Graham, D.L., Berton, O., Renthal, W., Russo, S.J., Laplant, Q., Graham, A., Lutter, M., Lagace, D.C., et al. (2007). Molecular adaptations underlying susceptibility and resistance to social defeat in brain reward regions. Cell *131*, 391–404.

Kuo, H., and Chang, H.T. (1992). Ventral pallido-striatal pathway in the rat brain: A light and electron microscopic study. J. Comp. Neurol. *321*, 626–636.

Kupchik, Y.M., Brown, R.M., Heinsbroek, J.A., Lobo, M.K., Schwartz, D.J., and Kalivas, P.W. (2015). Coding the direct/indirect pathways by D1 and D2 receptors is not valid for accumbens projections. Nat. Neurosci. *18*, 1230–1232.

Lammel, S., Hetzel, A., Häckel, O., Jones, I., Liss, B., and Roeper, J. (2008). Unique properties of mesoprefrontal neurons within a dual mesocorticolimbic dopamine system. Neuron *57*, 760–773.

Lammel, S., Lim, B.K., Ran, C., Huang, K.W., Betley, M.J., Tye, K.M., Deisseroth, K., and Malenka, R.C. (2012). Input-specific control of reward and aversion in the ventral tegmental area. Nature *491*, 212–217.

Li, B., Piriz, J., Mirrione, M., Chung, C., Proulx, C.D., Schulz, D., Henn, F., and Malinow, R. (2011). Synaptic potentiation onto habenula neurons in the learned helplessness model of depression. Nature *470*, 535–539.

Lim, B.K., Huang, K.W., Grueter, B.A., Rothwell, P.E., and Malenka, R.C. (2012). Anhedonia requires MC4R-mediated synaptic adaptations in nucleus accumbens. Nature *487*, 183–189.

Mahn, M., Prigge, M., Ron, S., Levy, R., and Yizhar, O. (2016). Biophysical constraints of optogenetic inhibition at presynaptic terminals. Nat. Neurosci. *19*, 554–556.

Murrough, J.W., Henry, S., Hu, J., Gallezot, J.D., Planeta-Wilson, B., Neumaier, J.F., and Neumeister, A. (2011). Reduced ventral striatal/ventral pallidal serotonin1B receptor binding potential in major depressive disorder. Psychopharmacology (Berl.) *213*, 547–553.

Neumaier, J.F., Root, D.C., and Hamblin, M.W. (1996). Chronic fluoxetine reduces serotonin transporter mRNA and 5-HT1B mRNA in a sequential manner in the rat dorsal raphe nucleus. Neuropsychopharmacology *15*, 515–522.

Osakada, F., and Callaway, E.M. (2013). Design and generation of recombinant rabies virus vectors. Nat Protoc. *8*, 1583–1601.

Pascoli, V., Terrier, J., Hiver, A., and Lüscher, C. (2015). Sufficiency of mesolimbic dopamine neuron stimulation for the progression to addiction. Neuron *88*, 1054–1066.

Proulx, C.D., Hikosaka, O., and Malinow, R. (2014). Reward processing by the lateral habenula in normal and depressive behaviors. Nat. Neurosci. *17*, 1146–1152.

Root, D.H., Melendez, R.I., Zaborszky, L., and Napier, T.C. (2015). The ventral pallidum: Subregion-specific functional anatomy and roles in motivated behaviors. Prog. Neurobiol. *130*, 29–70.

Rothwell, P.E., Fuccillo, M.V., Maxeiner, S., Hayton, S.J., Gokce, O., Lim, B.K., Fowler, S.C., Malenka, R.C., and Südhof, T.C. (2014). Autism-associated neuroligin-3 mutations commonly impair striatal circuits to boost repetitive behaviors. Cell *158*, 198–212.

Russo, S.J., and Nestler, E.J. (2013). The brain reward circuitry in mood disorders. Nat. Rev. Neurosci. *14*, 609–625.

Schwarz, L.A., Miyamichi, K., Gao, X.J., Beier, K.T., Weissbourd, B., DeLoach, K.E., Ren, J., Ibanes, S., Malenka, R.C., Kremer, E.J., and Luo, L. (2015). Viral-genetic tracing of the input-output organization of a central noradrenaline circuit. Nature *524*, 88–92.

Shabel, S.J., Proulx, C.D., Trias, A., Murphy, R.T., and Malinow, R. (2012). Input to the lateral habenula from the basal ganglia is excitatory, aversive, and suppressed by serotonin. Neuron *74*, 475–481.

Smith, K.S., Tindell, A.J., Aldridge, J.W., and Berridge, K.C. (2009). Ventral pallidum roles in reward and motivation. Behav. Brain Res. *196*, 155–167.

Steru, L., Chermat, R., Thierry, B., and Simon, P. (1985). The tail suspension test: A new method for screening antidepressants in mice. Psychopharmacology (Berl.) *85*, 367–370.

Tan, K.R., Yvon, C., Turiault, M., Mirzabekov, J.J., Doehner, J., Labouèbe, G., Deisseroth, K., Tye, K.M., and Lüscher, C. (2012). GABA neurons of the VTA drive conditioned place aversion. Neuron *73*, 1173–1183.

van Zessen, R., Phillips, J.L., Budygin, E.A., and Stuber, G.D. (2012). Activation of VTA GABA neurons disrupts reward consumption. Neuron *73*, 1184–1194.

Viswanathan, S., Williams, M.E., Bloss, E.B., Stasevich, T.J., Speer, C.M., Nern, A., Pfeiffer, B.D., Hooks, B.M., Li, W.-P., English, B.P., et al. (2015). High-performance probes for light and electron microscopy. Nat. Methods *12*, 568–576.

Walsh, J.J., Friedman, A.K., Sun, H., Heller, E.A., Ku, S.M., Juarez, B., Burnham, V.L., Mazei-Robison, M.S., Ferguson, D., Golden, S.A., et al. (2014). Stress and CRF gate neural activation of BDNF in the mesolimbic reward pathway. Nat. Neurosci. *17*, 27–29.

Wickersham, I.R., Lyon, D.C., Barnard, R.J.O., Mori, T., Finke, S., Conzelmann, K.-K., Young, J.A., and Callaway, E.M. (2007). Monosynaptic restriction of transsynaptic tracing from single, genetically targeted neurons. Neuron *53*, 639–647.

Yamanaka, H., Yokoyama, C., Mizuma, H., Kurai, S., Finnema, S.J., Halldin, C., Doi, H., and Onoe, H. (2014). A possible mechanism of the nucleus accumbens and ventral pallidum 5-HT1B receptors underlying the antidepressant action of ketamine: A PET study with macaques. Transl. Psychiatry *4*, e342.

Zahm, D.S., Williams, E., and Wohltmann, C. (1996). Ventral striatopallidothalamic projection: IV. Relative involvements of neurochemically distinct subterritories in the ventral pallidum and adjacent parts of the rostroventral forebrain. J. Comp. Neurol. *364*, 340–362.

STAR★METHODS

KEY RESOURCES TABLE

REAGENT or RESOURCE	SOURCE	IDENTIFIER
Antibodies		
Rabbit anti-Tyrosine Hydroxylase (1:1000)	Millipore	Ab152; RRID: AB_390204
Guinea pig anti-VGluT1 (1:500)	Millipore	Ab5905; RRID: AB_2301751
Guinea pig anti-VGluT2 (1:1000)	Millipore	Ab2251; RRID: AB_1587626
Rabbit anti-NeuN (1:2000)	Abcam	Ab177487; RRID: AB_2532109
Mouse anti-GAD65 (1:500)	DSHB at U of Iowa	AB_528264; RRID: AB_528264
Mouse anti-PV (1:500)	Sigma	Cat#P3088
Guinea pig anti-Substance P (1:500)	Abcam	Ab10353; RRID: AB_297089
Rabbit anti-dsred (1:500)	Clontech	Cat#632496
Rabbit anti-FLAG (1:1000)	Sigma	Cat#F7425
Goat anti-myc (1:1000)	Abcam	Ab9132; RRID: AB_307033
Mouse anti-V5 (1:1000)	Life Technologies	Cat#R960-25
Rat anti-HA (1:1000)	Roche	Cat#11 867 423 001
Donkey anti-rabbit Alexa Fluor 647	Life Technologies	A31573
Donkey anti-goat Alexa Fluor 488	Life Technologies	A11055
Donkey anti-mouse Alexa Fluor 405	Abcam	Ab175658
Donkey anti-rat Alexa Fluor 568	Life Technologies	A21209
Bacterial and Virus Strains		
EnvA-pseudotyped *g*-deleted rabies virus; EnvA-RVΔG-eGFP	Lim Lab	N/A
g-deleted rabies virus; RVΔG-GFP	Lim Lab	N/A
g-deleted rabies virus; RVΔG-tdTomato	Lim Lab	N/A
g-deleted rabies virus; RVΔG-mTagBFP2	This paper	N/A
g-deleted rabies virus; RVΔG-iRFP670	This paper	N/A
g-deleted rabies virus; RVΔG-smFP-HA	This paper	N/A
g-deleted rabies virus; RVΔG-smFP-Myc	This paper	N/A
g-deleted rabies virus; RVΔG-smFP-FLAG	This paper	N/A
g-deleted rabies virus; RVΔG-smFP-V5	This paper	N/A
Pseudotyped equine infectious anemia virus; RG-EIAV-CAG-DIO-Flp	This paper	N/A
Pseudotyped equine infectious anemia virus; RG-EIAV-CAG-fDIO-Cre	This paper	N/A
Chemicals, Peptides, and Recombinant Proteins		
CTb, AlexaFluor 488 conjugate	Thermo Fisher	Cat#C22841
CTb, AlexaFluor 647 conjugate	Thermo Fisher	Cat#C34778
Clozapine N-oxide	Enzo Life Sciences	MBL-NS105-0025
Fluoxetine hydrochloride	Spectrum Chemical	Cat#F1200
NBQX	Tocris	Cat#0373
QX314 chloride	Tocris	Cat#2313
Picrotoxin	Sigma	Cat#P1675
Cocaine hydrochloride	Sigma	Cat#C5776
Critical Commercial Assays – probes for RNAscope		
PV	ACD	421931
tdTomato	ACD	317041
Preproenkephalin (PENK)	ACD	318761
Somatostatin (SST)	ACD	404631
Corticotropin-releasing hormone (CRH)	ACD	316091

(*Continued on next page*)

Continued

REAGENT or RESOURCE	SOURCE	IDENTIFIER
Prkcd (PKC delta)	ACD	441791
Drd1a	ACD	406491
Drd2	ACD	406501
Slc32a1 (VGAT)	ACD	319191
Slc17a6 (VGlut2)	ACD	319171
EGFP	ACD	400281
Experimental Models: Organisms/Strains		
Mouse: PV-Cre: B6.Cg-Pvalb$^{tm1.1(cre)Aibs}$/J	The Jackson Laboratory	012358
Mouse: PV-Flp: B6.Cg-Pvalb$^{tm4.1(flpo)Hze}$/J	The Jackson Laboratory	022730
Mouse: CD-1, retired breeders	Charles River	022
Mouse: Ai14: B6;129S6-Gt(ROSA)26Sor$^{tm14(CAG-tdTomato)Hze}$/J	The Jackson Laboratory	007914
Mouse: VGlut2-Cre: Slc17a6$^{tm2(cre)Lowl}$/J	The Jackson Laboratory	016963
Mouse: DAT-Cre: B6.SJL-Slc6a3$^{tm1.1(cre)Bkmn}$/J	The Jackson Laboratory	006660
Mouse: TH-GFP	Dr. Davide Dulcis (UCSD)	N/A
Mouse: GAD67-GFP	Dr. Yuchio Yanagawa	N/A
Recombinant DNA		
AAV_{DJ}-hSyn-DIO-mRuby2-P2A-Synaptophysin-eGFP	This paper	N/A
AAV_{DJ}-EF1α-DIO-Synaptophysin-eGFP	This paper	N/A
AAV_{DJ}-EF1α-DIO-Synaptophysin-smFP-FLAG	This paper	N/A
AAV_{DJ}-EF1α-fDIO-eGFP	This paper	N/A
AAV_{DJ}-EF1α-fDIO-tdTomato	This paper	N/A
AAV_{DJ}-EF1α-fDIO-oPBG	This paper	N/A
AAV_{DJ}-EF1α-DIO-$Kir_{2.1}$-T2A-ZsGreen	Lim et al., 2012	N/A
AAV_{DJ}-hSyn-fDIO-hM4D(Gi)-mCherry	This paper	N/A
AAV_{DJ}-EF1α-DIO-hChR2(H134R)-eYFP	Plasmid: Karl Deisseroth Production: Lim Lab	Addgene #55639
AAV_{DJ}-EF1α-DIO-eNpHR3.0-eYFP	Plasmid: Karl Deisseroth Production: Lim Lab	N/A
Software and Algorithms		
Origin Lab	Origin Lab	http://www.originlab.com/index.aspx?go=Products/Origin/Statistics
Illustrator CS6	Adobe	http://www.adobe.com/products/illustrator.html
FIJI (ImageJ)	NIH	https://fiji.sc/
Viewer II	Biobserve	http://www.biobserve.com/behavioralresearch/products/viewer
Other		
Optogenetic fibers (LHb and VTA)	Doric	N/A

CONTACT FOR REAGENT AND RESOURCE SHARING

Further information and requests for resources and reagents should be directed to and will be fulfilled by the Lead Contact, Dr. Byungkook Lim (bklim@ucsd.edu).

EXPERIMENTAL MODEL AND SUBJECT DETAILS

Mice

All procedures to maintain and use mice were approved by the Institutional Animal Care and Use Committee (IACUC) at the University of California, San Diego. Mice were maintained on a 12-h:12-h light: dark cycle with regular mouse chow and water ad libitum. CD-1 male retired breeders and C57BL6 mice were purchased from Charles River Laboratories and Jackson Laboratories, respectively.

Pvalb-ires-Cre, Rosa-CAG-LSL-tdTomato (Ai14), and PV-Flp mice were obtained from the Jackson Laboratory (00869, 007914, 022730, respectively). TH-GFP and GAD67-GFP mice were gifts from Dr. Davide Dulcis and Dr. Yuchio Yanagawa, respectively. The social defeat stress protocol used requires male C57BL6 mice (Golden et al., 2011), thus all subjects for behavior and electrophysiological experiments were 8-12 week adult hemizygous transgenic male mice and heterozygous knockin males on a C57BL6/JL background. For behavioral experiments, all animals were singly housed after undergoing SDS. In all other cases, animals were group-housed. For tracing experiments, 8-12 week old male and female mice were used. No difference between sexes were observed so data were combined.

METHOD DETAILS

Virus generation

AAV vector plasmids were constructed using standard molecular cloning methods. Synaptophysin-eGFP, oPBG, and hM4D(Gi)-mCherry DNA fragments were obtained from pAAV-phSyn1(S)-FLEX-tdTomato-T2A-SypEGFP-WPRE (a gift from Hongkui Zeng; Addgene plasmid #51509), pAAV-hSyn-DIO-hM4D(Gi)-mCherry (a gift from Bryan Roth; Addgene plasmid # 44362), and pAAV-EF1α-DIO-oPBG (a gift from Edward M. Callaway), respectively. All 'spaghetti monster' fluorescent protein (smFP) DNA fragments were obtained from pCAG-smFP-FLAG, pCAG-smFP-HA, pCAG-smFP-Myc, and pCAG-smFP-V5 (gifts from Loren Looger; Addgene #59756-59759). A Flp-dependent, double-floxed inverted open reading frame (fDIO) was constructed with two heterospecific pairs of FRT and FRT5 sequences based on pAAV-EF1α-fDIO-hChR2(H134R)-eYFP (a gift from Karl Deisseroth; Addgene #55639). AAV vector plasmids encoding ChR2 (H134R variant) and eNPHR3.0 were gifts from Karl Deisseroth. We used EF1α promoter to drive the expression of target constructs for all AAV vectors except for AAV-DIO-mRuby2-T2A-Synaptophysin-eGFP which is driven by the human synapsin promoter.

All AAV vectors used in this study were packaged as serotype DJ and generated as previously described (Lim et al., 2012). In brief, AAV vectors were produced by transfection of AAV293 cells (Agilent) with three plasmids: an AAV vector plasmid carrying target constructs (DIO-mRuby2-T2A-Synaptophysin-eGFP, DIO-Synaptophysin-eGFP, DIO-Synaptophysin-smFP-FLAG, fDIO-eGFP, fDIO-oPBG, fDIO-mRuby2-P2A-TVA, DIO-ChR2(H134R)-eYFP, DIO-eNpHR3.0-eYFP, DIO-eYFP, fDIO-hM4D(Gi)-mCherry, or DIO-$Kir_{2.1}$-T2A-ZsGreen), AAV helper plasmid (pHELPER; Agilent), and AAV rep-cap helper plasmid (pRC-DJ, gift from M. Kay). At 72 hr post-transfection, the cells were collected and lysed by a repeated freeze-thaw procedure. Viral particles were then purified by an iodixanol step-gradient ultracentrifugation and subsequently concentrated using a 100-kDa molecular cutoff ultrafiltration device (Millipore). The genomic titer was determined by quantitative PCR. The AAV vectors were diluted in PBS to a working concentration of approximately 10^{13} viral particles/mL.

EIAV genomic vector plasmids were constructed from the initial pEIAV-SIN6.1-CBGFPW (a gift from John Olsen; Addgene #44173) by replacing eGFP coding sequence with DNA fragments containing DIO-Flp and fDIO-Cre, respectively. RG-EIAV vectors were generated by a modified version of a published protocol (Cetin and Callaway, 2014). Briefly, HEK293-T cells were transfected with three plasmids: an EIAV genomic vector (pEIAV-DIO-Flp or pEIAV-fDIO-Cre), a helper packaging plasmid (pEV53B; a gift from Edward M. Callaway), and a pseudotyping plasmid encoding fusion protein FuG-B2 (a gift from Kazuto Kobayashi). At 72 hr post-transfection, viral particles were harvested from the media by centrifugation using SureSpin630 swinging bucket rotor (Thermo Scientific) at 5,700 rpm and 16,200 rpm for 16 hr and 2 hr, respectively. EIAV viral particles were reconstituted from the pellets with PBS and immediately stored at −80°C.

Rabies viruses were designed and generated from a full-length cDNA plasmid containing all components of the virus (a gift from Karl-Klaus Conzelmann) as previously described (Osakada and Callaway, 2013). We replaced the coding sequence for viral glycoprotein with tdTomato, mTagBFP2, iRFP670, smFP-HA, smFP-Myc, or smFP-V5 to produce rabies viruses expressing three different fluorescent markers. In brief, B7GG cells were transfected with a total of five plasmids: four plasmids expressing the viral components pcDNA-SADB16N, pcDNA-SADB16P, pcDNA-SADB16L, pcDNA-SADB16G and the aforementioned rabies virus genomic vector. The virus-containing media was collected 3-4 days post-transfection and used for further amplification. Viral particles were harvested from the media by centrifugation using SureSpin630 rotor at 20,000 rpm for 2 hr. Rabies viral particles were reconstituted from the pellets with PBS and immediately stored at −80°C. To generate EnvA-pseudotyped, glycoprotein-deleted rabies virus expressing eGFP (EnvA-RVΔG-eGFP), we used a modified version of a published protocol (Osakada and Callaway, 2013). Plasmids expressing the rabies viral components, B7GG, BHK-EnvA and HEK-TVA cells were gifts from Edward M. Callaway.

Stereotaxic injections and optic fiber/cannula implantations

Animals were group housed in a 12 hr dark/light cycle (lights on 07:00) prior to surgery. Mice were anesthetized with a mixture of ketamine (*100 mg/kg*) and dexmedetomidine (*1 mg/kg*) and placed in a stereotaxic apparatus (David Kopf Instruments) as previously described. All animals were kept on a heating pad while recovering from anesthesia. All tracing experiments were conducted in either male or female PV-Cre adult mice (8-12 weeks) and infused unilaterally. Stereotactic coordinates were derived from Paxinos and Franklin mouse brain atlas and empirically adjusted. Empirically determined coordinates were on average shifted 0.5 mm anterior relative to atlas. For experiments examining outputs of VP PV neurons, 250 nL AAV-DIO-mRuby-T2A-Synaptophysin-eGFP was infused into VP (anteroposterior, 0.65 mm; mediolateral, +/− 1.45 mm; dorsoventral, −4.85 mm from top of skull).

For input-output mapping experiments with EnvA-pseudotyped rabies virus (SADΔG-eGFP(EnvA)), 250 nL of RG-EIAV-DIO-Flp was unilaterally infused into either VTA (AP, −2.9 mm; ML, +/− 0.6 mm; DV, −4.4 mm skull) or LHb (AP, −1.45 mm; ML, +/− 0.41 mm; DV, −3.0 mm skull) along with a 1:1 mixture of AAV-fDIO-oPBG and AAV-fDIO-TVA-tdTomato into ipsilateral VP at a rate of 100 nL/min. In order to control for leakage in the relatively small LHb, 175 nL was infused at a rate of 75 nL/min. After allowing for 3 weeks of expression, animals were again anesthetized as previously described and SADΔG-eGFP(EnvA) was infused into ipsilateral VP using scar on skull as guide validation. Six day post SADΔG-eGFP(EnvA) infusion animals were sacrificed for circuit mapping analysis.

For downstream targets of neurons in LHb or VTA, 250 nL of AAV-DIO-Synaptophysin-eGFP or AAV-DIO-Synaptophysin-smFP-FLAG was infused into unilateral VP of PV-Cre mice. After 2 weeks of expression, animals were injected with 300 nL RVΔG-tdTomato, RVΔG-mTagBFP2, and RVΔG-iRFP670; or, RVΔG-smFP_myc, RVΔG-smFP_V5, and RVΔG-smFP_HA into either DRN (AP, −4.3 mm; ML, 0.0 mm; DV, −2.8 mm skull), NAc medial shell (AP, 1.9 mm; ML, 0.5 mm; DV, −4.4 mm skull), NAc lateral shell (AP, 1.65 mm; ML, 1.8 mm; DV, −4.4 mm skull), RMTg (AP, −3.65 mm; ML, −0.4 mm; DV, −4.0 mm skull), VTA, LHb, or VP. Different rabies and smFPs were randomly assigned to brain areas and interleaved between animals.

For electrophysiology experiments, 8 week old PV-Flp × Ai14 (Ai14-LSL-tdTomato) double transgenic males were injected bilaterally with RV-EIAV-fDIO-Cre into VTA or LHb using same volumes and coordinates as previously stated. Two weeks were given before animals were sacrificed for electrophysiology. For VTA or LHb target recordings, AAV-DIO-ChR2-eYFP was infused bilaterally into VP of PV-Cre animals.

For optogenetic behavioral experiments, adult (8-12 weeks) male PV-Cre animals were bilaterally injected with 250nL AAV-DIO-ChR2-eYFP into VP. Bilateral chronic optic fiber cannulae (200 um, 0.22 NA; Doriclenses, Canada) were implanted during same surgery session above either lateral habenula (LHb) or ventral tegmental area (VTA). One initial layer of adhesive cement (C&B metabond; Parkell) was used to cement fiber in place. Once dried, a second layer of dental cement was used to secure implant to skull. Finally, sutures and sterile tissue adhesive (Vetbond; 3M) was used to close up head incision. Four weeks were given for viral expression in terminals before behavioral testing commenced. Upon completion of behavioral experiments, viral injections, and fiber placement were confirmed.

Ex vivo electrophysiology

Mice were deeply anesthetized with isoflurane inhalation. Acute 250 μm coronal brain sections were prepared after intracardial perfusion of ice-cold choline-based slicing solution containing (in mM): 25 $NaHCO_3$, 1.25 NaH_2PO_4, 2.5 KCl, 7 $MgCl_2$, 25 glucose, 0.5 $CaCl_2$, 110 choline chloride, 11.6 ascorbic acid, 3.1 pyruvic acid). Brain was quickly transferred and sliced in the same solution with vibratome (LeicaVT1200). Sections were transferred to a recovery chamber and incubated for 15-20 min at 28-31°C in recovery solution consisting of (in mM): 118 NaCl, 2.6 $NaHCO_3$, 11 gluocse, 15 HEPES, 2.5 KCl, 1.25 NaH_2PO_4, 2 sodium pyruvate, 0.4 sodium ascorabate, 2 $CaCl_2$, 1 $MgCl_2$. Slices were maintained at room temperature for at least one hour until transferred to bath for recording. Cutting solution, recovery solution, and ACSF were constantly bubbled with 95% O_2/5% CO_2.

For recordings from VP neurons, slices were transferred to a recording chamber on an upright fluorescent microscope continuously perfused with oxygenated ACSF (in mM):125 NaCl, 25 $NaHCO_3$, 2.5 KCl, 1.25 NaH_2PO_4, 11 glucose, 1.3 $MgCl_2$ and 2.5 $CaCl_2$ at 28-31°C using a feedback temperature controller. Neurons labeled by fluorescent markers were visualized with a 40X water-immersion objective (Olympus) with epifluorescence and infrared differential interference contrast video microscopy.

For current clamp recording, patch pipettes (3-6 MΩ) were pulled from borosilicate glass (G150TF-4; Warner Instruments) and filled with internal solution containing (in mM): 135 K-gluconate, 5 KCl, 10 HEPES, 0.1 EGTA, 2 MgCl2, 2 Mg^{2+}-ATP, and 0.2 Na^{+}-GTP, pH 7.35 (290-300 mOsm, pH 7.4). Electrophysiological recordings were made using a MultiClamp700B amplifier and PClamp software (Molecular Devices). Data were low-pass filtered at 1 kHz and digitized at 10 kHz with Digidata 1440 (Molecular Devices). For measuring firing frequency, steady-state current was injected in +20 pA increments from −100 pA to 200 pA. All action potential properties and excitability recordings in Figure S8 were performed in the presence of 10 μM NBQX and 100 μM picrotoxin.

Action potential threshold was measured as the change in voltage from rest at which the slope = 20 V/s. Peak amplitude measured as change in voltage from threshold to peak, after hyperpolarization (AHP) the change in voltage and time from threshold to minimum after peak (see Figure S8A). Half-width calculated in Clampfit software (Molecular Devices) as full-width at half max amplitude. All measures quantified while eliciting a single action potential. Capacitance was calculated by Clampfit during the first minute after breaking in to cell. Membrane resistance was calculated from the change in voltage elicited after a 50 ms 5 mV hyperpolarizing step from −70 mV (the last 10 ms of the step from baseline was taken as ΔV).

For measuring the ratio of excitatory and inhibitory inputs (E/I ratio), a Cs-based internal solution was used containing (in mM): 115 Cs^{+}-methanesulphonate, 10 HEPES, 1 EGTA, 1.5 MgCl2, 4 Mg^{2+}-ATP, 0.3 Na^{+}-GTP, 10 Na^{+}-phosphocreatine, 2 QX 314-Cl, 10 BAPTA-tetracesium (290-300 mOsm, pH 7.4). EPSCs and IPSCs were recorded at the reversal potential for IPSCs (−70 mV) and EPSCs (0 mV), respectively. E/I ratio was calculated by dividing amplitude of AMPA-mediated EPSC while voltage-clamping at −70 mV by amplitude of GABA-mediated IPSC at 0 mV. Spontaneous EPSC and IPSC were also recorded at −70mV and 0mV, respectively. Liquid junction potential (5-8 mV) was not corrected for any experiments.

For target recordings in the LHb or VTA, AAV-DIO-ChR2-eYFP was injected into the VP of PV-Cre animals and cells in the LHb or VTA near $eYFP^{+}$ fibers were patched. For photostimulation of ChR2-expressing axon terminals, 5 ms blue light pulse was emitted from a collimated light-emitting diode (473 nm; Thorlabs) driven by a T-Cube LED Driver (Thorlabs) under the control of an Axon

Digidata 1440A Data Acquisition System and pClamp software. Light was delivered through the reflected light fluorescence illuminator port and the 40X objective (light power at max setting measured at 10.68 mW). AMPA-mediated EPSCs were blocked by bath-application of 15 μM of NBQX, $GABA_A$-mediated IPSCs with 100 μM picrotoxin. (Tocris). All recordings were excluded if holding current exceeded −200 pA or if series resistance was greater than 30 MΩ. Quantitation for electrophysiological records was performed in either Clampfit (Molecular Devices) or OriginPro 2016 (Origin Lab).

Immunohistochemistry

Immunohistochemistry was performed as previously described (Lammel et al., 2012). Briefly, animals were intracardially perfused with 4% paraformaldehyde in PBS and post-fixed at 4°C overnight. 50 μm coronal sections were sliced on a Leica VT1000 vibratome. Primary antibodies used were: guinea pig anti-Vglut1 (1:250; Millipore), guinea pig anti-Vglut2 (1:1000; Millipore), rabbit anti-TH (1:1000; Millipore), rabbit anti-NeuN (1:2000; Abcam), mouse anti-GAD65 (1:250; DSHB U. of Iowa), guinea pig anti-substance P (1:500; Abcam). For spaghetti monster experiments, epitope antibodies used were: rabbit anti-FLAG (1:1000; Sigma), goat anti-myc (1:1000; Abcam), mouse anti-V5 (1:1000; Life Technologies), rat anti-HA (1:1000; Roche). Alexa Fluor dyes conjugated to either 405, 488, 568, or 647 were used for secondary antibodies (Life Technologies, Abcam). All dilutions used were 1:1000 except for Alexa Fluor 405 at 1:500. All images were acquired with an Olympus FluoView FV1200 confocal microscope.

Circuit mapping quantitation

For whole-brain circuit mapping, cell counting was quantified as previously described with slight alterations (Beier et al., 2015). Briefly, 60 μm coronal sections were obtained across the antero-posterior axis of the brain and imaged on an Olympus VS120 slide scanner. Every third section was quantitated and all GFP-positive input neurons were counted excluding the site of SADΔG-eGFP(EnvA) injection. Data are presented as a percentage of total brain-wide inputs. That is, (total cells quantified in region / all cells quantified across brain). Fourteen total animals were injected; however, only those that had the majority of starter cells located in VP were quantified (final n = 7). Brain regions were determined by anatomical landmarks and based on Mouse Brain Atlas in Stereotaxic Coordinates, Franklin and Paxinos, 2nd edition. Olfactory cortex (Olfactory ctx) included anterior olfactory areas, piriform cortex, and olfactory tubercle. Preoptic – lateral preoptic area, medial preoptic area, medial preoptic nucleus. STN – subthalamic nucleus and parasubthalamic nucleus. Areas that exhibited < 1% of all inputs for both LHb-PV and VTA-PV populations were not included in graph. Virus titer and signal of SADΔG-eGFP(EnvA) was sufficiently high, so GFP signal was not amplified with immunofluorescence.

For VP PV neuronal fiber quantitation, images were taken on Olympus FluoView FV1200 confocal microscope. All images were taken in roughly the same imaging area, as denoted in Figure S2A. Images were acquired at 20X with 2x zoom, 570 HSV (PMT sensitivity), 5.8% laser power, using a high-sensitivity Gallium arsenide phosphide (GaAsP) detector. Analysis was conducted in Fiji (ImageJ) and quantified as a percentage of area of thresholded pixels normalized to the RG-EIAV injection site. Qualitatively determined threshold values were maintained consistent throughout animals and obtained by determining the level that best mirrored the original image without introducing background.

For spaghetti monster downstream connectivity quantitation, images of RV-smFP$^+$ (myc, V5, or HA) labeled neurons were imaged at 60X zoom 2 magnification. Z stacks, step size 2 μm were taken to fully capture labeled dendritic tree (60 μm slices). Number of synaptophysin-smFP_FLAG$^+$ puncta on cell body and dendrites were manually quantitated using FV10 Viewer (Olympus) to ensure puncta were in same z-plane as soma and neurites.

FISH assay

PV-Flp × Ai14 animals were injected with RG-EIAV-fDIO-Cre into LHb or VTA to label LHb-PV or VTA-PV subpopulations, respectively. Fresh-frozen brains were collected from mice and frozen down with isopentane (Sigma) chilled with dry ice in 70% ethanol. 20 μm coronal brain slices were sectioned on a cryostat (Thermo-Fisher). Sample preparation and mRNA labeling was performed exactly as described in RNAscope online protocol (ACD; Advanced Cell Diagnostics). All probes were purchased from ACD.

Behavioral Assays

For ChR2-mediated stimulation experiments optical fibers (Doric) were connected to a 473 nm blue laser diode (OEM Laser Systems). For LHb stimulation, 5 ms pulses of 20 Hz light were delivered as outlined in previous studies that optogenetically manipulated LHb (Shabel et al., 2012). For VTA, phasic firing has been shown to induce depressive-like symptoms in mice (Chaudhury et al., 2013). As such, phasic stimulation (5 pulses of 40ms light at 20Hz, once every 10 s) was used in SI and subthreshold/sufficiency experiments. For all others, 20 Hz, 5 ms pulse was used as previously described (Beier et al., 2015). Laser power was measured (Thorlabs) before each experiment and measured to be 10-15 mW (measured from bilateral fibers, assumed that roughly half power would be delivered to each hemisphere). For NpHR-mediated inhibition, fibers were connected to a 593 nm yellow laser diode. For both LHb and VTA inhibition, 0.1 Hz 9000 ms duration (9 s on, 1 s off) was delivered.

Chronic social defeat stress

Chronic social defeat stress (SDS) was carried out as previously described (Golden et al., 2011). Briefly, prior to experiment retired male breeder CD1 mice were screened on three consecutive days for aggressive characteristics. For ten consecutive days, experimental male C57BL6/JL mice (intruder) were subjected to physical contact and defeat by the aggressive CD1 (resident) in resident home cage for ten minutes (one defeat / day). After physical defeat a clear, perforated divider was placed in the cage preventing

physical, yet allowing for sensory contact between intruder and resident. Sensory defeat stage of SDS continued for 24h until next bout of physical defeat. Intruder mice always faced novel residents. After 10 days of SDS, animals were singly housed and tested 24h later for social avoidance behavior. Control animals were housed together separated by the perforated barrier, and switched each day. They were never in physical or sensory contact with CD1s.

Fluoxetine injections were performed as previously described (Cao et al., 2010). Briefly, animals were injected intraperitoneally with fluoxetine (20 mg/kg; Spectrum Chemical) from 9:00 A.M. – 10:00 A.M. once per day for 14-28 days. The day prior to sacrifice, animals underwent one more round of SI test to ascertain whether behavioral deficits were reversed. If animals did not exhibit reversal (judged to be SI ratio > 1), then animals were not used for FLX recordings. Control animals were treated identically except with 100 μL i.p. saline injection.

Social interaction and avoidance

Social avoidance behavior was measured using the two-stage social interaction (SI) test. In the first stage, animals were placed in an open field arena (44 cm x 44 cm x 44 cm) with an empty metal cage (9.5 cm x 9.5 cm x 8 cm). In all behavioral experiments, animals were monitored with the BIOBSERVE video-tracking software. Time spent in an area surrounding the cage ('interaction zone,' 8 cm region flanking cage), and the area along the wall opposite to the cage ('opposing zone' 9 cm region along wall opposing cage) was measured. The time spent in the interaction zone in this first stage was termed 'NO CD1.' Animals were then returned to home cage for one minute. In the second stage, a novel, aggressive CD1 mouse was placed in the cage and the same metrics were measured. From these two stages, an SI index was calculated (SI = time spent interaction zone CD1 / time spent interaction zone NO CD1). Animals were deemed susceptible if SI < 1, and resilient if SI > 1.

For initial optogenetic manipulation experiments, animals were subjected to light epochs of 3 min OFF / 3 min ON / 3 min OFF in NO CD1 stage to determine whether stimulation or inhibition changed interaction with an empty cage. Since no change was seen, most experiments omitted the 3 min OFF / 3 min ON / 3 min OFF light epochs for NO CD1 stage, and restricted light stimulation or inhibition to only CD1 stage. Both conditions were pooled together. To represent light-mediated increases or decreases in social interaction, data are presented as a ratio: time in interaction zone CD1 light ON / time in interaction zone CD1 light OFF. Thus, a ratio of 1 indicates no change, while a ratio > 1 indicates increased time in interaction zone and vice versa. For post-stress optogenetic social interaction experiments, data from only susceptible mice was reported as resilient animals would readily approach CD1 interaction zone. Previous reports indicate that SDS is not a simple fear memory of the CD1, as avoidance behavior is present with novel C57 mice as well so these were not carried out in the present study (Chaudhury et al., 2013).

For DREADD experiments, to account for difference in time course of CNO-mediated inhibition relative to optogenetics, social interaction was increased to 10 min. 24 hr after SDS completion, mice underwent 10 min NO CD1 SI. Animals were then injected with saline and 30 min later were tested for 10 min in the SI test with CD1. From this ratio, it was determined whether an animal was resilient or susceptible (only susceptible animals were tested with CNO). 24 hr later, animals were injected with CNO, and 30 min after CNO injection were again subjected to SI test with CD1.

Conditioned-place preference/aversion

For context-dependent CPP/CPA (Figure S6), a three chambered rectangular arena was used with two chambers on each side (28 × 24 cm) separated by a neutral central chamber (11.5 cm x 24 cm) (Lammel et al., 2012). In one side chamber, the floor had punched, checker-like flooring with black and white checkered pattern on the walls. The opposite chamber contained a metal grill floor with black and white stripe patterns on the walls. The central, neutral chambers had solid, clear flooring with white walls. The CPP/CPA experiments took place over 3 days as habituation, training, and testing phases. During habituation, animals were placed in the center chamber and allowed free access to explore all chambers for fifteen minutes while time spent in each chamber was recorded with BIOBSERVE. On day 2, animals were placed and restricted to one context and received no stimulation for 15 min. After, animals were restricted to the opposite context and received either blue light stimulation or yellow light inhibition for 15 min. Animals were randomly assigned which context would receive light treatment and alternated between subjects. On day 3, animals were again allowed free access to all chambers. To represent acquired preference or aversion, two metrics were calculated. CPP index represents the time spent in the stimulated side on day 3 (testing) divided by time spent in stimulated side on day 1 (habituation). 1 would indicate no change, while > 1 and < 1 indicates preference and aversion, respectively. To more clearly represent aversion and preference, the data were also presented as a difference score. Instead of dividing, $time_{habituation}$ was subtracted from $time_{testing}$. In this manner, negative values denoted acquired aversion, and positive values preference. After trends were established after first rounds of experiments, a biased CPP procedure was used. In order to account for potential chamber preferences between animals, NpHR inhibition was restricted to the *non-preferred* side while ChR2 stimulation was restricted to the *preferred* side. Thus, optogenetic experiments worked against the animals' innate preference. Since no significant differences were seen between these two approaches, results were pooled together. CPP with cocaine experiments were carried out in identical fashion with the exception that on day 2 animals received an intraperitoneal saline injection with no light stimulation in one context, and light delivery was paired with a 20 mg/kg i.p. injection of cocaine in the other.

Open field test

A plain, 44 × 44 cm open field arena was used while total locomotor activity was measured. After a 3 min habituation period, locomotion was measured in 3 min light epochs (3 min OFF / 3 min ON / 3 min OFF). Time spent in center (20 × 20 cm) and surround of arena was also measured. For non-optogenetic experiments, locomotion was recorded in one 10 min session.

Elevated plus maze

Mice were placed in the center of a plus-shaped apparatus (each arm protruding 30 cm from center, 6.35 cm wide) containing two closed arms facing each other, and two open arms. Closed arms had walls flanking the platform (15.24cm high), while closed arms had small (2 cm) 'railings' to prevent animals falling. Apparatus was elevated 30.5 cm off the ground. Time spent in closed and open arms, excluding the middle neutral area, was recorded in 5 min light OFF / 5 min light ON / 5 min light OFF epochs.

Sucrose preference test

In home cage, animals were presented with choice of two identical bottles with ball-bearing sipper tubes, one containing water and the other containing a 1% sucrose solution (bottle locations were randomly assigned and flipped at 12h to control for preference in side). The amount of liquid consumed from each bottle was measured at 0, 12, and 24h time points. No difference between 12h and 24h time points were observed, so data are presented at 12h.

Tail suspension test

TST was performed as previously described (Steru et al., 1985). Briefly, mice were suspended by tails with adhesive tape 1 cm from tip of tail and roughly 50 cm above ground so no contact could be made. Plastic tubes were placed over mouse tails to ensure mice could not climb or hang on to their tail. Animals were video recorded for 5 min and time spent immobile was quantitated over the full 5 min interval post hoc. For optogenetic experiments, to control for fatigue over a 10 min interval, animals were subjected to two separate 5 min bouts (light OFF, then light ON) separated by 5 min of rest.

For DREADD experiments, animals were tested on consecutive days, 24 hr apart. First day animals were always injected with saline, and the second day with CNO. Animals were tested 30 min post injection.

Stimulation sufficiency

All light delivery was performed in the home cage of single-housed animals and stimulation protocol was performed as previously indicated. Two times a day (08:00 and 20:00) animals received blue light stimulation for ten minutes. 24h after day 10, animals underwent SI test and later, other behavior tests (Figures S7I and S7J). After behavior, animals were sacrificed to check for injection site and fiber placement.

Subthreshold defeat protocol was performed as previously described (Chaudhury et al., 2013). Briefly, experimental C57BL6/JL mouse was subjected to 3 consecutive bouts of 3 min physical defeat and 10 min sensory defeat on a single day. Light stimulation was delivered during sensory portion of defeat. 5 min of rest in home cage was given between sensory defeat and subsequent bout of physical defeat.

QUANTIFICATION AND STASTISTICAL ANALYSIS

Student's t tests, Mann-Whitney U-tests, and one- or two-way ANOVA tests were used as appropriate to determine statistical differences using OriginPro 2016 software (Origin Labs). Shapiro-Wilk test was used to assess normality. Tukey post test was applied in ANOVAs to ascertain differences within groups and to correct for multiple comparisons. Clampfit (Molecular Devices) was used for event detection in electrophysiological experiments. All statistical data can be found in figure legends with corresponding sample sizes. Statistical significance was set at * $p < 0.05$, ** $p < 0.001$, *** $p < 0.0001$. All data are presented as mean ± SEM.

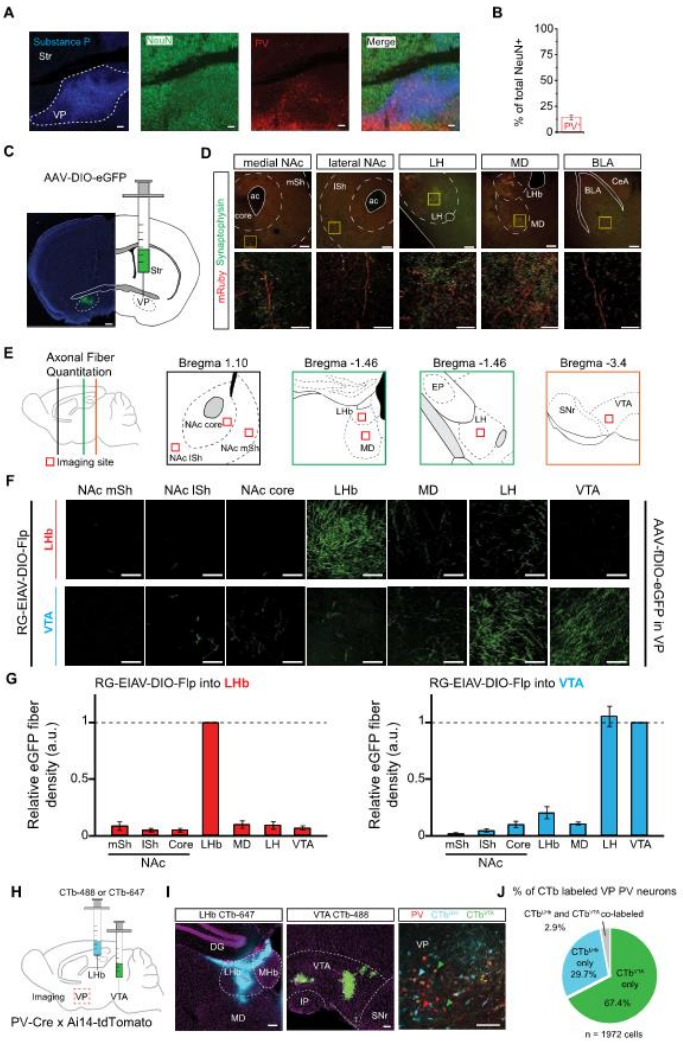

Figure S1. $PV^{VP \rightarrow LHb}$ and $PV^{VP \rightarrow VTA}$ Neurons Represent Distinct Subpopulations, Related to Figure 1

(A) Immunofluorescent images showing staining for Substance P (to delineate VP border), PV (from PV-tdTomato mouse), and NeuN (neuronal marker). Scale: 100 μm.

(B) Quantitation of PV neurons as a percentage of the total population of ventral pallidal neurons. PV neurons comprise 14% (# PV^+ neurons / total # $NeuN^+$ neurons within borders of Substance P staining). > 25,000 neurons across 4 animals quantified. Data presented as mean + SEM.

(C) Validation showing virus expression can be precisely localized to the VP without leakage into surrounding brain areas. 250 nL of AAV-DIO-eGFP injected into a PV-Cre mouse. Scale: 400 μm.

(legend continued on next page)

(D) Other outputs of VP PV neurons. Yellow boxes indicate zoomed areas in bottom row. Scale bars: 50 μm top, 150 μm bottom. Related to Figures 1C–1E.
Abbreviations: NAc, nucleus accumbens; mSh, medial shell; lSh, lateral shell; LH, lateral hypothalamus; MD, mediodorsal nucleus of the thalamus; BLA, basolateral amygdala.
(E) Sagittal view showing areas along antero-posterior axis images are taken for fiber quantitation analysis. Coronal views of the areas in which confocal images in (B) are taken (red squares).
(F) Representative images of fibers in target areas after RG-EIAV-DIO-Flp injection into either LHb (top) or VTA (bottom) and AAV-fDIO-eGFP into VP. Scale: 80 μm.
(G) Fiber quantitation of $PV^{VP \rightarrow LHb}$ and $PV^{VP \rightarrow VTA}$ neurons. Dashed line indicates normalized level of injection site. For analysis, 3-4 images were taken for each brain area within an individual animal (n = 4) and averaged. Data presented as mean + SEM.
(H) Experimental schematic. Cholera toxin subunit B conjugated to Alexa Fluor 488 and 647 injected into LHb or VTA in a PV-Cre x Ai14-tdTomato animal to label $PV^{VP \rightarrow LHb}$ and $PV^{VP \rightarrow VTA}$ neurons.
(I) Representative images of bead injection sites in LHb (left) and VTA (middle) and retrograde labeling in VP (right). Green arrows depict colocalization of CTb^{VTA} beads and PV-tdT, blue arrow CTb^{LHb} and PV-tdT, and red arrow PV neuron with no bead expression that likely projects to a separate target. Scales: 100 μm.
(J) Quantitation of VP PV neurons that colocalized with CTb beads injected into the VTA, LHb (CTb^{VTA} and CTb^{LHb}, respectively), or both. Only 2.9% of bead-labeled PV neurons projected to both LHb and VTA indicating minimal overlap between these two populations (n = 1972 neurons).
Abbreviations: NAc, nucleus accumbens; mSh, medial shell; lSh, lateral shell; ac, anterior commissure LH, lateral hypothalamus; MD, mediodorsal nucleus of the thalamus; BLA, basolateral amygdala; EP, entopeduncular nucleus; SNr, substantia nigra reticulata.

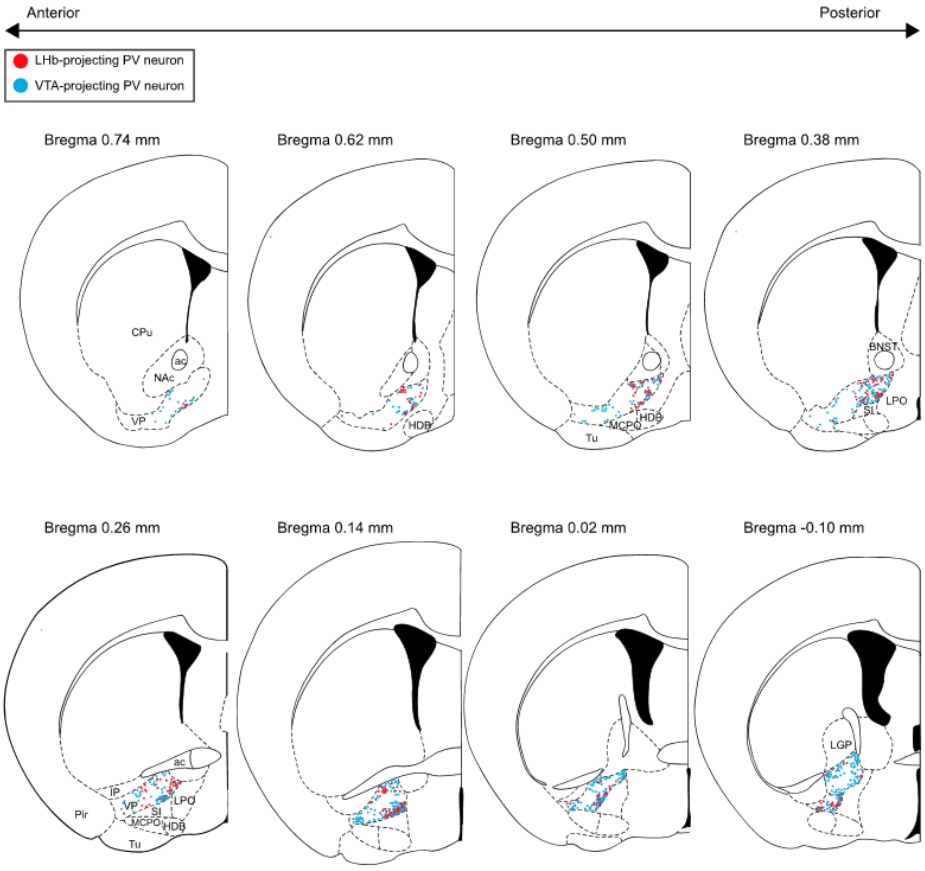

Figure S2. Anatomical Localization of $PV^{VP \rightarrow LHb}$ and $PV^{VP \rightarrow VTA}$ Neurons, Related to Figure 1

Localization of $PV^{VP \rightarrow LHb}$ (red) and $PV^{VP \rightarrow VTA}$ (blue) neurons across the A-P axis in VP. Only cells in VP are shown. Each dot represents a single neuron. All neurons presented are cumulative across 4 animals for each.

NAc, nucleus accumbens; ac, anterior commissure; CPu, caudate putamen; VP, ventral pallidum; HDB, horizontal diagonal band; MCPO, magnocellular preoptic nucleus; SI, substantia inominata; BNST, bed nucleus of stria terminalis; LPO, lateral preoptic area; IP, interstitial nucleus; Pir, piriform cortex; Tu, olfactory tubercle; LGP, lateral globus pallidus.

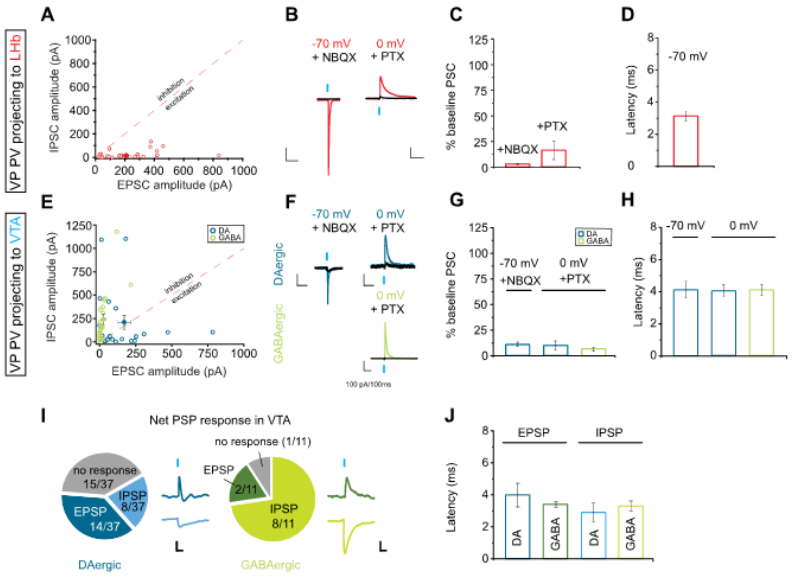

Figure S3. PV$^{VP \rightarrow LHb}$ Neurons Are Primarily Glutamatergic, While PV$^{VP \rightarrow VTA}$ Neurons Send Inhibitory Projections to GABAergic Neurons and Mixed Excitatory Projections to Dopaminergic Neurons, Related to Figure 1

(A and E) Absolute amplitude of eEPSCs and eIPSCs of LHb (n = 40; (A)) and VTA (green, GABAergic neurons, n = 25; blue, dopaminergic (DA) neurons, n = 40; (E)) neurons evoked by light-stimulation of axonal terminals of VP PV neurons. Individual responses depicted in Figure 1J quantitation. The filled circle and error bars represent overall average and SEM.

(B and F) Representative traces of LHb (B) and VTA (F) neurons. Colored traces represent baseline responses, and black traces after bath-application of indicated drug. Scale: (B) 50 pA, 100 ms; (F, blue) 25 pA, 50 ms; (D, green) 100 pA, 100 ms.

(C and G) Average EPSC and IPSC amplitude after bath application of NBQX and PTX. Data presented as normalized % of PSC amplitude after drug application. For (C): n = 5 each condition. For (G, DA): n = 5, 3 for NBQX, PTX respectively. (G, GABA): n = 5. Data presented as mean + SEM.

(D and H) Latency of beginning of synaptic response to initiation of light delivery on slice. Data presented as mean + SEM.

(I) Quantitation of net post-synaptic potential (PSP) responses using a potassium gluconate-based internal in DAergic and GABAergic VTA neurons in current-clamp mode. Example traces of evoked IPSPs and EPSPs on right. Scale: 2 mV, 100 ms.

(J) Latencies of EPSP and IPSP responses in GABAergic and DAergic VTA neurons to initiation of light delivery on slice.

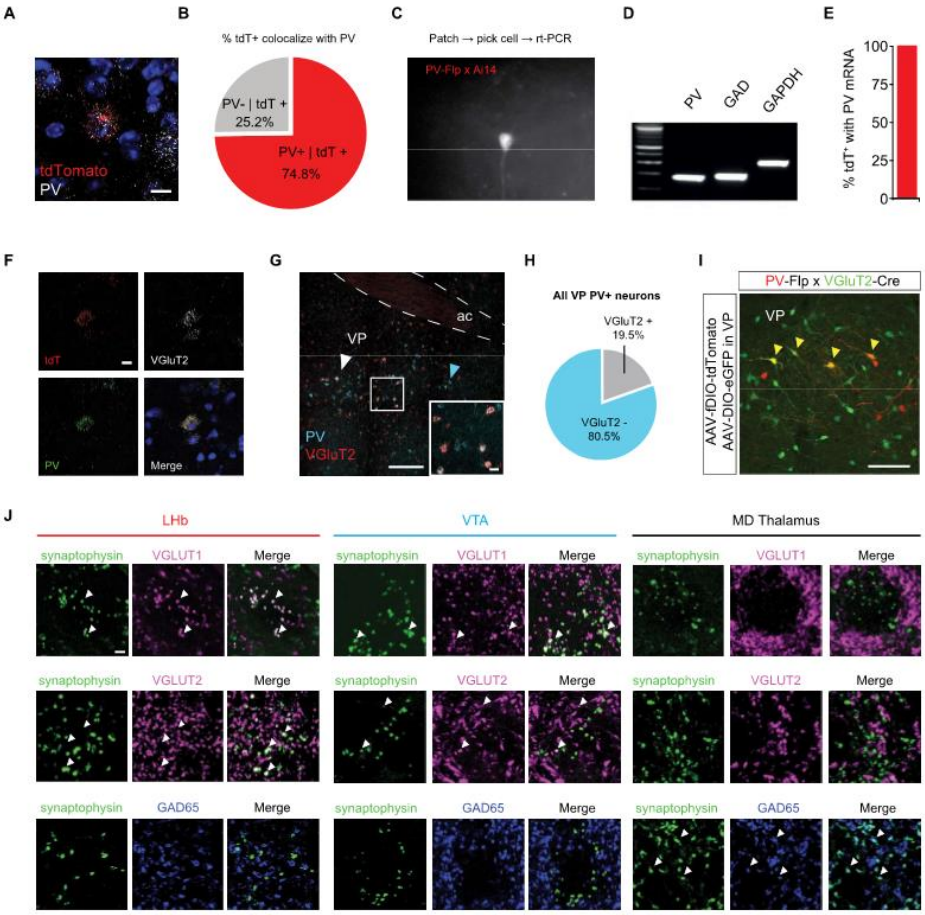

Figure S4. Validation of Ventral Pallidal Glutamatergic Parvalbumin Neurons, Related to Figure 1

(A) mRNA labeling of PV and tdTomato (from PV-Flp x Ai14 animal injected with RG-EIAV-fDIO-Cre, related to Figures 1K and 1L) depicting specificity of RG-EIAV virus. tdTomato mRNA localizes predominantly to PV^+ neurons. Scale: 10 μm.

(B) mRNA viral validation quantitation. Roughly 75% of $tdTomato^+$ neurons colocalize with PV mRNA.

(C) Image shows labeled PV-$tdTomato^+$ neuron in prepared ex vivo slice with same viral labeling strategy used in (A).

(D) The RT-PCR of picked $tdTomato^+$ neurons in slice to further validate RG-EIAV virus specificity. Example gel showing bands for GAPDH (control), PV, and GAD (glutamate decarboxylase, marker for GABAergic neurons).

(E) 100% of $tdTomato^+$ neurons patched and picked (n = 7) expressed mRNA for PV.

(F) Fluorescent mRNA labeling showing triple co-expression of probes to tdTomato (from PV-Flp x Ai14 mouse injected with RG-EIAV-fDIO-Cre), PV, and VGluT2. Validation that virally labeled cells (tdT^+) are also PV^+ and $VGluT2^+$. Scale: 20 μm.

(G) mRNA labeling for PV and VGluT2 in the VP. Scale: 200 μm, inset 50 μm. White arrowhead indicates PV/VGluT2 co-localization, blue arrowhead indicates $VGluT2^-$ PV^+ neuron.

(H) Quantitation of all VP PV neurons imaged (non-projection specific) that either co-localized ($VGluT2^+$ | PV^+, 19.5%) or did not co-localize ($VGluT2^-$ | PV^+, 80.5%) with VGluT2 probe. n = 67 / 343 neurons $VGluT2^+$ | PV^+, from 2 animals.

(legend continued on next page)

(I) Viral labeling of PV$^+$ neurons (red) and VGluT2$^+$ neurons (green) by viral injections in double transgenic (PV-Flp × VGluT2-Cre) animals. Colocalized VGluT2/PV-positive neurons denoted by yellow arrows. Scale: 100 μm.
(J) Immunohistochemistry showing co-expression of synaptophysin-eGFP puncta with VGluT1 and VGluT2, but not GAD65 in LHb (left), and VTA (middle). AAV-DIO-Synaptophysin-eGFP was injected in VP of PV-Cre mice. Dense colocalization of synaptophysin to GAD65 was observed in the MD thalamus. Arrowheads indicate synaptophysin-eGFP puncta co-localized with respective marker. Scale: 2 μm.

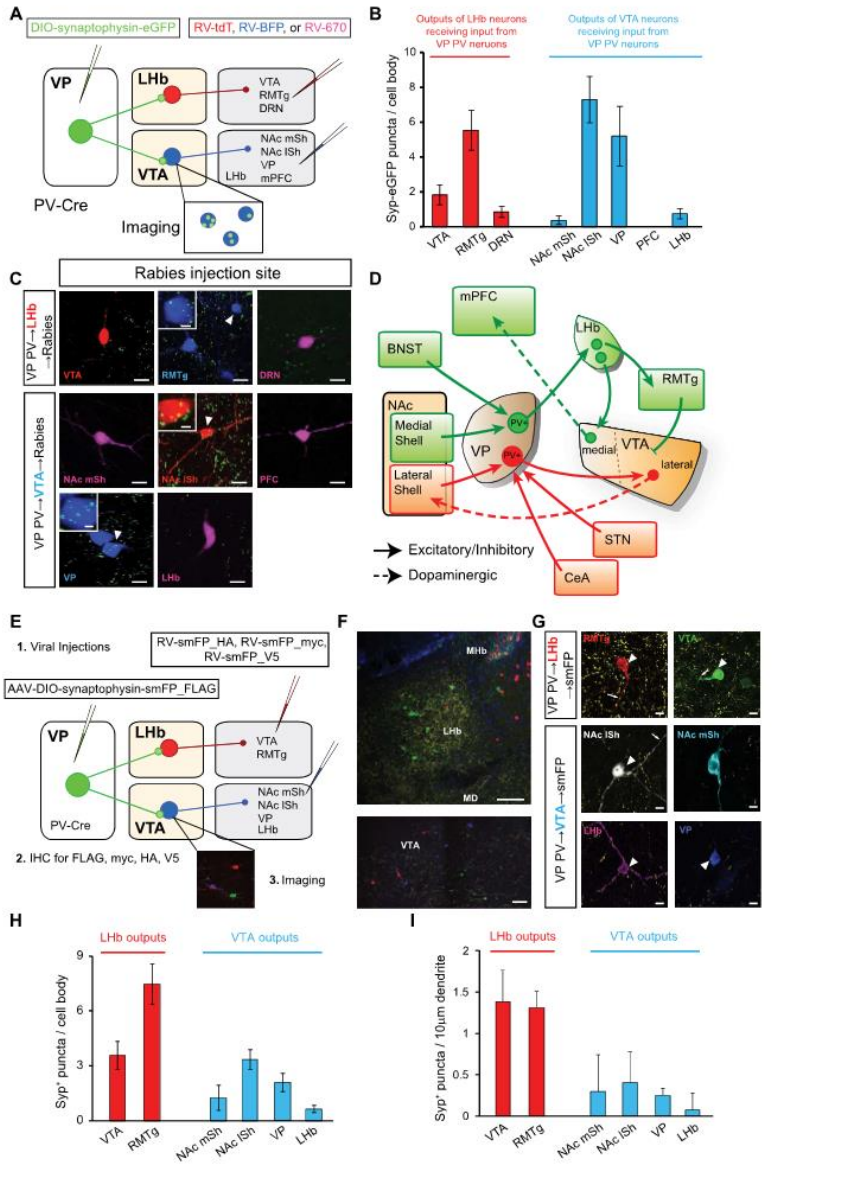

(legend on next page)

Figure S5. Projection Targets of VTA and LHb Neurons Receiving Input from VP PV Neurons, Related to Figure 2

(A) Schematic of viral injections labeling outputs of neuronal targets of $PV^{VP \rightarrow LHb}$ and $PV^{VP \rightarrow VTA}$ neurons. AAV-DIO-Synaptophysin-eGFP was injected into VP of PV-Cre mice. After 2 weeks of expression, same animals were injected with retrograde rabies viruses expressing various fluorophores including RVΔG-tdTomato, RVΔG-mTagBFP2, and RVΔG-iRFP670 into output structures of LHb and VTA (RMTg, DRN, and VTA for LHb; NAc medial shell (mSh), NAc lateral shell (lSh), VP, prefrontal cortex (PFC), and LHb for VTA). Colors and brain structures were alternated across animals. RV^+ neurons were imaged and synaptophysin-eGFP puncta colocalizing with RV^+ soma were quantitated.

(B) Quantitation of puncta/rabies$^+$ cell body, data presented as mean ± SEM n = 8 total animals. Cells: LHb outputs (VTA, n = 18; RMTg, n = 13; DRN, n = 7), VTA outputs (NAc mSh, n = 8; NAc lSh, n = 17; PFC, n = 3; VP, n = 5; LHb, n = 8).

(C) Representative confocal images. Scale: 10 μm, inset 4 μm. Arrow denotes zoomed in area. NAc mSh and mPFC projecting VTA neurons were located predominantly in medial VTA, as such very few if any puncta were located nearby.

(D) Overall inputs, outputs, and targets of outputs circuit diagram of LHb-PV and VTA-PV neurons. NAc, nucleus accumbens; mSh, medial shell; lSh, lateral shell; RMTg, rostromedial tegmental nucleus; DRN, dorsal raphe nucleus; PFC, prefrontal cortex.

(E) Schematic of spaghetti monster fluorescent proteins (smFPs) tracing experiments. AAV-DIO-synaptophysin-smFP_FLAG injected into VP of PV-Cre mouse while. RV-smFP_HA, RV-smFP_myc, and RV-smFP_V5 injected into output targets of VTA or LHb (1). After viral expression, IHC to epitope tags performed to enhance and amplify fluorescent signal (2). Animals are then perfused and imaged (3).

(F) Representative low-magnification confocal images at 20X. Top: RMTg-projecting LHb neurons in green, VTA-projecting LHb neurons in red, DRN-projecting LHb neurons in blue. VP PV synaptophysin terminals in yellow. Bottom: NAc lSh-projecting neurons in red, NAc mSh-projecting neurons in green, VP-projecting neurons in blue. Scale: 100 μm.

(G) Representative high-magnification images of LHb- or VTA-output neurons. Scale: 10 μm. Arrowheads indicate synaptic contact with cell body, arrows indicate synaptic contact with dendrite.

(H and I) Quantitation for number of synaptophysin$^+$ puncta/cell body (H) or per 10 μm of dendrite (I). N = 12, 11, 8, 14, 12, 11 cell bodies and n = 6, 14, 9, 28, 14, 19 dendrites for VTA, RMTg, NAc lSh, NAc mSh, VP, LHb, respectively.

All data presented as mean + SEM.

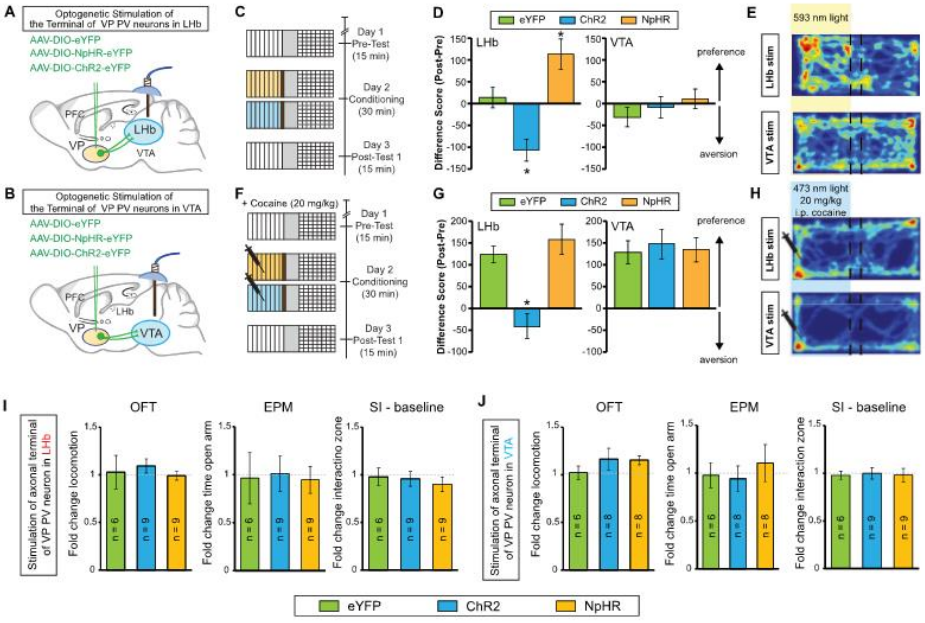

Figure S6. PV$^{VP \rightarrow LHb}$, but Not PV$^{VP \rightarrow VTA}$ Neurons, Bidirectionally Modulate Reward and Aversion, Related to Figure 3

(A and B) Schematic of viral injections in the VP and optical fiber implantations in the LHb and VTA for optogenetic-mediated terminal stimulation (AAV-DIO-ChR2), inhibition (AAV-DIO-NpHR), or control (AAV-DIO-eYFP).

(C) Behavioral paradigm of conditioned place preference or aversion (CPP or CPA).

(D) Quantitation of CPP/CPA. Activation or silencing of axonal fibers in LHb, but not in VTA, produces aversion and preference, respectively. LHb: one-way ANOVA $F_{2,25} = 13.95$, $p < 0.001$. Tukey post hoc test to determine significance between individual groups. *$p < 0.05$, eYFP-NpHR *$p < 0.05$, ChR2-NpHR **$p < 0.001$. n = 9, 9, 10 for eYFP, ChR2, NpHR groups, respectively. n = 5, 8, 8 for each group in VTA-implant animals.

(E) Example behavior heatmap of CPP/CPA on day 3. Shaded yellow area on left indicates side where yellow light was delivered on day 2. Warmer colors denote more time spent in designated area. Dashed lines indicate neutral center area.

(F) Same CPP/CPA behavior paradigm, except i.p. injection of cocaine (20 mg / kg) was paired with light delivery.

(G) Terminal stimulation of VP PV neurons in LHb, but not in VTA, is sufficient to block expression of cocaine-induced CPP. LHb: one-way ANOVA $F_{2,18} = 4.804$, $p < 0.05$, Tukey post test: eYFP-ChR2 *$p < 0.05$. n = 5, 8, 8 for eYFP, ChR2, and NpHR respectively in both LHb and VTA animals.

(H) Representative trace of animal track on day 3, blue shading and needle indicate side on day 2 where light delivery and cocaine was administered.

(I and J) Optogenetic stimulation or inhibition of VP PV terminals in LHb (A) and VTA (B) does not induce changes in locomotion (OFT), anxiety (EPM), or basal social interaction (SI test). Data presented as fold change in light ON epoch divided by light OFF epoch. Dashed line indicates no change.

All data presented as mean + SEM.

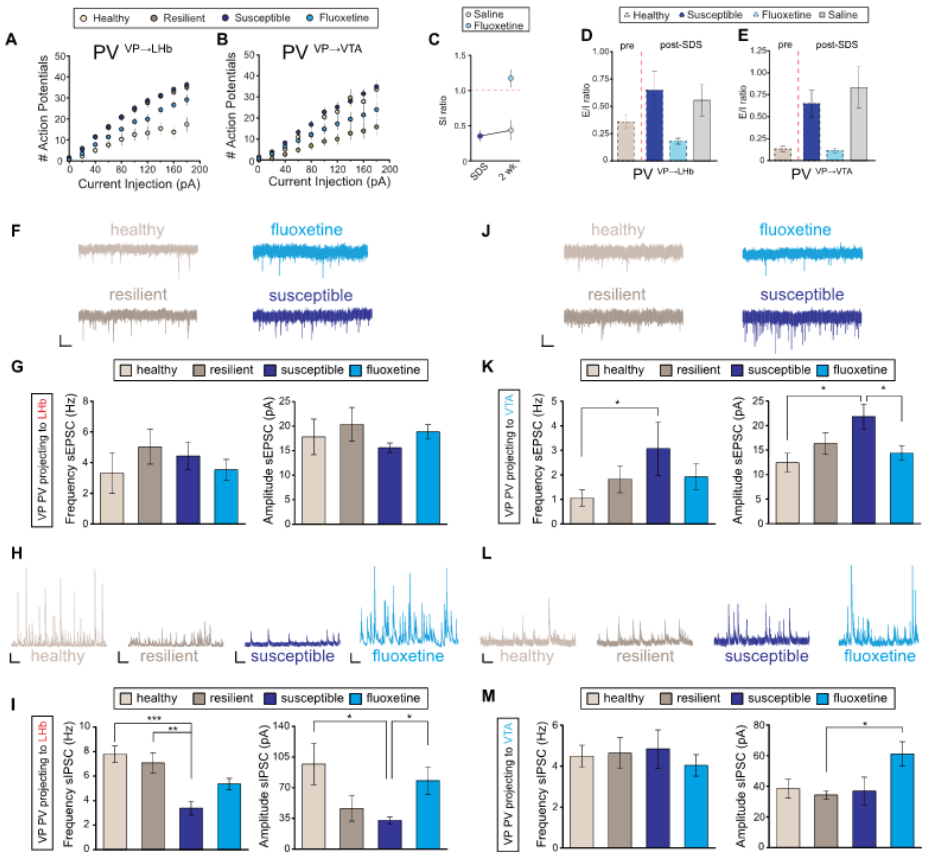

Figure S7. Differential Changes in Spontaneous Synaptic Activity in $PV^{VP\rightarrow LHb}$ and $PV^{VP\rightarrow VTA}$ Neurons after SDS, Related to Figure 3

(A and B) Spikes elicited at all current injection levels. Supplemental to Figures 3E and 3K. For (A): two-way ANOVA with main effect on SDS group, $F_{3,345} = 54.1$, *$p < 0.001$. n = 9, 11, 10, 8 cells for healthy, resilient, susceptible, FLX, respectively. For (B): two-way ANOVA with main effect on SDS group, $F_{3,358} = 32.58$ *$p < 0.001$. n = 12, 10, 10, 8 cells from each group.

(C) SI ratio before and after 2 weeks FLX or saline injections in susceptible animals. FLX data point adapted from Figure 3C. No spontaneous recovery observed 2 weeks post SDS.

(D and E) E/I ratio of susceptible animals administered 2 weeks saline injections (gray bar). Other data points adapted from Figures 3H and 3N for comparison (dashed lines around bars).

(F to I) Differential changes in spontaneous excitatory (F and G) and inhibitory (H and I) postsynaptic currents (sEPSC, sIPSC, respectively) in control, resilient, susceptible, and FLX mice (light tan, brown, light blue, navy, respectively) in $PV^{VP\rightarrow LHb}$ neurons. Amplitude of sEPSCs and sIPSCs (right) and frequency (left). Scale in (F): 10 pA, 500 ms. For (H): control, 100 pA, 500 ms; resilient, susceptible, and FLX, 50 pA, 500ms. Significant decreases in sIPSC frequency (left, $F_{3,37} = 8.468$, $p < 0.001$) and amplitude (right, $F_{3,37} = 3.916$, $p < 0.05$) in susceptible animals in $PV^{VP\rightarrow LHb}$ neurons, with recovery in amplitude in FLX animals.

(J to M) $PV^{VP\rightarrow VTA}$ neurons in susceptible animals exhibit significant increases in frequency (left) and amplitude (right) of sEPSCs (J and K), but not sIPSCs (L and M) with recovery in FLX animals. (K) frequency, $F_{3,38} = 3.606$, $p < 0.05$; amplitude, $F_{3,38} = 4.699$, $p < 0.01$. (G) amplitude, $F_{3,41} = 3.389$, $p < 0.05$. Scale for (J): 10 pA, 500 ms. (L): 20 pA, 500 ms. $PV^{VP\rightarrow LHb}$ neurons: n = 6, 8, 13, 14 from 3, 4, 4, 4 animals in control, resilient, susceptible, FLX groups, respectively. $PV^{VP\rightarrow VTA}$ cells: n = 9, 14, 8, 14 from 3, 4, 4, 4 animals in control, resilient, susceptible, FLX groups, respectively.

***$p < 0.001$, **$p < 0.01$, *$p < 0.05$. All tests conducted one-way ANOVA with post hoc Tukey test for multiple comparisons. All data presented as mean + SEM.

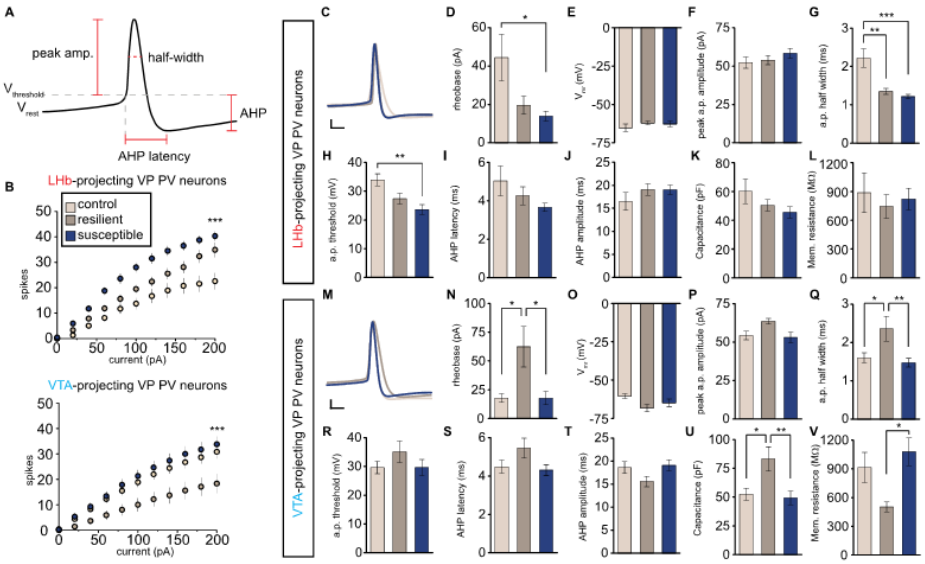

Figure S8. Social Defeat Stress-Induced Changes in Action Potential and Membrane Properties in $PV^{VP \rightarrow LHb}$ and $PV^{VP \rightarrow VTA}$ Neurons, Related to Figure 3 and 4

(A) Schematic defining how certain action potential (a.p.) properties were quantified (for further information see STAR Methods). All measurements were recorded in the presence of the synaptic blockers NBQX and picrotoxin. AHP: after-hyperpolarization.

(B) Spikes elicited in $PV^{VP \rightarrow LHb}$ (top) or $PV^{VP \rightarrow VTA}$ (bottom) neurons in response to current injection. Same as Figures S7A and S7B, but with synaptic blockers. For $PV^{VP \rightarrow LHb}$ neurons, $F_{2, 359} = 106.72$, $p < 0.001$; n = 11, 13, 12 cells from 3, 4, 4 animals for control, resilient, susceptible, respectively. $p < 0.01$ for all individual group interactions. For $PV^{VP \rightarrow VTA}$ neurons, $F_{2, 387} = 49.33$, $p < 0.001$; n = 12, 10, 14 cells from 4, 4, 4 animals for control, resilient, susceptible, respectively. Susceptible and control significantly different from resilient. $p < 0.001$ for healthy-resilient and susceptible-resilient comparisons. Two-way ANOVA with post hoc Tukey test for multiple comparisons, main effect on stress condition for both.

(C and M) Sample a.p. traces of $PV^{VP \rightarrow LHb}$ and $PV^{VP \rightarrow VTA}$ neurons in healthy, resilient, and susceptible animals. Scale: 2 ms, 10 mV.

(D-L) Rheobase (D, minimum current required to elicit a.p. $F_{2,32} = 4.19$, $p < 0.05$), resting membrane potential (E, V_{mr}), peak a.p. amplitude (F), a.p. half width (G, full width at half max. $F_{2,31} = 11.83$, $p < 0.001$), a.p. threshold (H, $F_{2,31} = 6.48$, $p < 0.01$), AHP latency (I), AHP amplitude (J), membrane capacitance (K), and membrane resistance (L) for $PV^{VP \rightarrow LHb}$ neurons.

(N-V) Rheobase (N, $F_{2,35} = 4.68$, $p < 0.05$), V_{mr} (O), peak a.p. amplitude (P), a.p. half width (Q; $F_{2,36} = 5.86$, $p < 0.01$), a.p. threshold (R), AHP latency (S), AHP amplitude (T), membrane capacitance (U; $F_{2,36} = 6.99$, $p < 0.01$), and membrane resistance (V; $F_{2,36} = 5.12$, $p < 0.05$) for $PV^{VP \rightarrow VTA}$ neurons.

All data presented as mean ± SEM. *$p < 0.05$, **$p < 0.01$, ***$p < 0.001$. All data except for (B) tested on one-way ANOVA with Tukey post hoc test to assess inter-group differences. Two-way ANOVA used for (B).

Chapter I, in full, is a reprint of the material as it appears in Knowland D, Lilascharoen V, Pacia CP, Shin S, Wang EHJ and Lim BK. *Distinct Ventral Pallidal Neural Populations Mediate Separate Symptoms of Depression*. Cell, 170.2 (2017): 284-297. The dissertation author was the primary investigator and author of this paper.

CHAPTER II:

Cocaine Induced Structural Plasticity in Input Regions to Distinct Cell Types in Nucleus Accumbens

Cindy Barrientos*, **Daniel Knowland***, Mingche MJ Wu, Varoth Lilascharoen, Kee Wui Huang, Robert C. Malenka, Byung Kook Lim

* These authors contributed equally to this work.

Abstract

Background:

The nucleus accumbens (NAc) is an extensively studied brain region implicated in pathological motivated behaviors such as drug addiction and is comprised predominantly of two discrete populations of neurons, dopamine receptor-1 and dopamine receptor-2 expressing medium spiny neurons (D1-MSNs and D2-MSNs, respectively). It is unclear whether these populations receive inputs from different brain areas and whether input regions to these cell-types undergo distinct structural adaptations in response to administration of addictive drugs such as cocaine.

Methods:

Using a modified rabies virus-mediated tracing method, we present a comprehensive brain-wide monosynaptic input map to NAc D1- and D2-MSNs. Next, we analyze nearly 2,000 dendrites and over 125,000 spines of neurons across four input regions (prelimbic cortex (PrL), medial orbitofrontal cortex (MO), basolateral amygdala (BLA), and ventral hippocampus (vHPC)) at four separate time points during cocaine administration and withdrawal to examine changes in spine density in response to repeated intraperitoneal cocaine injection.

Results:

D1- and D2-MSNs display overall similar input profiles, with the exception that D1-MSNs receive significantly more input from the MO. We find that neurons in distinct brain areas projecting to D1- and D2-MSNs display different adaptations in dendritic spine density during different stages of cocaine administration and withdrawal.

Conclusions:

While NAc D1- and D2-MSNs receive input from generally similar brain structures, spine density changes in specific input regions in response to cocaine administration are quite distinct and dynamic. While previous studies have focused on input-specific postsynaptic changes within NAc MSNs in response to cocaine, these findings emphasize the dramatic changes that occur in the afferent input regions as well.

Introduction

The nucleus accumbens (NAc) is a brain region critical for processing motivationally salient information from the environment and is one of the first brain areas to robustly respond to drugs of abuse (Grueter et al., 2012; Kalivas and Volkow, 2005; Lüscher and Malenka, 2011; Nestler, 2001; Russo et al., 2010). Indeed, animals will work to electrically self-stimulate the NAc to the exclusion of basic needs such as water and food (Olds and Milner, 1954). In addition to responding to rewarding stimuli, the NAc also plays a role in mediating aversive states (Al-Hasani et al., 2015). These seemingly opposite functions may arise in part because of the cellular diversity of the NAc. D1-MSNs and D2-MSNs represent largely non-overlapping NAc cell populations and comprise ~95**%** of all neurons in the region (Le Moine and Bloch, 1995). Indeed, optogenetic manipulations suggest that D1-MSN stimulation is rewarding, while D2-MSN stimulation is aversive (Lobo et al., 2010). Furthermore, D1-MSNs and D2-MSNs undergo distinct synaptic adaptations in response to cocaine administration (Bock et al., 2013; Creed et al., 2016; Grueter et al., 2012; Lee et al., 2006; Lüscher and Malenka, 2011; MacAskill et al., 2014; Russo et al., 2010), possibly reflecting their different functional roles.

In addition to these cell-type specific differences, the NAc also receives brain-wide input from many different regions. The dense innervation of the NAc by ventral tegmental area dopaminergic neurons is thought to be critically important for the response to rewarding stimuli, in particular drugs of abuse (Nestler, 2004). Recent research has also uncovered critical roles for glutamatergic inputs from various brain regions including but not limited to the medial prefrontal cortex (mPFC), basolateral amygdala (BLA), and ventral hippocampus (vHPC)(Grueter et al., 2012; Lüscher and Malenka, 2011; Russo and Nestler, 2013). These

excitatory afferents to the NAc have been suggested to underlie separate components of addictive behavior with the vHPC encoding contextual information, the BLA relaying emotional context, and the mPFC providing operational value (Russo and Nestler, 2013). Recent reports have also underscored the importance of the paraventricular nucleus of the thalamus (PVT) and its synaptic connections with D2-MSNs during protracted drug use (Bock et al., 2013; Zhu et al., 2016). Thus, consideration of both cell type- and input-specific plasticity within the NAc is necessary to fully capture the mechanistic complexity underlying drug-induced neural adaptations.

Drug-induced structural changes in neurons may play a particularly important role in mediating the long-lasting behavioral adaptations caused by repetitive administration of drugs of abuse (Russo et al., 2010). For example, increased spine density, a structural correlate of synaptic plasticity, and Delta-FosB expression after chronic cocaine treatment is stably maintained during long periods of withdrawal in D1-MSNs, but not in D2-MSNs (Lee et al., 2006; Russo et al., 2010). Additionally, BLA inputs to D1-MSNs, but not vHPC inputs, exhibit an increase in both spine density and excitatory synaptic strength after repeated cocaine exposure (MacAskill et al., 2014). While spine changes have been thoroughly described in NAc MSNs, much less is known about whether similar cocaine-induced changes extend to the input structures themselves. Do cells projecting to NAc in input regions such as the mPFC, BLA, and vHPC exhibit spine density changes that parallel those observed in the NAc? Might such changes lie upstream of aberrant alterations seen in the NAc in response to cocaine administration?

To begin to address these questions, we provide a brain-wide characterization of all inputs to NAc D1- and D2-MSNs using viral-mediated monosynaptic circuit tracing. While such a characterization has been performed for the dorsal striatum (Wall et al., 2013), it has yet to be performed for the NAc. We then examine cocaine-induced changes in dendritic spine density in input region cells which specifically contact NAc D1- or D2-MSNS, at several distinct time points following chronic cocaine administration. Our findings suggest that cocaine-induced structural changes in neurons sending inputs to NAc are highly specific and depend both on the MSN subtype they contact and the time point at which they are analyzed following cocaine administration.

Materials and Methods

Animals

All procedures to maintain and use mice were approved by the Institutional Animal Care and Use Committee (IACUC) at the University of California, San Diego. Mice were maintained on a 12-h:12-h light:dark cycle with regular mouse chow and water ad libitum. Adult Adora2a-cre (GENSAT 036158-UCD, for labelling D2-MSNs) and Drd1a-cre (GENSAT 017264-UCD, for D1-MSNs) congenic mice on a C57BL6/JL background were obtained from GENSAT and backcrossed with wild type C57BL mice for several generations. Animals were randomly assigned to either control or experimental groups. Surgeries were performed between 10-12 weeks of age.

Virus generation

All AAV vectors used in this study were packaged as serotype DJ and generated as previously described (Lim et al., 2012). In brief, AAV vectors were produced by transfection

of AAV293 cells (Agilent) with three plasmids: an AAV vector plasmid carrying target constructs (DIO-tdTomato-P2A-TVA, AAV-DIO-RVG), AAV helper plasmid (pHELPER; Agilent), and AAV rep-cap helper plasmid (pRC-DJ, gift from M. Kay). At 72 h post-transfection, cells were collected and lysed by a repeated freeze-thaw procedure. Viral particles were purified by an iodixanol step-gradient ultracentrifugation and concentrated using a 100-kDa molecular cutoff ultrafiltration device (Millipore). Genomic titer was determined by quantitative PCR and diluted in PBS to a working concentration of approximately 10^{13} viral particles/mL.

Rabies virus was designed and generated as previously described (Osakada and Callaway, 2013). Briefly, B7GG cells were transfected with a total of five plasmids: four plasmids expressing the viral components pcDNA-SADB16N, pcDNA-SADB16P, pcDNA-SADB16L, pcDNA-SADB16G and a full-length cDNA plasmid containing all components of the virus where the glycoprotein coding sequence is replaced by eGFP (a gift from Karl-Klaus Conzelmann). Virus-containing media was collected 3-4 days post-transfection and used for further amplification. Viral particles were harvested from the media by centrifugation using SureSpin630 rotor at 20,000 rpm for 2h. Rabies viral particles were reconstituted from with PBS and immediately stored at -80 °C.

To generate EnvA-pseudotyped, glycoprotein-deleted rabies virus expressing eGFP (RV□G-eGFP(EnvA)), we used a modified version of a published protocol (Osakada and Callaway, 2013). Plasmids expressing the rabies viral components, B7GG, BHK-EnvA and HEK-TVA cells were gifts from Edward M. Callaway.

Surgeries

Mice were anesthetized with a mixture of ketamine (*75 mg/kg*) and dexmedetomidine (*0.5 mg/kg*) and placed in a stereotaxic apparatus (David Kopf Instruments). All viruses were intracranially infused at a rate of 100 nL/min using a Harvard Apparatus syringe pump into the right NAc core with coordinates relative to bregma: anterior/posterior +1.5, medial/lateral +1.0, dorsal/ventral -4.4.

For 5 day cocaine and saline control groups, AAV-DIO-tdTomato-TVA and AAV-DIO-RVG were diluted in a 1:1:8 mixture with PBS. 250 nL of the mixture was injected unilaterally into the right NAc core 14 days prior to the first cocaine injection. Two days prior to the first saline habituation injection, 250 nL RV□G-eGFP(EnvA) was injected into the same location and the animal sacrificed 24 hours after the final cocaine or saline injection.

For challenge groups, 250 nL of the same diluted mixture of AAV-DIO-tdTomato-TVA and AAV-DIO-RVG was injected into the NAc core 2 days prior to the first saline habituation injection. Then, 8 days before the challenge shot, RV□G-eGFP(EnvA) was injected and the animal perfused 24 hours after challenge. These regiments were used to ensure the same duration of RV□G-eGFP(EnvA) expression between acute and challenge groups.

Locomotor sensitization

All tests were conducted in a 27.25 x 27.25 cm open field arena with white opaque walls. Prior to acute cocaine or saline administration, all groups were given two consecutive days of a single i.p. saline injection for habituation. After 2 days of habituation, animals were given one shot of either saline or cocaine (*20 mg/kg*) once per day for five consecutive days and locomotion monitored. Animals were re-weighed each day prior to behavior in order to

account for potential fluctuations in weight. After injections, animals were immediately placed into the open field arena and locomotion was monitored using BIOBSERVE automated behavioral analysis software for 15 minutes. Animals were all injected at the same time of day $\pm$ 2 hours and sacrificed 24 hours after final injection.

For challenge groups, animals were injected daily *20 mg/kg* cocaine for 5 consecutive days at the same time ± 2 hours and monitored for locomotor sensitization. The animals then underwent a 2 week withdrawal in their home cage in which no saline or cocaine was administered. After 2 weeks withdrawal, a single *20 mg/kg* cocaine or saline challenge shot was administered. Animals were sacrificed 24 hours later. All animals were singly housed.

Spine imaging and quantitation

Secondary dendrites were identified and imaged under an Olympus Fluoview FV1200 confocal microscope using a 100x objective (1.4 NA) at 3.5x zoom in which each pixel corresponded to 0.035 x 0.035 x 0.15 µm. Z-stacks were acquired on FV10-ASW software. A high sensitive gallium arsenide phosphide (GaAsP) detector was used in most cases to ensure complete visualization of spines. For more accurate quantitation and morphological analysis, images were post-processed with AutoQuant X3 deconvolution software prior to analysis.

Deconvolved images were imported and analyzed through NeuronStudio (25). The software allows for automated and unbiased spine counting and spine type classification; however, to ensure accurate counting and classification, a human experimenter manually verified each spine. All imaging and quantitation was performed blind to the experimental condition and genotype.

Whole brain input quantitation

Cell counting for whole-brain input quantitation was performed as previously described (Knowland et al., 2017). Briefly, mice were deeply anesthetized with isoflurane and intracardially perfused with PBS and post-fixed overnight with 4% paraformaldehyde at 4°C. After wash with PBS, the entire brain was sectioned into 60 µm coronal slices on a Leica VT1000s vibratome and immediately mounted on slides with DAPI mounting medium. Brains were imaged at 10X on an Olympus VS120 slide scanning microscope. Every third section across the antero-posterior axis was quantified and all GFP-positive neurons were counted with the exclusion of those at the injection site (all local inputs in NAc or starter cells were not included). Double-labeled starter cells were verified to primarily localize to NAc (Supplemental Figure S2.1). Animals were excluded if significant spread outside of NAc existed. Brain regions were determined by anatomical landmarks and based on Mouse Brain Atlas in Stereotaxic Coordinates, Franklin and Paxinos, 2nd edition. Quantitation is represented as total number of inputs in a brain region normalized to all inputs quantified across the entire brain (excluding injection site).

Brain regions were clustered into generalized umbrella regions for Figure 2.1 and further refined into subregions in Figure 2.2, Supplemental Figure S2.2. Brain areas with < 1% of total inputs were not included in graphs. If not delineated in Figure 2.2 or Supplemental Figure S2.2, the following brain regions were clustered as follows (all these regions exhibited inputs to NAc):

Olfactory areas: lateral olfactory tract, olfactory tubercle, piriform cortex, rostral ventral olfactory areas.

Pallidum: ventral pallidum, interstitial nucleus of the anterior commissure, ventral diagonal band, magnocellular preoptic nucleus, horizontal diagonal band, substantia innominata, lateral globus pallidus.

Hippocampus: CA1, CA3, Subiculum, amygdalohippocampal area.

Midbrain: ventral tegmental area, periaqueductal grey, dorsal raphe nucleus, median raphe nucleus, pedunculopontine tegmental nucleus, substantia nigra pars compacta, substantia nigra pars reticulata, interpeduncular nucleus, premammillary nucleus.

Results

Viral labeling of inputs to D1-MSNs and D2-MSNs in NAc

To identify all brain-wide monosynaptic inputs to either NAc D1- or D2-MSNs in an unbiased fashion, we used a viral tracing strategy that depends on a glycoprotein-deleted EnvA-pseudotyped rabies virus (Figure 2.1A*;* (Wickersham et al., 2007)). First, we expressed an exogenous avian receptor for the EnvA ligand (TVA) in either D1- or D2-MSNs by injecting adeno-associated virus (AAV) expressing TVA receptor together with the red fluorescent protein, tdTomato, (AAV-DIO-tdTomato-TVA) in a Cre-recombinase dependent manner into the NAc core of D1-Cre or A2A-Cre mice (for labelling of D1- or D2-MSNs, respectively). We simultaneously supplied the rabies virus glycoprotein (RVG) *in trans* by injecting AAV-DIO-RVG into the NAc core as well. After allowing adequate TVA-receptor and RVG expression, we injected glycoprotein-deleted EnvA-pseudotyped rabies conjugated to eGFP (EnvA-RV□G-eGFP) and after waiting an additional 7 days, processed the brains for unbiased brain-wide analysis of labeled neurons (Figure 2.1B*;* (Wall et al., 2010; Wickersham et al., 2007)). Using this method, double-labeled tdTomato- and GFP-positive neurons are

known as “starter neurons”, which are the postsynaptic partners of monosynaptically connected input neurons that are retrogradely labeled with only GFP (Figure 2.1C; Supplemental Figure S2.1).

Brain-wide quantitation of all inputs to NAc D1- or D2-MSNs revealed quantitatively similar proportions of labelled input neurons to both MSN cell types from general brain areas such as cortex and hippocampus, although D2-MSNs received proportionally, but not significantly, stronger inputs from the amygdala and pallidum (Figure 2.1C, D). Strikingly, we find that the NAc MSNs receive direct synaptic input from over 50 distinct subregions across the brain. Closer examination of subregions within the cortex revealed that D1-MSNs receive significantly more input from medial orbitofrontal cortex (MO), yet similar proportions of inputs from prelimbic (PrL) and infralimbic (IL) cortex (Figure 2.2A, B), components of the mPFC that have been implicated in playing important roles in cocaine use (Miller and Marshall, 2004; Winstanley et al., 2009). Interestingly, we found that across all individual brain regions, D2-MSNs received the greatest input from the PVT (Figure 2.2C, D), suggesting that this pathway may be more critical to the function of NAc D2-MSNs than previously thought (Neumann et al., 2016) (Figure 2.2C).

Since our tracing results revealed a strong trend of D2-MSNs receiving more input from the amygdaloid complex, we reasoned that different subdivisions of the amygdala may have a difference in their projection preference. However, closer examination revealed no statistical difference in the inputs from amygdalar subnuclei to either NAc D1- or D2-MSNs (Figure 2.2E, F). Additionally, no quantitative differences in the proportion of inputs onto D1- and D2-MSNs were observed in hypothalamic, pallidal, or hippocampal subregions

(Supplemental Figure S2.2A-C, data not shown). Collectively, we find that D1- and D2-MSNs receive overall quantitatively similar brain-wide inputs, with the lone exception that D1-MSNs receive significantly more input from MO cortex.

Input labeling at different stages of cocaine administration

Spines are small structural protrusions of dendrites known to be sites of excitatory synaptic contact due to the high concentrations of PSD-95 protein, AMPA receptors, and NMDA receptors. Disruption of their formation has been shown to lead to profound synaptic and functional deficits (Hering and Sheng, 2001; Vogl et al., 2015). Changes in spine density and composition may thus serve as a useful structural proxy for synaptic alterations at the cellular level. Previous reports indicate that dendritic spines of NAc D1- and D2-MSNs exhibit differential plasticity after chronic cocaine administration (Dobi et al., 2011; Dumitriu et al., 2012; MacAskill et al., 2012). It is unknown, however, whether this spine plasticity extends to neurons sending projections to the NAc and if this plasticity changes during the course of cocaine administration and withdrawal from cocaine. To address this topic, we used the viral strategy described above and also asked whether cocaine-induced spine plasticity in input neurons differed depending on whether they contacted D1- or D2-MSNs.

After NAc injection of the TVA and RVG expressing AAV's, mice received one of four treatments: 1) one injection of saline per day for five days (5d saline), 2) one injection of cocaine per day (20 mg/kg) for five days (5d cocaine), 3) daily injection of cocaine (20 mg/kg) for five days followed by a 2 week withdrawal period with a single injection of saline on withdrawal day 14 (saline challenge), 4) same as 3, except a single shot of cocaine (20 mg/kg) was given on withdrawal day 14 (cocaine challenge; Figure 2.3A, B). For treatments 1

and 2, NAc rabies virus injections were made the day before the 5 day treatment regime; for treatments 3 and 4, rabies virus was injected into the NAc on withdrawal day 7 (Figure 2.3A, B). These regimens were chosen because they are similar to those used previously to model some of the separate stages of drug abuse, discriminating the neural adaptations that occur during the initial stages of cocaine administration (acute cocaine) from those that occur during withdrawal (Kourrich et al., 2007; Rothwell et al., 2011).

After each cocaine or saline administration, animals' locomotor activity was assayed to test cocaine's efficacy and confirm the occurrence of behavioral sensitization (Sanchis-segura and Spanagel, 2006). As expected, locomotor activity increased over successive cocaine, but not successive saline, injections (Figure 2.3C, D). Locomotor activity in the cocaine challenge group remained elevated to levels comparable to the fifth day of acute cocaine administration, suggesting that despite two weeks of withdrawal, animals retained the neural adaptations that mediated the enhanced locomotor response to cocaine.

BLA neurons projecting to NAc MSNs are differentially affected by cocaine

Since differential changes in synaptic strength at the BLA, vHPC, and mPFC inputs to NAc D1- and D2-MSNs in response to cocaine administration have been previously described, we focused our spine analysis on these input regions (MacAskill et al., 2012, 2014). Additionally, since our tracing analysis identified the MO as one of the brain regions preferentially targeting D1-MSNs over D2-MSNs, we included this area in our analysis as well. Input neurons were easily identified by the presence of GFP, which allowed collection of high-resolution confocal z-stack images of secondary dendritic branches and high-precision quantitation of spine density and spine morphological subtype at different stages of cocaine

administration. Unbiased 3D spine morphometric analysis was performed using NeuronStudio software semi-automatically and manually double-checked and adjusted in a blinded fashion (Rodriguez et al., 2008).

We observed that BLA neurons projecting to NAc D1-MSNs, but not D2-MSNs exhibited distinct changes in dendritic spine density in all treatment groups that received cocaine (Figure 2.3E-G). Specifically, spine density of BLA neurons projecting to NAc D1-MSNs increased after 5 days of cocaine injections and continued to increase after 14 days of withdrawal with both saline and cocaine challenge injections (Figure 2.3E-G). In marked contrast, BLA neurons projecting to NAc D2-MSNs exhibited no significant changes in spine density due to cocaine administration (Figure 2.3I, J). These results parallel a previous report suggesting that BLA synapses on NAc D1-, but not D2-MSNs exhibit an increase in synaptic strength after 5 days of cocaine administration (MacAskill et al., 2014).

Spines can be further classified based on their individual morphology as thin, stubby, or mushroom-shaped, each thought to represent differing levels of maturation and plasticity (Hering and Sheng, 2001; Peters and Kaiserman-Abramof, 1970). Thus, we next analyzed whether specific spine subtypes in BLA neurons displayed dynamic plasticity in response to cocaine administration based on their target neurons in NAc. Five days of cocaine treatment followed by a withdrawal period resulted in a significant decrement in the relative number of thin spines and a concomitant increase in the number of mushroom spines in D1-MSN projecting BLA neurons (Supplemental Figure S2.3A). This may reflect maturation of thin spines to mushroom spines during the withdrawal period (Nimchinsky et al., 2002). Although no net change in overall spine density was observed in BLA neurons projecting to D2-MSNs,

a dynamic rearrangement of the relative proportion of the three spines subtypes was observed (Supplemental Figure S2.3B). This rearrangement of different spine subtypes may offset each other, thereby resulting in the observed lack of net change in average spine density. Together, these results demonstrate distinct types of cocaine-induced structural plasticity in NAc-projecting BLA neurons based on their target cell types in NAc.

Dendritic spine density increases in D1-MSN projecting vHPC neurons after 14 day withdrawal

Ventral hippocampal (vHPC) neurons projecting to NAc, mostly located in the subiculum subregion, have prominent apical and basal dendritic structures (Harris et al., 2001). It has been suggested that discrete regions of dendrites receive inputs from different brain structures and can exhibit differential plasticity (Losonczy et al., 2008; Makara et al., 2009). To account for this, we analyzed spine density in both subregions of these neurons' dendritic tree – apical and basal dendrites. Unlike NAc-projecting BLA neurons, 5 day acute cocaine administration caused no detectable changes in spine density on apical or basal dendrites of vHPC neurons projecting to either D1-MSNs or D2-MSNs (Figure 2.4). However, after cocaine administration following two weeks of withdrawal we observed an increase in spine density in both apical and basal dendrites of vHPC neurons projecting to D1-MSNs, but not to D2-MSNs (Figure 2.4). We observed a trend towards a reduction in the relative proportion of stubby spines in vHPC apical dendrites projecting to D1-, but not D2-MSNs, after 2 week withdrawal from cocaine; however, this did not reach significance (Supplemental Figure 3C, D). Similarly, basal dendrites in vHPC neurons projecting to D1-MSNs exhibited a significant decrease in the proportion of stubby spines after the 14 day

withdrawal period in both challenge groups suggesting that this dynamic spine subtype remodeling may not depend on the NAc cell-type it targets (Supplemental Figure S2.3E, F). Thus, similar to NAc-projecting BLA neurons, dendrites on vHPC neurons display differential structural plasticity dependent on the target NAc cell-type.

Cocaine administration induces a decrease in spine density of PrL neurons projecting to D1-MSNs, but not D2-MSNs

Like vHPC neurons, PrL neurons projecting to NAc also have long, elaborated dendritic structures along the different layers of prelimbic cortex (Radley et al., 2008). Since different layers of the cortex receive inputs from different brain areas, we again separately examined apical dendritic spines, which are located in the lower, more superficial layers of cortex, and basal dendrites located in the higher, deeper layers of cortex. In contrast to NAc-projecting BLA and vHPC neurons, cocaine administration followed by two weeks of withdrawal induced a decrease in spine density in apical dendrites of PrL neurons innervating D1-MSNs (Figure 2.5A-C). Although we observed a trend, 5 days of cocaine administration was not sufficient to induce a reduction in apical spine density in this group. Despite observing a decrease in average spine density, these changes were not accompanied by significant changes in spine subtypes (Supplemental Figure S2.4A).

While we observed changes in apical dendrite spine density of PrL neurons projecting to D1-MSNs in response to cocaine administration, no change was observed in D2-MSN projecting PrL neuronal apical dendrites (Figure 2.5D, E). Interestingly, despite no net changes in density, we observed dynamic structural reorganization of individual spines on apical dendrites evidenced by alterations in thin and stubby spine ratios: apical dendrites

exhibited a decrease in thin spines after 5 days cocaine administration and a proportional increase in stubby spines (Supplemental Figure S2.4B).

Basal dendrites on D1-MSN projecting PrL neurons displayed a more pronounced effect, as the average spine density decreased after 5 days cocaine exposure and persisted after 14 days of withdrawal with both saline and cocaine challenge shots (Figure 2.5F-H). However, consistent with the apical dendrite group, this was not accompanied by any changes in spine subtype composition (Supplemental Figure S2.4C). On the other hand, basal dendrites on D2-MSN projecting PrL neurons exhibited no significant changes in spine density but, similar to apical dendrites, showed dynamic spine subtype remodeling (Figure 2.5I, J; Supplemental Figure 4D). A decrement in thin spines was observed along with an increase in stubby spines after 5 days cocaine injection that persisted after withdrawal and a saline challenge shot (Supplemental Figure 4D). This increase in stubby spines may serve to offset the reduction in thin spines and could explain why we observed no significant difference in average spine density.

Cocaine administration decreases spine density in dendrites of MO inputs to both D1-MSNs and D2-MSNs

The MO and the PrL, collectively known as the medial prefrontal cortex, are known to exhibit different anatomical connections and functions (Boulougouris et al., 2007; Capriles et al., 2003; Volkow and Fowler, 2000). Our anatomical analysis revealed that D1-MSNs received proportionally more input from NAc-projecting MO neurons compared to D2-MSNs (Figure 2.2A). Furthermore, previous reports have shown that D1-, but not D2-receptor antagonist infusion into the MO blocks cocaine seeking (Cosme et al., 2018). For these

reasons, we decided to subdivide these regions in our analysis to see if cocaine administration may differentially affect them. Spine quantitation revealed a significant reduction in density of both basal and apical dendrites in MO neurons projecting to D1-MSNs after 5 days of cocaine administration, similar to what was observed in the PrL cortex (Figure. 6A-C, F-G). However, unlike PrL neurons projecting to D2-MSNs which showed no change, we observed a significant reduction in spine density of MO neurons projecting to D2-MSNs in both apical and basal dendrites after 5 days of cocaine administration as well (Figure 2.6D, E, I, H). Interestingly, while the MO was an area we identified as sending more proportional inputs to D1-MSNs, this was the only brain region projecting to D2-MSNs in which we measured significant changes in spine density (Figure 2.6I, H). This reduction is driven primarily through reduced mushroom-type spines (Supplemental Figure S2.4E-H). The decrease in spine density after acute cocaine administration was not sustained after 14 days of withdrawal, as both saline and cocaine challenge groups had spine density levels similar to saline controls. Collectively, these data indicate that MO neurons projecting to NAc show a non-discriminatory decrease in spine density after 5 days cocaine administration.

Discussion

Brain-wide anatomical organization of NAc D1- and D2-MSN specific inputs

Here, using virus-mediated circuit mapping together with transgenic mice expressing Cre-recombinase in specific cell types, we characterize the brain-wide distributions of afferent inputs to D1-MSNs and D2-MSNs in the NAc core. While previous studies have provided a basic framework of synaptic organizations of D1- and D2-MSNs and their different roles, no study has provided a thorough delineation of brain-wide inputs to specific cell types in NAc

(Creed et al., 2016; MacAskill et al., 2012, 2014). We find that over 50 distinct brain subregions provide direct synaptic inputs onto NAc MSNs, a finding that presumably reflects the critical importance of the NAc in integrating very diverse types of information in the service of its role in translating motivation into action (Mogenson et al., 1980).

Our whole-brain input tracing with rabies virus identifies many of the same principal input brain regions as previous studies using different retrograde tracers (Fluorogold and wheatgerm agglutinin) such as the mPFC, vHPC, BLA, VTA, and PVT (Brog et al., 1993; Novejarque, 2011; Phillipson and Griffiths, 1985) and confirmed via anterograde tracer injection (50). While the mPFC, vHPC, and BLA are the most heavily studied inputs to the nucleus accumbens, our brain-wide analysis revealed that the paraventricular nucleus of the thalamus (PVT) sends proportionally more input to the NAc than any other brain area, as defined by total number of input cells. However, we emphasize that this measure does not take into account the relative synaptic strength of these input brain regions onto the NAc. While recent studies have begun to focus on the PVT-NAc circuit (Neumann et al., 2016; Su and Bentivoglio, 1990; Wunsch et al., 2017), future studies are required to further uncover its functional roles, particularly as it pertains to differential plasticity compared to mPFC, vHPC, and BLA afferents to the NAc. Indeed, recent studies have reported separate changes in synaptic plasticity in the PVT-NAc circuit after cocaine withdrawal compared to BLA- and mPFC-NAc circuits (Joffe and Grueter, 2016; Neumann et al., 2016).

Despite the extensive literature reporting distinct synaptic effects and functional roles of D1- and D2-MSNs (Joffe and Grueter, 2016; Khibnik et al., 2016; MacAskill et al., 2014), our trans-synaptic tracing surprisingly demonstrates largely non-discriminatory monosynaptic

innervation to the two-different populations in NAc core across the antero-posterior axis of the brain (Figure 2.1). One exception is that D1-MSNs receive significantly more inputs than D2-MSNs from NAc-projecting MO neurons (Figure 2.2A, B). The unexpected large degree of similarity in regards to inputs to D1- and D2-MSNs may in part reflect the fact that a substantial fraction of D1-MSNs show the same output projection pattern as that of D2-MSNs, sending projections to the ventral pallidum (VP) rather than to the ventral tegmental area (VTA) (Kupchik et al., 2015). These populations of VP-projecting D1-MSNs and D2-MSNs may share similar brain-wide inputs, in contrast to VTA-projecting D1-MSNs. Further analysis using additional methods will be required to differentiate inputs to distinct populations of D1-MSNs projecting to VTA or VP (Schwarz et al., 2015).

Curiously, we find that D1- and D2-MSNs receive small amounts of input from the central amygdala (CeA). While previous studies have reported that the CeA sends small amounts of input to the NAc in comparison to the BLA and other regions (Phillipson and Griffiths, 1985), most studies have noted a distinct absence of this pathway (Brog et al., 1993; Novejarque, 2011). The bed nucleus of the stria terminalis (BNST) lies immediately adjacent to the posterior border of the NAc and receives significant input from the CeA (Dong et al., 2001). Furthermore, cells in the oval subnuclei of the BNST can be labeled using the same Drd1a-Cre animal used in the this study (Kim et al., 2013). Thus, it is possible that viral leakage of $Drd1a^{+}$ starter cells in the BNST could account for the labeling we see in the CeA. Despite this, since we see CeA labeling in A2A-Cre animals as well and are careful to exclude animals that exhibit significant starter cell leakage we do not believe this to be the case. However, we note that the posterior end of the NAc and anterior portion of the BNST come into almost continuous apposition of each other around the anterior commissure. This area

does express both Drd1a and A2A (Allen Brain Atlas), and thus we believe that while CeA input labeling was much less robust than that of the BLA, a proportion of these may be due to this anterior BNST leak.

Finally, previous reports have identified separate input patterns, functions, and structural changes based on whether MSNs are located in the NAc core, medial shell, or lateral shell (Dumitriu et al., 2012; Lammel et al., 2008). Since our circuit analysis is limited to inputs to the NAc core, it remains plausible that significant differences in afferent organization between D1- and D2-MSNs exist in the NAc medial or lateral shell. Future work will be required to dissect the input patterns to D1- and D2-MSNs in separate sub-compartments of the NAc.

Cocaine administration-induced stage-specific structural plasticity in afferent inputs to NAc

The progression to recurrent drug use initiates as recreational use, which eventually evolves into compulsive use, suggesting that distinct brain areas are engaged at different stages of drug addiction. Although it has been proposed that adaptations in upstream excitatory neurons projecting to NAc may contribute to the long-lasting drug-induced neural adaptations in NAc (Britt et al., 2012), how those inputs are engaged at different stages of cocaine administration has not been fully addressed. We find that both repeated exposure to cocaine and exposure followed by a withdrawal period elicits robust but distinct changes in structural plasticity in neurons upstream of NAc MSNs. These changes are dependent on three key factors: 1) the brain structure which monosynaptically projects to the NAc, 2) the cell-

type within the NAc that is targeted and, 3) the stage of cocaine exposure at which the spine analysis is performed..

In our first analysis we find a selective increase in spine density in BLA neurons projecting to D1-MSNs, but not D2-MSNs (Figure 2.3). Since spines are putative sites of excitatory synaptic contact, we may expect that an increase in spine density enhances spiking activity of these neurons. This observation is consistent with recent work showing a selective increase in BLA innervation of D1-MSNs by repeated cocaine administration (MacAskill et al., 2014). Even after 14 days of abstinence structural changes persisted in D1-MSN-projecting BLA neurons suggesting that spine changes represent a lasting adaptation to repeated cocaine use and not just an acute, transient process. Future examination of how manipulation of spine dynamics may affect cocaine seeking are required. Furthermore, since BLA neurons have been shown to encode both rewarding and aversive signals (Kim et al., 2017; Beyeler et al., 2016), it is possible that distinct BLA neuronal subpopulations differentially project to D1-MSNs and D2-MSNs. Further study is needed to examine the molecular and functional identity of BLA neurons that target distinct neuronal populations in NAc.

Second, the spine density of vHPC neurons projecting to D1-MSNs, but not to D2-MSNs, showed a significant increase only when animals were challenged by cocaine after 14 days withdrawal. Previous reports show that silencing vHPC neurons projecting to the NAc inhibits cocaine induced locomotor sensitization, and that cocaine administration reduces excitatory synaptic drive at the vHPC-to-D2-MSN synapse (Britt et al., 2012; MacAskill et al., 2014). Thus, the increase in spine density of vHPC neurons projecting to D1-MSNs may

lie upstream of synaptic changes at the NAc MSN synapse during periods of cocaine seeking or challenge. This idea is also supported by studies showing that vHPC inputs to NAc are potentiated by withdrawal after repeated exposure to cocaine (Britt et al., 2012).

Third, prefrontal cortical neurons in both MO and PrL showed a significant reduction in their spine density following 5 days of cocaine administration. These findings are consistent with recent results using high resolution two-photon imaging of cortical neurons in chronic cocaine administration (Muñoz-Cuevas et al., 2013). However, this report as well as our data are not consistent with previous findings with Golgi-staining preparation (Li et al., 2004; Robinson, 1999; Robinson et al., 2001). This discrepancy may be due to the nature of Golgi staining which randomly and sparsely labels neurons without a clear known mechanism together with low-magnification imaging. In contrast, our methods examine specific cortical populations projecting to distinct cell types within the NAc.

The overall increase in spine density in BLA and vHPC neurons and decrease in prefrontal (PrL and MO) spine density in response to cocaine administration may parallel the previously defined roles for these projections to the NAc. For example, since the BLA appears to encode emotional valence, it is possible that the acute increase in spine density is necessary to form the initial affective response to cocaine, which often persists after withdrawal. On the other hand, vHPC spine density only increased 14 days after withdrawal and after a cocaine challenge. Since the vHPC is thought to link experience with contextual information (Rogers and See, 2007) it is plausible that the 14 day withdrawal period is required for strengthening the vHPC-NAc pathway to maintain the contextual representation of cocaine seeking induced during the initial 5 day cocaine administration. Finally, the

decrease in spine density in the mPFC immediately following the 5 day cocaine administration period may reflect that in the developing stages of addiction, individuals experience a loss of top-down control and aberrant action-outcome evaluation, both of which are associated with mPFC activity (Volkow and Fowler, 2000).

What then is driving the spine changes of these regions? In addition to sending inputs to the NAc, the MO, PrL, BLA, and vHPC also send and receive reciprocal connections amongst themselves. The vHPC is known to send efferents to the BLA and PrL, PrL sends and receives reciprocal connections to and from the BLA, and goal-directed valuation depends on BLA input to the MO (Hoover and Vertes, 2007; Pitkanen et al., 2006; Schoenbaum et al., 2003). This network of reciprocal connections and interconnected regions makes it difficult to ascertain which changes beget which. Recent computational work has gone towards understanding the directionality of neural activity between the BLA and PrL regions during behavior (Burgos-Robles et al., 2017). More studies employing these techniques may shed light on which kind of changes, both physiologically and structurally, lie upstream or downstream of each other.

In general, we find that spines on D1-MSN projecting neurons appear to be more plastic than D2-MSN projecting neurons in all the brain structures that we examined. This likely reflects the different roles that these two major cell types play in mediating the behavioral functions of the NAc. However, it is important to note that our viral tracing strategy does not eliminate the possibility that individual neurons in the mPFC, BLA, or vHPC may project to both D1- and D2-MSNs. Thus, labeling D1-MSN projecting neurons does not exclude the possibility that these neurons may also project to D2-MSNs as well.

Unfortunately, until we are able to carry out single neuronal tracing with an anterograde transsynaptic tracer or retrogradely label two cell-type specific populations within the same animal, we cannot entirely eliminate this possibility.

The fact that we see D1-MSNs consistently displaying more structural plasticity than D2-MSNs across brain regions supports, but does not confirm, the fact that we are likely labeling distinct populations. Previous reports have also shown that stimulating vHPC inputs to the NAc while recording from adjacent D1- and D2-MSNs elicits separate spike probabilities (MacAskill et al., 2012), possibly due to separate populations of presynaptic vHPC neurons. Furthermore, differences in the frequency of quantal excitatory post synaptic currents from the BLA between D1- and D2-MSNs after cocaine administration were measured, suggesting a presynaptic mechanism and the likelihood that these neurons receive inputs from separate populations (MacAskill et al., 2014).

Our results highlight the pressing need for increased specificity in regards to cell-type, brain-area, and stage-specific aspects of neural adaptations in response to drugs of abuse such as cocaine. While the majority of studies have focused on structural and synaptic adaptations within NAc MSNs, our results demonstrate that potentially important structural changes occur in upstream brain regions. Clearly, further study of the many different upstream neuronal populations that influence NAc activity is needed for a more comprehensive understanding of the neural adaptations underlying complex neuropsychiatric disorders such as addiction.

Acknowledgements and Disclosures

We thank X. Wang for technical assistance, H. Pribiag and Lim laboratory for comments on manuscript. This work was supported by Klingenstein foundation, Searle scholar program (Kinship foundation), Whitehall foundation, and grants from NIH (DA040030, DA008227). V.L. is also supported by Anandamahidol Foundation Fellowship.

The authors report no biomedical financial interests or potential conflicts of interest.

Article Information

From the Neurobiology Section in the Division of Biological Sciences (CB, MW, VL, BKL) and the Neurosciences Graduate Program (DK) at the University of California, San Diego, La Jolla, California; and the Nancy Pritzker Laboratory in the Department of Psychiatry and Behavioral Sciences at Stanford University School of Medicine, Palo Alto, California (KWH, RCM).

Address correspondence to Byung Kook Lim, Ph.D., Department of Biological Sciences, University of California, San Diego, 9500 Gilman Dr. La Jolla, CA 92093; email: bklim@ucsd.edu.

CB and DK contributed equally to this work.

Chapter II, in full, is a reprint of Barrientos C, Knowland D, Wu MJ, Lilascharoen V, Huang KW, Malenka, RC, Lim BK. *Cocaine induced structural plasticity in input regions to distinct cell types in nucleus accumbens*. Biological Psychiatry (2018): in press. The dissertation author was the primary investigator and author of this paper with equal contribution from Cindy Barrientos. This work was included with generous consent by all co-authors.

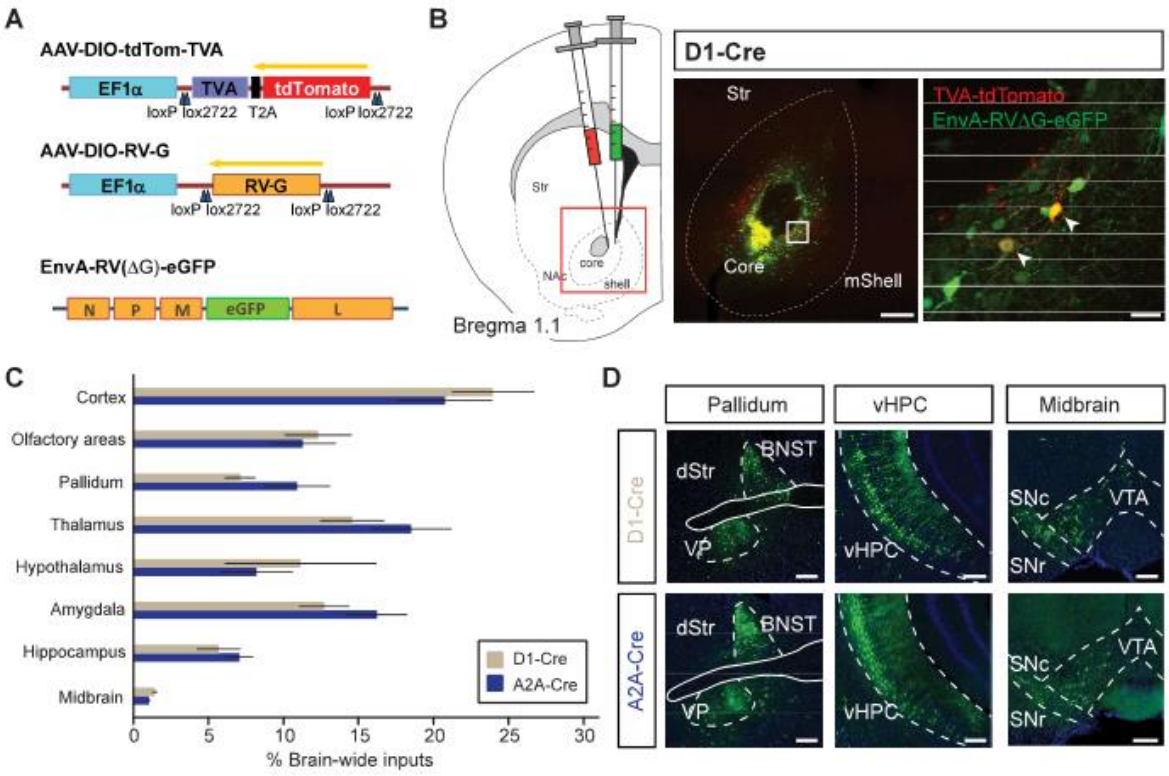

Figure 2.1. Brain-wide monosynaptic inputs to NAc D1- and D2-receptor expressing medium spiny neurons (D1-MSNs, D2-MSNs, respectively)

(*A*) (*Left*) Viral vectors used to express Cre-dependent TVA receptor, rabies glycoprotein, and G-deleted EnvA-pseudotyped rabies virus (AAV-DIO-tdTom-TVA, AAV-DIO-RV-G, EnvA-RV(ΔG)-eGFP, respectively). (*Right*) Schematic of viral injections targeting NAc core.

(*B*) Injection schematic. D1-Cre or A2A-Cre mice were unilaterally injected with viruses in (*A*) into nucleus accumbens (NAc) core (left). Representative images of injection site showing co-localized 'starter cells' (right). Box denotes area of zoom. Scale bar, 200 μm (left), 25 μm (right)

(*C*) Brain-wide quantitation of inputs to D1- and D2-MSNs (D1-Cre and A2A-Cre, respectively; n = 7 for each genotype). See methods for how brain regions were clustered.

(*D*) Representative images for different input brain regions. Green cells represent individual neurons sending monosynaptic input to D1- (top row) or D2-MSNs (bottom row) in the NAc. Scale: 250 um

Abbreviations: BNST, bed nucleus stria terminalis; VP, ventral pallidum; dStr, dorsal striatum; SNc, substantia nigra pars compacta; SNr, substantia nigra pars reticulate; VTA, ventral tegmental area.

Figure 2.2. D1- and D2-receptor expressing medium spiny neurons (D1-MSNs, D2-MSNs, respectively) exhibit different cortical input patterns

(*A*) Quantitation of inputs from subregions within the cortex. Two-tailed t-test, t = 3.38, * P < .05.

(*B*) Representative images of inputs from anterior cortical regions. D1-MSNs receive proportionally more input from medial orbitofrontal cortex (MO) than D2-MSNs.

(*C*) Quantitation of individual thalamic subregion inputs to D1- and D2-MSNs.

(*D*) Representative images of inputs from midline thalamic areas.

(*E*) Quantitation of inputs from amygdala subregions. Inset depicts percentage of all central amygdala inputs that localize to subdivisions within central amygdala (CeA) and representative image.

(*F*) Representative images of amygdala inputs to D1- and D2-MSNs.Abbreviations: 3V, 3rd ventricle; LO, lateral orbitofrontal cortex; VO, ventral orbitofrontal cortex; PrL: prelimbic cortex; IL, infralimbic cortex; CM, central medial thalamic nucleus; Re, nucleus reuniens; Rh, rhomboid thalamic nucleus; MD, mediodorsal thalamic nucleus; Pf, parafascicular nucleus; EAM, extended amydala; CeC, capsular nucleus of CeA; CeM, medial nucleus of CeA; CeL, lateral nucleus of CeA. All scale bars: 250 μm.

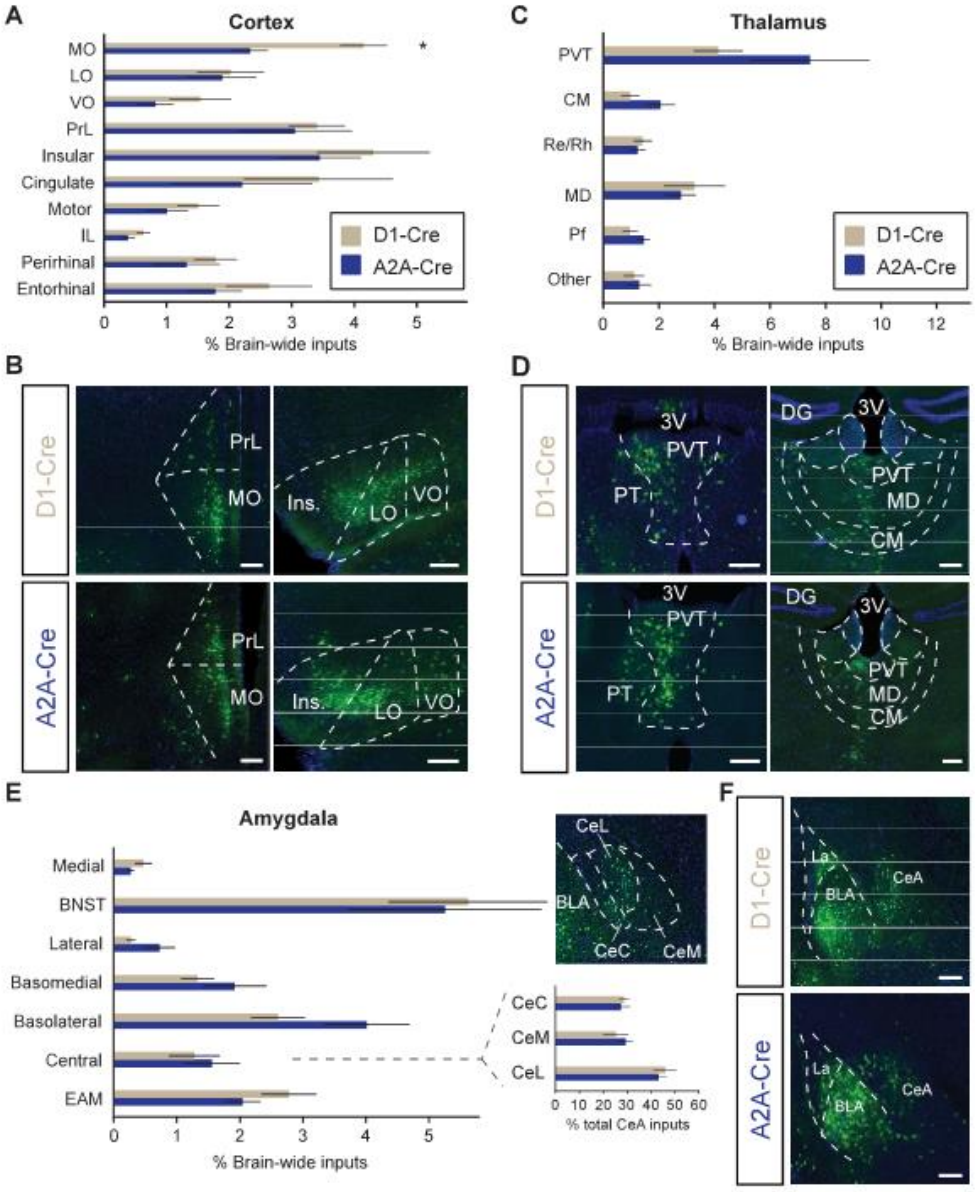
A
Cortex
MO
LO
VO
PrL
Insular
Cingulate
Motor
IL
Perirhinal
Entorhinal
*
D1-Cre
A2A-Cre
0 1 2 3 4 5
% Brain-wide inputs
C
Thalamus
PVT
CM
Re/Rh
MD
Pf
Other
D1-Cre
A2A-Cre
0 2 4 6 8 10 12
% Brain-wide inputs
B
D1-Cre
A2A-Cre
PrL
MO
Ins.
LO
VO
D
3V
PVT
PT
DG
MD
CM
E
Amygdala
Medial
BNST
Lateral
Basomedial
Basolateral
Central
EAM
0 1 2 3 4 5
% Brain-wide inputs
CeL
BLA
CeC
CeM
0 10 20 30 40 50 60
% total CeA inputs
F
D1-Cre
A2A-Cre
La
BLA
CeA

Figure 2.3. Stage- and cell-type specific structural plasticity in basolateral amygdala (BLA) inputs to nucleus accumbens (NAc)

(*A* and *B*) Experimental timeline of viral injections and cocaine/saline administrations for 5 day administration group (*A*) and 5 day cocaine with 2 week withdrawal followed by either saline or cocaine challenge injection (*B*).

(*C* and D) Both genotypes exhibit locomotor sensitization with successive injections of cocaine (*C*) that persists after 2 weeks withdrawal with a cocaine, but not saline, challenge shot (*D*).

(*E*) Representative confocal images of dendritic spines of BLA neurons projecting to D1- and D2-receptor expressing medium spiny neurons (D1-MSNs, D2-MSNs, respectively) in NAc at separate stages of cocaine administration. Scale: 1 μm.

(*F*) Cumulative distribution plot of spine density of all dendrites imaged in BLA projecting to D1-MSNs. n = 48, 50, 45, 48 dendrites for 5d S (5 mice), 5d C (5 mice), 14WD S (6 mice), 14WD C (6 mice) groups, respectively. $p < .05$ for 5d S – 5d C and 5d S – 14WD C. $p < .001$ for 5d S – 14WD S; K-S test.

(*G*) Average spine densities at separate stages of cocaine administration in BLA dendrites projecting to D1-MSNs. K-S test, dendrites sampled as in (*F*).

(*H*) Cumulative distribution plot of spine density of all dendrites imaged in BLA projecting to D2-MSNs. n = 47, 47, 35, 44 dendrites for 5d S (4 mice), 5d C (5 mice), 14WD S (5 mice), 14WD C (6 mice), respectively.

(*I*) Average spine densities at separate stages of cocaine administration in D2-MSN projecting BLA neuronal dendrites. K-S test, dendrites sampled as in (*H*).

All data in (*G* and *I*) presented as mean $\pm$ SEM. Abbreviations: 5d S, 5 day acute saline; 5d C, 5 day acute cocaine; 14WD S, 14 day withdrawal saline challenge; 14WD C, 14 day withdrawal cocaine challenge. K-S test * $P < .05$, *** $P < .001$.

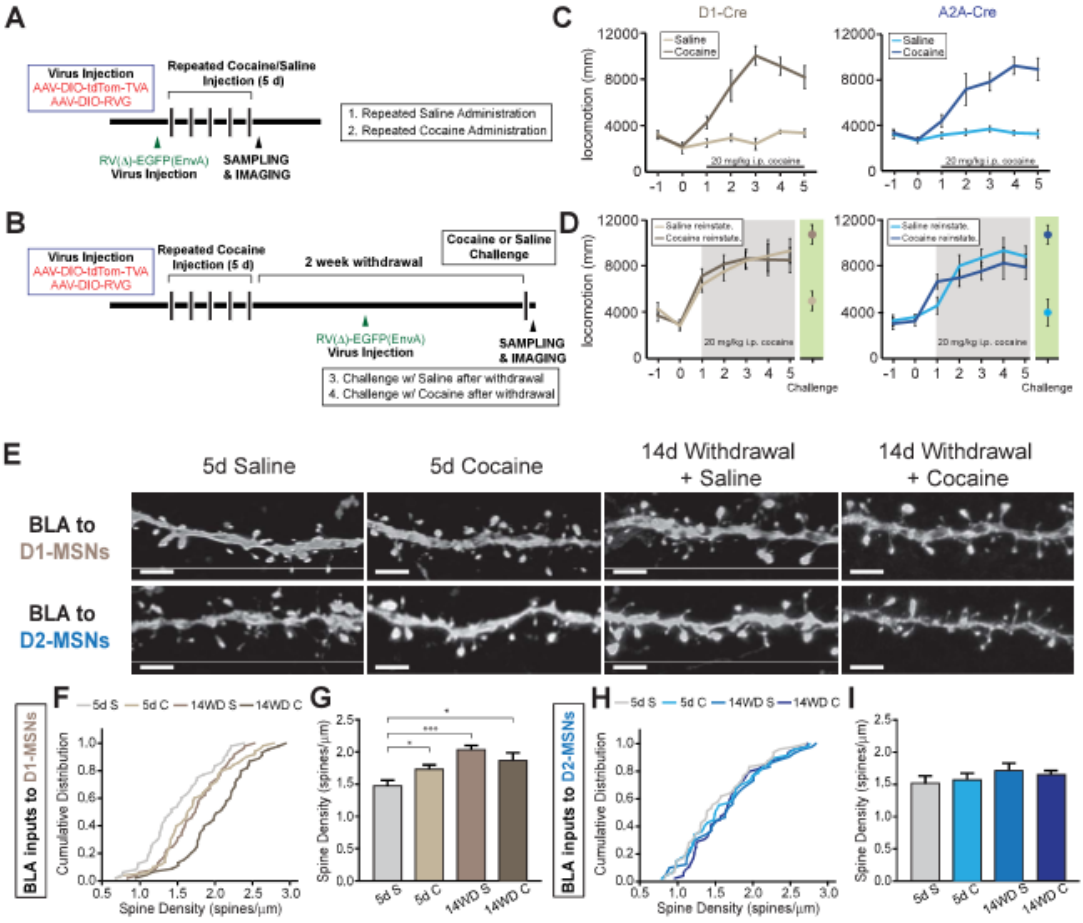
A
Virus Injection
AAV-DIO-tdTom-TVA
AAV-DIO-RVG
Repeated Cocaine/Saline
Injection (5 d)
1. Repeated Saline Administration
2. Repeated Cocaine Administration
RV(Δ)-EGFP(EnvA)
Virus Injection
SAMPLING
& IMAGING
B
Virus Injection
AAV-DIO-tdTom-TVA
AAV-DIO-RVG
Repeated Cocaine
Injection (5 d)
2 week withdrawal
Cocaine or Saline
Challenge
RV(Δ)-EGFP(EnvA)
Virus Injection
SAMPLING
& IMAGING
3. Challenge w/ Saline after withdrawal
4. Challenge w/ Cocaine after withdrawal
C
D1-Cre
A2A-Cre
Saline
Cocaine
locomotion (mm)
20 mg/kg i.p. cocaine
D
Saline reinstate
Cocaine reinstate
Challenge
E
5d Saline
5d Cocaine
14d Withdrawal
+ Saline
14d Withdrawal
+ Cocaine
BLA to
D1-MSNs
BLA to
D2-MSNs
F
5d S
5d C
14WD S
14WD C
BLA inputs to D1-MSNs
Cumulative Distribution
Spine Density (spines/μm)
G
Spine Density (spines/μm)
H
BLA inputs to D2-MSNs
I

Figure 2.4. Ventral hippocampal (vHPC) neurons projecting to D1-receptor expressing medium spiny neurons (D1-MSNs) exhibit increased dendrite spine density after withdrawal

(*A*) Representative images of apical dendritic spines in vHPC neurons projecting to NAc D1- and D2-receptor expressing MSNs (D2-MSNs) at different stages of cocaine administration. Scale: 1 μm .

(*B*) Cumulative distribution plots of apical vHPC dendrite density projecting to D1-MSNs. n = 37, 26, 25, 28 for 5d S (5 mice), 5d C (5 mice), 14WD S (5 mice), 14WD C (5 mice), respectively. $p < 0.01$ 5d S – 14WD C; Kolmogorov-Smirnov (K-S) test.

(*C*) Average spine densities of apical vHPC dendrites projecting to D1-MSNs at separate stages of cocaine administration. K-S test, dendrites sampled as in (*B*).

(*D*) Cumulative distribution plots of apical vHPC dendrite density projecting to D2-MSNs. n = 27, 33, 26, 25 for 5d S (4 mice), 5d C (5 mice), 14WD S (5 mice), and 14WD C (4 mice), respectively.

(*E*) Average spine densities of apical vHPC dendrites projecting to D2-MSNs at separate stages of cocaine administration. K-S test, dendrites sampled as in (*D*).

(*F*) Representative images of basal dendritic spines in vHPC neurons projecting to NAc D1- and D2-MSNs at different stages of cocaine administration. Scale: 1 μm.

(*G*) Cumulative distribution plots of basal vHPC dendrite density projecting to D1-MSNs. n = 46, 30, 20, 32 dendrites for 5d S (5 mice), 5d C (4 mice), 14WD S (4 mice), 14WD C (5 mice), respectively. $p < 0.001$ 5d S – 14WD C; K-S test.

(*H*) Average spine densities of basal vHPC dendrites projecting to D1-MSNs at separate stages of cocaine administration. K-S test, dendrites sampled as in (*G*).

(*I*) Cumulative distribution plots of basal vHPC dendrite density projecting to D2-MSNs. n = 29, 35, 25, 30 dendrites for 5d S (4 mice), 5d C (5 mice), 14WD S (4 mice), and 14WD C (5 mice), respectively.

(*J*) Average spine densities of basal vHPC dendrites projecting to D2-MSNs at separate stages of cocaine administration. K-S test, dendrites sampled as in (*I*).

Data in *(C, E, H, J)* presented as mean $\pm$ SEM. Abbreviations: 5d S, 5 day acute saline; 5d C, 5 day acute cocaine; 14WD S, 14 day withdrawal saline challenge; 14WD C, 14 day withdrawal cocaine challenge. K-S test ** $P < .01$.

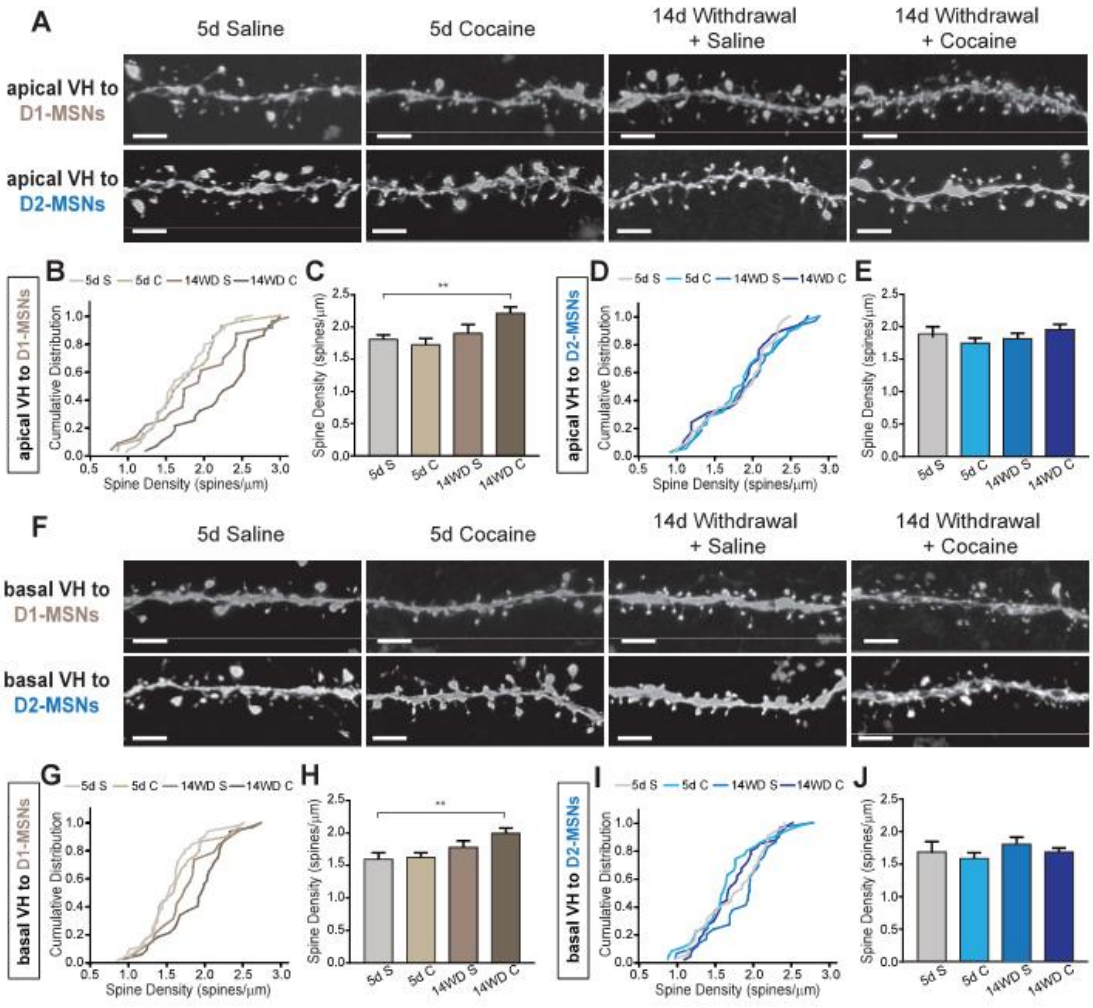
A
5d Saline
5d Cocaine
14d Withdrawal + Saline
14d Withdrawal + Cocaine
apical VH to D1-MSNs
apical VH to D2-MSNs
B
C
D
E
5d S
5d C
14WD S
14WD C
apical VH to D1-MSNs
apical VH to D2-MSNs
Cumulative Distribution
Spine Density (spines/µm)
F
basal VH to D1-MSNs
basal VH to D2-MSNs
G
H
I
J

Figure 2.5. Dendritic spine density of prelimbic cortex subregion (PrL) of medial prefrontal cortical (mPFC) neurons projecting to D1-receptor expressing, but not D2-receptor expressing medium spiny neurons (D1-MSN, D2-MSN, respectively) decrease after 14 day withdrawal.

(*A*) Representative confocal images of PrL neuronal apical dendrites and spines projecting to D1- and D2-MSNs. Scale: 1 μm

(*B*) Cumulative distribute plots of individual apical PrL dendrites projecting to D1-MSNs at different stages of cocaine administration. n = 44, 47, 36, 38 dendrites from 5d S (5 mice), 5d C (5 mice), 14WD S (5 mice), 14WD C (6 mice), respectively. $p < .05$ for 5d S – 14WD S, 5d S – 14WD C; Kolmogorov-Smirnov (K-S) test.

(*C*) Average spine densities of apical dendrites for D1-MSN projecting PrL neurons. K-S test, dendrites sampled as in (*B*).

(*D*) Cumulative distribute plots of individual apical PrL dendrites projecting to D2-MSNs at different stages of cocaine administration. n = 40 (5 mice), 37 (5 mice), 25 (4 mice), 40 (5 mice) dendrites for respective groups.

(*E*) Average spine densities of apical dendrites for D2-MSN projecting PrL neurons. K-S test, dendrites sampled as in (*D*).

(*F*) Representative confocal images of PrL neuronal basal dendrites and spines projecting to D1- and D2-MSNs. Scale: 1 μm.

(*G*) Cumulative distribute plots of individual D1-MSN projecting basal PrL dendrites at different stages of cocaine administration. n = 45, 45, 42, 40 dendrites from 5d S (5 mice), 5d C (5 mice), 14WD S (5 mice), 14WD C (6 mice), respectively. $P < .001$ for 5d S – 5d C, 5d S – 14WD C; $p < .05$ 5d S – 14WD S; all tested on K-S test.

(*H*) Average spine densities of basal dendrites for D1-MSN projecting PrL neurons. K-S test, dendrites sampled as in (*G*).

(*I*) Cumulative distribute plots of individual D2-MSN projecting basal PrL dendrites at different stages of cocaine administration. n = 30 (4 mice), 37 (5 mice), 26 (4 mice), 44 (5 mice) dendrites for respective groups.

(*J*) Average spine densities of basal dendrites for D2-MSN projecting PrL neurons. K-S test, dendrites sampled as in (*I*).

Data in *(C, E, H, J)* presented as mean $\pm$ SEM. Abbreviations: 5d S, 5 day acute saline; 5d C, 5 day acute cocaine; 14WD S, 14 day withdrawal saline challenge; 14WD C, 14 day withdrawal cocaine challenge. K-S test * $P < .05$, ** $P < .01$.

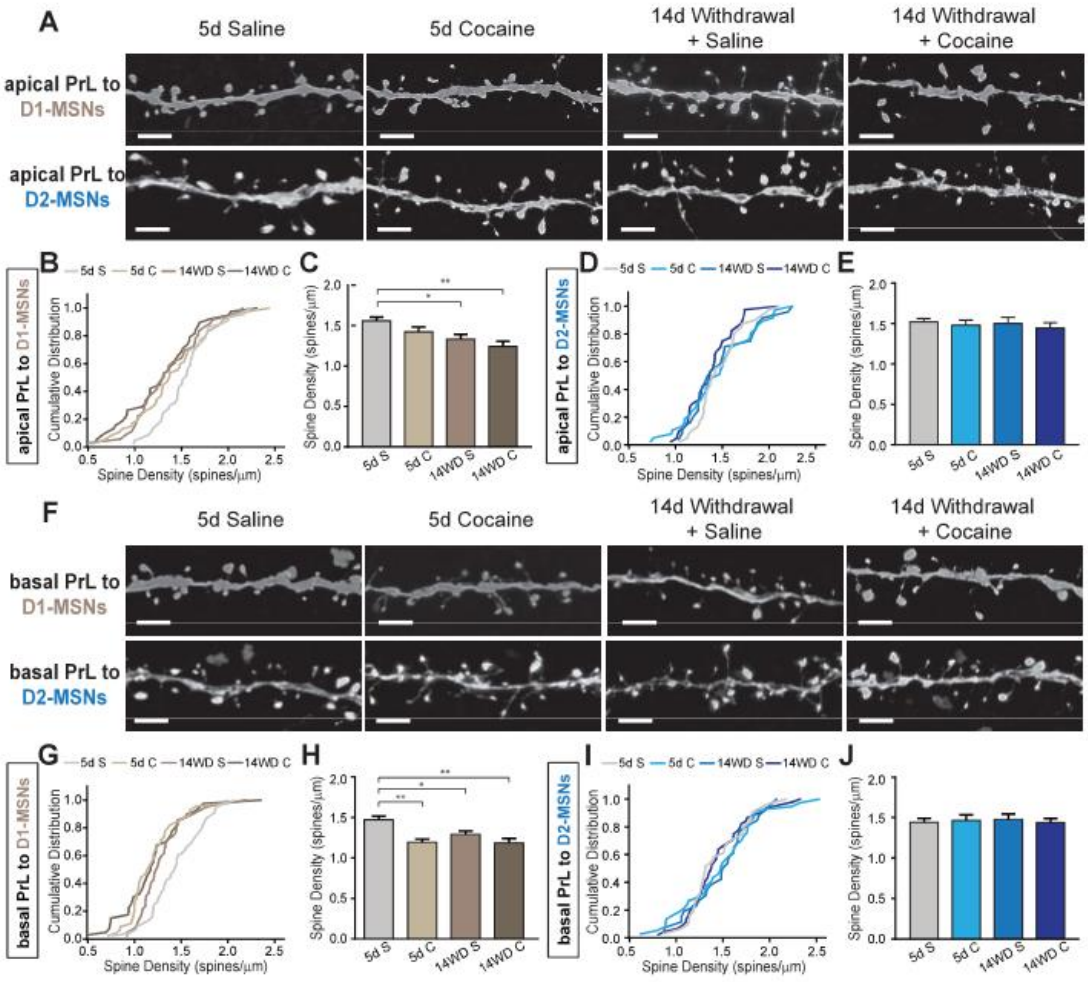
A
5d Saline
5d Cocaine
14d Withdrawal + Saline
14d Withdrawal + Cocaine
apical PrL to D1-MSNs
apical PrL to D2-MSNs
B
5d S
5d C
14WD S
14WD C
apical PrL to D1-MSNs
Cumulative Distribution
Spine Density (spines/µm)
C
Spine Density (spines/µm)
D
apical PrL to D2-MSNs
E
F
basal PrL to D1-MSNs
basal PrL to D2-MSNs
G
basal PrL to D1-MSNs
H
I
basal PrL to D2-MSNs
J

Figure 2.6. Dendrites of medial orbitofrontal cortical (MO) neurons non-discriminately decrease spine density after 5 day cocaine treatment.

(*A*) Representative images of apical dendrites of MO neurons projecting to either D1- or D2-receptor expressing medium spiny neurons (D1-MSNs, D2-MSNs, respectively) in nucleus accumbens (NAc). Scale: 1 μm .

(*B*) Cumulative distribute plot of individual apical MO dendrites projecting to D1-MSNs at different stages of cocaine administration. n = 41, 26, 36, 35 dendrites for 5d S (5 mice), 5d C (5 mice), 14WD S (6 mice), 14WD C (5 mice), respectively. $P < .001$ for 5d S – 5d C, 5d S – 14WD C; $p < .05$ 5d S – 14WD S; all tested on K-S test.

(*C*) Average spine densities of apical dendrites for D1-MSN projecting MO neurons. K-S test, dendrites sampled as in (*B*).

(*D*) Cumulative distribute plot of individual apical MO dendrites projecting to D2-MSNs at different stages of cocaine administration. n = 35, 45, 23, 34 dendrites for 5d S (4 mice), 5d C (5 mice), 14WD S (4 mice), 14WD C (5 mice), respectively. $P < .05$ for 5d S – 5d C; K-S test.

(*E*) Average spine densities of apical dendrites for D2-MSN projecting MO neurons. K-S test, dendrites sampled as in (*D*).

(*F*) Representative images of apical dendrites of MO neurons projecting to either D1- or D2-MSNs in NAc. Scale: 1 μm.

(*G*) Cumulative distribute plots of individual basal MO dendrites projecting to D1-MSNs at different stages of cocaine administration. n = 40, 39, 35, 27 dendrites for 5d S (5 mice), 5d C (4 mice), 14WD S (5 mice), 14WD C (5 mice), respectively. $P < .05$ for 5d S – 5d C; K-S test.

(*H*) Average spine densities of basal dendrites for D1-MSN projecting MO neurons. K-S test, dendrites sampled as in (*G*).

(*I*) Cumulative distribute plots of individual basal MO dendrites projecting to D2-MSNs at different stages of cocaine administration. N = 36, 48, 24, 34 dendrites for 5d S (4 mice), 5d C (5 mice), 14WD S (5 mice), 14WD C (5 mice), respectively. $P < .05$ for 5d S – 5d C; K-S test.

(*H*) Average spine densities of apical dendrites for D2-MSN projecting MO neurons. K-S test, dendrites sampled as in (*I*).

Data in *(C, E, H, J)* presented as mean $\pm$ SEM. Abbreviations: 5d S, 5 day acute saline; 5d C, 5 day acute cocaine; 14WD S, 14 day withdrawal saline challenge; 14WD C, 14 day withdrawal cocaine challenge. K-S test * $P < .05$, ** $P < .01$.

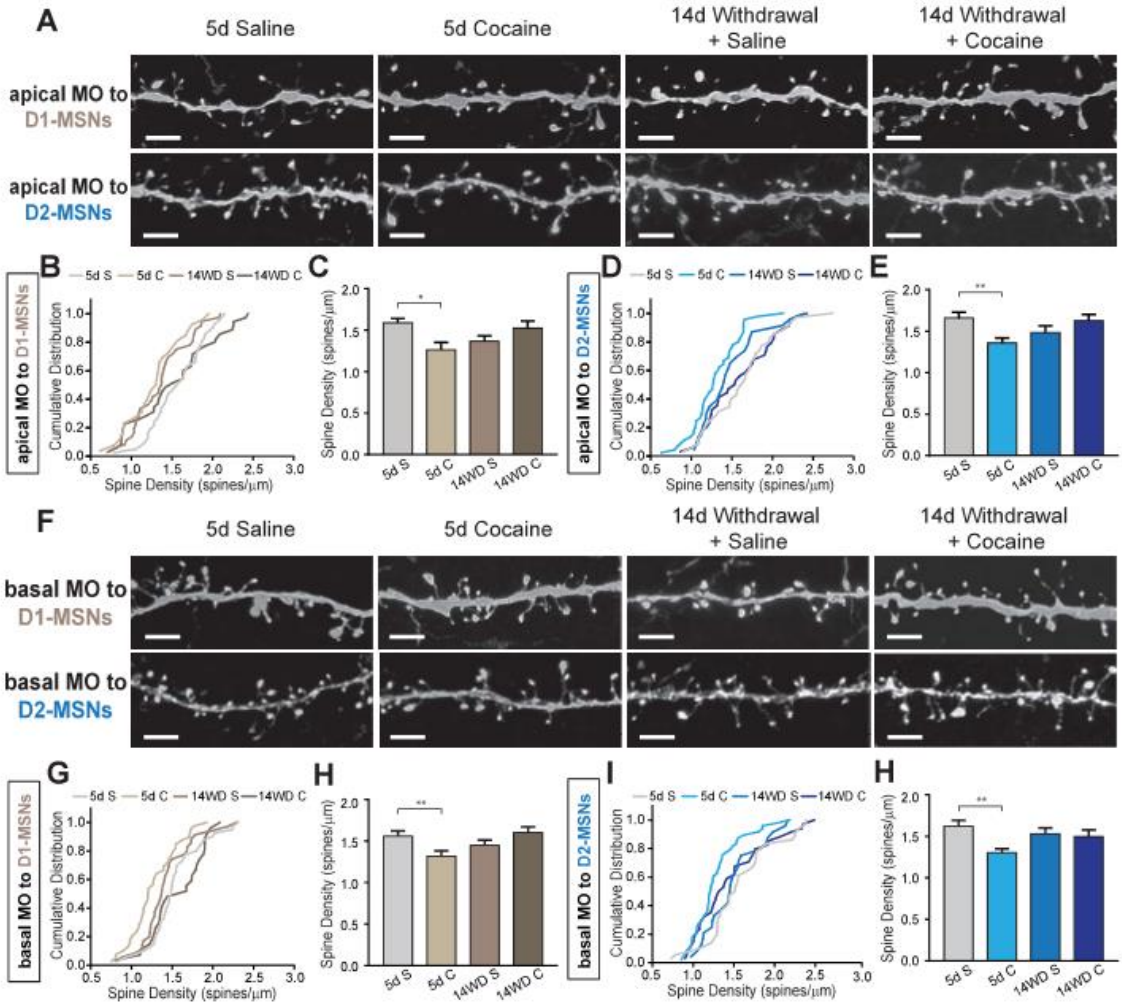
A
5d Saline
5d Cocaine
14d Withdrawal + Saline
14d Withdrawal + Cocaine
apical MO to D1-MSNs
apical MO to D2-MSNs
B
C
D
E
5d S
5d C
14WD S
14WD C
Cumulative Distribution
Spine Density (spines/μm)
F
basal MO to D1-MSNs
basal MO to D2-MSNs
G
H
I

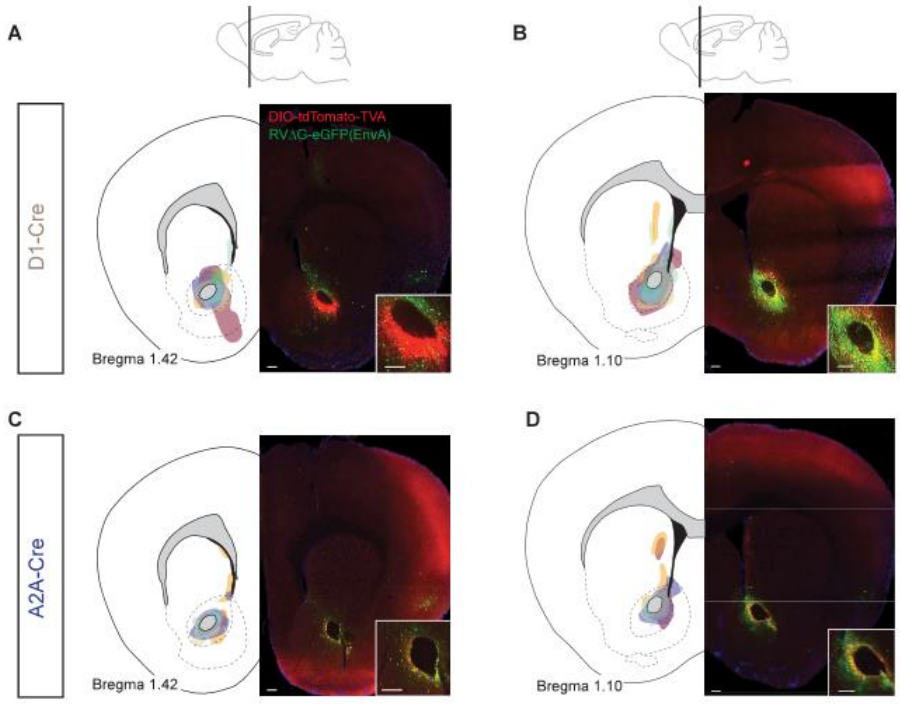

Figure S2.1. Injection site rabies viral spread.

(*A-D*) Spread of colocalized yellow 'starter cells' at injection site across two locations in the NAc across antero-posterior axis. Different colors represent individual animals. Borders indicate max spread of starter cells, and do not represent density or number of cells. Insets represent zoomed image of injection site for D1-Cre (*A* and *B*) or A2A-Cre (*C* and *D*) mice. Schematics in (*A)* and (*B*) show sagittal locations of images presented across A-P axis Scale: 200 μm.

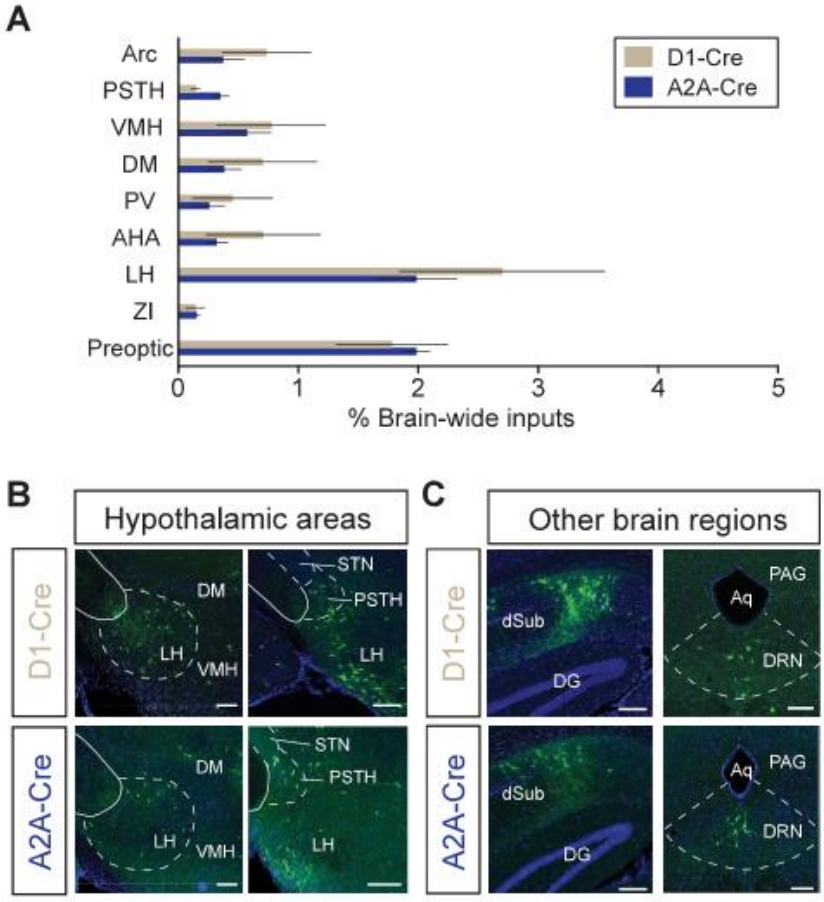

Figure S2.2. Hypothalamic regional inputs to D1- and D2-MSNs.

(*A*) Quantitation of separate hypothalamic subregion inputs to D1- and D2-MSNs as a percentage of all brain inputs. Data presented as mean ± SEM.

(*B*) Representative images of hypothalamic inputs to D1- or D2-MSNs. Scale: 500 □m .

(*C*) Representative images of other brain regions such as the dorsal raphe nucleus (DRN) and dorsal subiculum (dSub) sending input to D1- and D2-MSNs. Scale: 200 □m

Abbreviations: Arc, arcuate nucleus; PSTH, parasubthalamic nucleus; VMH, ventromedial hypothalamic nucleus; DM, dorsomedial hypothalamic nucleus; PV, paraventricular hypothalamic nucleus; AHA, anterior hypothalamic area; LH, lateral hypothalamus; ZI, zona incerta; DG, dentate gyrus of hippocampus; PAG, periaqueductal grey; Aq, cerebral aqueduct.

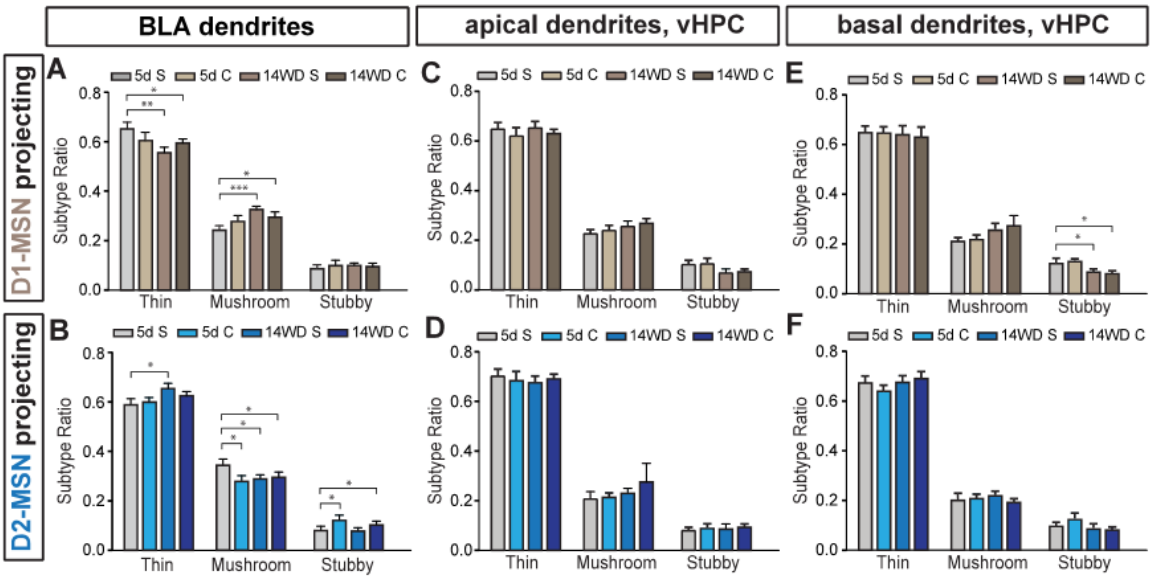

Figure S2.3. Changes in basolateral amygdala (BLA) and ventral hippocampus (vHPC) dendritic spine subtype are observed throughout different stages of cocaine administration.

(*A*, *B*) Average composition of dendritic spine subtypes of BLA dendrites projecting to D1- (*A*) and D2-receptor (*B*) expressing medium spiny neurons (D1-MSNs, D2-MSNs, respectively) at separate stages of cocaine administration. One-way analysis of variance (ANOVA) for each spine subtype. D1-MSNs (*A*): for thin spines, $F(3,159) = 4.455$, $P < 0.01$; mushroom spines, $F(3,159) = 5.658$, $P < 0.001$; stubby spines, $F(3, 159) = 0.3238$, $P > 0.05$. D2-MSNs (*B*): for thin spines, $F(3,144) = 2.772$, $P < 0.05$; mushroom spines, $F(3,144) = 3.613$, $P < 0.05$; stubby spines, $F(3, 144) = 6.098$, $P < 0.001$.

(*C*, *D*) Average spine subtypes of apical vHPC dendrites projecting to D1-MSNs (*C*) and D2-MSNs at separate stages of cocaine administration. One-way ANOVA for each spine subtype. D1-MSNs (*C*): for thin spines, $F(3,107) = 0.2592$, $P > 0.05$; mushroom spines, $F(3,107) = 0.7364$, $P > 0.05$; stubby spines, $F(3, 107) = 2.906$, $P > 0.05$. D2-MSNs (*D*): for thin spines, $F(3,106) = 0.2951$, $P > 0.05$; mushroom spines, $F(3,106) = 0.8965$, $P > 0.05$; stubby spines, $F(3, 106) = 0.4808$, $P > 0.05$.

(*E*, *F*) Average spine subtypes of basal vHPC dendrites projecting to D1-MSNs (*E*) or D2-MSNs (*F*) at separate stages of cocaine administration. One-way ANOVA for each spine subtype. D1-MSNs (*E*): thin spines, $F(3,115) = 0.1325$, $P > 0.05$; mushroom spines, $F(3,115) = 2.298$, $P > 0.05$; stubby spines, $F(3, 115) = 5.589$, $P < 0.01$. D2-MSNs (*F*): for thin spines, $F(3,115) = 0.1325$, $P > 0.05$; mushroom spines, $F(3,115) = 2.298$, $P < 0.1$; stubby spines, $F(3, 115) = 5.589$, $P > 0.05$.

All data presented as mean $\pm$ SEM. Abbreviations: 5d S, 5 day acute saline; 5d C, 5 day acute cocaine; 14WD S, 14 day withdrawal saline challenge; 14WD C, 14 day withdrawal cocaine challenge. Tukey post-hoc test used to test for differences between individual groups. * $P < .05$, ** $P < .01$, *** $P < .001$.

Figure S2.4. Dendritic spine subtype changes in prelimbic (PrL) and medial orbitofrontal cortex (MO) neurons projecting to nucleus accumbens (NAc) D2-receptor expressing medium spiny neurons (D2-MSNs), but not D1-receptor expressing medium spiny neurons (D1-MSNs).

(*A*, *B*) Average spine subtypes of apical PrL dendrites projecting to D1-MSNs (*A*) and D2-MSNs (*B*) in NAc at separate stages of cocaine administration. One-way analysis of variance (ANOVA) for each spine subtype. D1-MSNs (*A*): for thin spines, $F(3,142) = 0.3264$, $P > 0.05$; mushroom spines, $F(3,142) = 0.6174$, $P > 0.05$; stubby spines, $F(3, 142) = 0.7248$, $P > 0.05$. D2-MSNs (*B*): for thin spines, $F(3,115) = 2.872$, $P < 0.05$; mushroom spines, $F(3,115) = 0.9585$, $P > 0.05$; stubby spines, $F(3, 115) = 7.562$, $P < 0.01$.

(*C*, *D*) Average spine subtypes of basal PrL dendrites projecting to D1-MSNs (*C*) or D2-MSNs (*D*) at separate stages of cocaine administration. One-way ANOVA for each spine subtype. D1-MSNs (*C*): thin spines, $F(3,142) = 0.3264$, $P > .05$; mushroom spines, $F(3,142) = 0.6174$, $P > 0.05$; stubby spines, $F(3, 142) = 0.7248$, $P > 0.05$. D2-MSNs (*D*): for thin spines, $F(3,125) = 3.281$, $P < 0.05$; mushroom spines, $F(3,125) = 0.8961$, $P > 0.05$; stubby spines, $F(3, 125) = 4.966$, $P < 0.01$.

(*E*, *F*) Average spine subtypes of apical MO dendrites projecting to D1-MSNs (*E*) D2-MSNs (*F*) in NAc at separate stages of cocaine administration. One-way ANOVA for each spine subtype. D1-MSNs (*E*): for thin spines, $F(3,123) = 0.7273$, $P > 0.05$; $F(3,123) = 2.539$, $P < 0.05$; stubby spines $F(3, 123) = 0.7248$, $P > 0.05$. D2-MSNs (*F*): for thin spines, $F(3,118) = 0.505$, $P > 0.05$; mushroom spines, $F(3,118) = 0.848$, $P < 0.05$; stubby spines, $F(3, 118) = 3.338$, $P < 0.05$.

(*G*, *H*) Average spine subtypes of basal MO dendrites projecting to D1-MSNs (*G*) or D2-MSNs (*H*) at separate stages of cocaine administration. One-way ANOVA for each spine subtype. D1-MSNs (*G*): thin spines, $F(3,121) = 3.977$, $P > 0.05$; mushroom spines, $F(3,121) = 5.753$, $P < 0.01$; stubby spines, $F(3, 121) = 0.9059$, $P > 0.05$. D2-MSNs (*H*): for thin spines, $F(3,122) = 0.9532$, $P > 0.05$; mushroom spines, $F(3,122) = 3.276$, $P < 0.05$; stubby spines, $F(3, 122) = 1.134$, $P > 0.05$.

All data presented as mean $\pm$ SEM. Abbreviations: 5d S, 5 day acute saline; 5d C, 5 day acute cocaine; 14WD S, 14 day withdrawal saline challenge; 14WD C, 14 day withdrawal cocaine challenge. Tukey post-hoc test used to test for differences between individual groups. * $P < .05$, ** $P < .01$, *** $P < .001$.

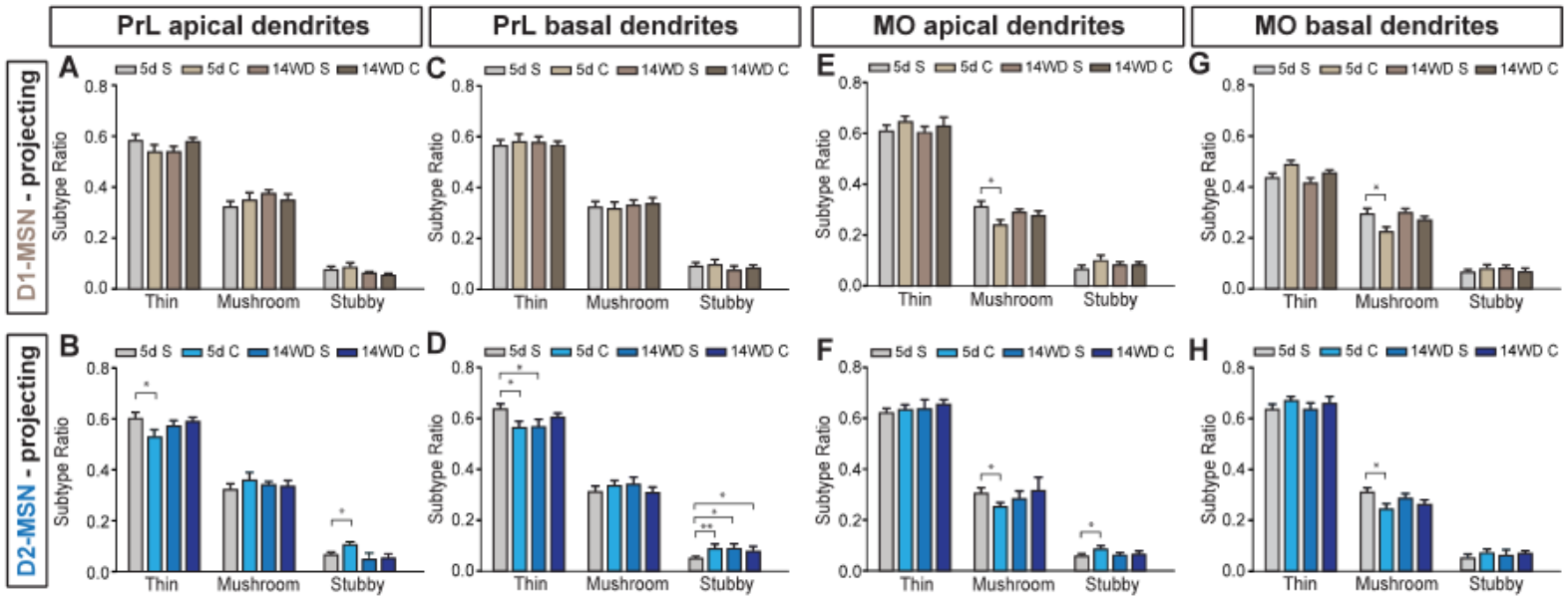
PrL apical dendrites
PrL basal dendrites
MO apical dendrites
MO basal dendrites
D1-MSN - projecting
D2-MSN - projecting
A
B
C
D
E
F
G
H
5d S
5d C
14WD S
14WD C
Subtype Ratio
0.0
0.2
0.4
0.6
0.8
Thin
Mushroom
Stubby

References

Al-Hasani, R., McCall, J.G., Shin, G., Gomez, A.M., Schmitz, G.P., Bernardi, J.M., Pyo, C.O., Park, S. Il, Marcinkiewcz, C.M., Crowley, N.A., et al. (2015). Distinct Subpopulations of Nucleus Accumbens Dynorphin Neurons Drive Aversion and Reward. Neuron *87*, 1063–1077.

Beyeler, A., Namburi, P., Glober, G.F., Luck, R., Wildes, C.P., Tye Correspondence, K.M., Simonnet, C.M., Calhoon, G.G., Conyers, G.F., and Tye, K.M. (2016). Divergent Routing of Positive and Negative Information from the Amygdala during Memory Retrieval. Neuron *90*, 348–361.

Bock, R., Shin, J.H., Kaplan, A.R., Dobi, A., Markey, E., Kramer, P.F., Gremel, C.M., Christensen, C.H., Adrover, M.F., and Alvarez, V.A. (2013). Strengthening the accumbal indirect pathway promotes resilience to compulsive cocaine use. Nat. Neurosci. *16*, 632–638.

Boulougouris, V., Dalley, J.W., and Robbins, T.W. (2007). Effects of orbitofrontal, infralimbic and prelimbic cortical lesions on serial spatial reversal learning in the rat. Behav. Brain Res. *179*, 219–228.

Britt, J.P., Benaliouad, F., McDevitt, R.A., Stuber, G.D., Wise, R.A., and Bonci, A. (2012). Synaptic and Behavioral Profile of Multiple Glutamatergic Inputs to the Nucleus Accumbens. Neuron *76*, 790–803.

Brog, J.S., Salyapongse, A., Deutch, A.Y., and Zahm, D.S. (1993). The patterns of afferent innervation of the core and shell in the "Accumbens" part of the rat ventral striatum: Immunohistochemical detection of retrogradely transported fluoro-gold. J. Comp. Neurol. *338*, 255–278.

Burgos-Robles, A., Kimchi, E.Y., Izadmehr, E.M., Porzenheim, M.J., Ramos-Guasp, W.A., Nieh, E.H., Felix-Ortiz, A.C., Namburi, P., Leppla, C.A., Presbrey, K.N., et al. (2017). Amygdala inputs to prefrontal cortex guide behavior amid conflicting cues of reward and punishment. Nat. Neurosci. *advance on*.

Capriles, N., Rodaros, D., Sorge, R.E., and Stewart, J. (2003). A role for the prefrontal cortex in stress- and cocaine-induced reinstatement of cocaine seeking in rats. Psychopharmacology (Berl). *168*, 66–74.

Cosme, C. V., Gutman, A.L., Worth, W.R., and LaLumiere, R.T. (2018). D1, but not D2, receptor blockade within the infralimbic and medial orbitofrontal cortex impairs cocaine seeking in a region-specific manner. Addict. Biol. *23*, 16–27.

Creed, M., Ntamati, N.R., Chandra, R., Lobo, M.K., and Lüscher, C. (2016). Convergence of Reinforcing and Anhedonic Cocaine Effects in the Ventral Pallidum. Neuron 214–226.

Dobi, A., Seabold, G.K., Christensen, C.H., Bock, R., and Alvarez, V. a (2011). Cocaine-induced plasticity in the nucleus accumbens is cell specific and develops without

prolonged withdrawal. J. Neurosci. *31*, 1895–1904.

Dong, H.W., Petrovich, G.D., and Swanson, L.W. (2001). Topography of projections from amygdala to bed nuclei of the stria terminalis. Brain Res. Rev. *38*, 192–246.

Dumitriu, D., Laplant, Q., Grossman, Y.S., Dias, C., Janssen, W.G., Russo, S.J., Morrison, J.H., and Nestler, E.J. (2012). Subregional, dendritic compartment, and spine subtype specificity in cocaine regulation of dendritic spines in the nucleus accumbens. J. Neurosci. *32*, 6957–6966.

Groenewegen, H.J., Mulder, A.B., Beijer, A.V.J., Wright, C.I., Silva, F.H.L. Da, and Pennartz, C.M. a. (1999). Hippocampal and amygdaloid interactions in the nucleus accumbens. Psychobiology *27*, 149–164.

Grueter, B. a, Rothwell, P.E., and Malenka, R.C. (2012). Integrating synaptic plasticity and striatal circuit function in addiction. Curr. Opin. Neurobiol. *22*, 545–551.

Harris, E., Witter, M.P., Weinstein, G., and Stewart, M. (2001). Intrinsic connectivity of the rat subiculum: I. Dendritic morphology and patterns of axonal arborization by pyramidal neurons. J. Comp. Neurol. *435*, 490–505.

Hering, H., and Sheng, M. (2001). Dentritic spines: structure, dynamics and regulation. Nat. Rev. Neurosci. *2*, 880–888.

Hoover, W.B., and Vertes, R.P. (2007). Anatomical analysis of afferent projections to the medial prefrontal cortex in the rat. Brain Struct. Funct. *212*, 149–179.

Joffe, M.E., and Grueter, B.A. (2016). Cocaine Experience Enhances Thalamo-Accumbens N-Methyl-D-Aspartate Receptor Function. Biol. Psychiatry *80*, 671–681.

Kalivas, P.W., and Volkow, N.D. (2005). The Neural Basis of Addiction:A Pathology of Motivation and Choice. Am. J. Psychiatry *162*, 1403–1413.

Khibnik, L.A., Beaumont, M., Doyle, M., Heshmati, M., Slesinger, P.A., Nestler, E.J., and Russo, S.J. (2016). Stress and Cocaine Trigger Divergent and Cell Type-Specific Regulation of Synaptic Transmission at Single Spines in Nucleus Accumbens. Biol. Psychiatry *79*, 898–905.

Kim, J., Zhang, X., Muralidhar, S., Leblanc, S.A., Kim, J., Zhang, X., Muralidhar, S., Leblanc, S.A., and Tonegawa, S. (2017). Basolateral to Central Amygdala Neural Circuits for Appetitive Behaviors: Neuron. Neuron *93*, 1464–1479.e5.

Kim, S.-Y., Adhikari, A., Lee, S.Y., Marshel, J.H., Kim, C.K., Mallory, C.S., Lo, M., Pak, S., Mattis, J., Lim, B.K., et al. (2013). Diverging neural pathways assemble a behavioural state from separable features in anxiety. Nature *496*, 219–223.

Knowland, D., Lilascharoen, V., Pham Pacia, C., Shin, S., Hou-Jen Wang, E., and Kook Lim, B. (2017). Distinct Ventral Pallidal Neural Populations Mediate Separate Symptoms of Depression. Cell *170*, 1–14.

Kourrich, S., Rothwell, P.E., Klug, J.R., and Thomas, M.J. (2007). Cocaine Experience

Controls Bidirectional Synaptic Plasticity in the Nucleus Accumbens. J. Neurosci. *27*, 7921–7928.

Kupchik, Y.M., Brown, R.M., Heinsbroek, J. a, Lobo, M.K., Schwartz, D.J., and Kalivas, P.W. (2015). Coding the direct/indirect pathways by D1 and D2 receptors is not valid for accumbens projections. Nat. Neurosci. *18*, 1230–1232.

Lammel, S., Hetzel, A., Häckel, O., Jones, I., Liss, B., and Roeper, J. (2008). Unique Properties of Mesoprefrontal Neurons within a Dual Mesocorticolimbic Dopamine System. Neuron *57*, 760–773.

Lee, K.-W., Kim, Y., Kim, A.M., Helmin, K., Nairn, A.C., and Greengard, P. (2006). Cocaine-induced dendritic spine formation in D1 and D2 dopamine receptor-containing medium spiny neurons in nucleus accumbens. Proc. Natl. Acad. Sci. U. S. A. *103*, 3399–3404.

Li, Y., Acerbo, M.J., and Robinson, T.E. (2004). The induction of behavioural sensitization is associated with cocaine-induced structural plasticity in the core (but not shell) of the nucleus accumbens. Eur. J. Neurosci. *20*, 1647–1654.

Lim, B.K., Huang, K.W., Grueter, B. a, Rothwell, P.E., and Malenka, R.C. (2012). Anhedonia requires MC4R-mediated synaptic adaptations in nucleus accumbens. Nature *487*, 183–189.

Lobo, M.K., Covington, H.E., Chaudhury, D., Friedman, A.K., Sun, H., Damez-Werno, D., Dietz, D.M., Zaman, S., Koo, J.W., Kennedy, P.J., et al. (2010). Cell Type-Specific Loss of BDNF Signaling Mimics Optogenetic Control of Cocaine Reward. Science (80-.). *327*, 385–391.

Losonczy, A., Makara, J.K., and Magee, J.C. (2008). Compartmentalized dendritic plasticity and input feature storage in neurons. Nature *452*, 436–441.

Lüscher, C., and Malenka, R.C. (2011). Drug-Evoked Synaptic Plasticity in Addiction: From Molecular Changes to Circuit Remodeling. Neuron *69*, 650–663.

MacAskill, A.F., Little, J.P., Cassel, J.M., and Carter, A.G. (2012). Subcellular connectivity underlies pathway-specific signaling in the nucleus accumbens. Nat. Neurosci. *15*, 1624–1626.

MacAskill, A.F., Cassel, J.M., and Carter, A.G. (2014). Cocaine exposure reorganizes cell type– and input-specific connectivity in the nucleus accumbens. Nat. Neurosci. *17*, 1198–1207.

Makara, J.K., Losonczy, A., Wen, Q., and Magee, J.C. (2009). Experience-dependent compartmentalized dendritic plasticity in rat hippocampal CA1 pyramidal neurons. Nat. Neurosci. *12*, 1485–1487.

Miller, C.A., and Marshall, J.F. (2004). Altered Prelimbic Cortex Output during Cue-Elicited Drug Seeking. J. Neurosci. *24*, 6889–6897.

Mogenson, G.J., Jones, D.L., and Yim, C.Y. (1980). From motivation to action: Functional

interface between the limbic system and the motor system. Prog. Neurobiol. *14*, 69–97.

Le Moine, C., and Bloch, B. (1995). D1 and D2 dopamine receptor gene expression in the rat striatum: Sensitive cRNA probes demonstrate prominent segregation of D1 and D2 mRNAS in distinct neuronal populations of the dorsal and ventral striatum. J. Comp. Neurol. *355*, 418–426.

Muñoz-Cuevas, F.J., Athilingam, J., Piscopo, D., and Wilbrecht, L. (2013). Cocaine-induced structural plasticity in frontal cortex correlates with conditioned place preference. Nat. Neurosci. *16*, 1367–1369.

Nestler, E.J. (2001). Molecular Basis of Long-term Plasticity Underlying Addiction. Nat. Rev. Neurosci. *2*, 119–128.

Nestler, E.J. (2004). Historical review: Molecular and cellular mechanisms of opiate and cocaine addiction. Trends Pharmacol. Sci. *25*, 210–218.

Neumann, P.A., Wang, Y., Yan, Y., Wang, Y., Ishikawa, M., Cui, R., Huang, Y.H., Sesack, S.R., Schlüter, O.M., and Dong, Y. (2016). Cocaine-Induced Synaptic Alterations in Thalamus to Nucleus Accumbens Projection. Neuropsychopharmacology *41*, 2399–2410.

Nimchinsky, E.A., Sabatini, B.L., and Svoboda, K. (2002). Structure and function of dendritic spines. Annu. Rev. Physiol. *64*, 313–353.

Novejarque, A. (2011). Amygdaloid projections to the ventral striatum in mice: direct and indirect chemosensory inputs to the brain reward system. Front. Neuroanat. *5*, 1–20.

Olds, J., and Milner, P. (1954). Positive reinforcement produced by electrical stimulation of septal area and other regions of rat brain. 419–427.

Osakada, F., and Callaway, E.M. (2013). Design and generation of recombinant rabies virus vectors. Nat. Protoc. *8*, 1583–1601.

Peters, A., and Kaiserman-Abramof, I.R. (1970). The small pyramidal neuron of the rat cerebral cortex. The perikaryon, dendrites and spines. Am. J. Anat. *127*, 321–355.

Phillipson, O.T., and Griffiths, A.C. (1985). The topographic order of inputs to nucleus accumbens in the rat. Neuroscience *16*, 275–296.

Pitkanen, A., Pikkarainen, M., Nurminen, N., and Ylinen, A. (2006). Reciprocal Connections between the Amygdala and the Hippocampal Formation, Perirhinal Cortex, and Postrhinal Cortex in Rat: A Review. Ann. N. Y. Acad. Sci. *911*, 369–391.

Radley, J.J., Rocher, A.B., Rodrigues, A., Ehlenberger, D.B., Dammann, M., Mcewen, B.S., Morrison, J.H., Wearne, S.L., and Hof, P.R. (2008). Repeated Stress Alters Dendritic Spine Morphology in the Rat Medial Prefrontal Cortex. J. Comp. Neurol. *507*, 1141–1150.

Robinson, T.E. (1999). Alterations in the morphology of dendrites and dendritic spines in the

nucleus accumbens and prefrontal cortex following repeated treatment with amphetamine or cocaine. Eur. J. Neurosci. *11*, 1598–1604.

Robinson, T.E., Gorny, G., Mitton, E., and Kolb, B. (2001). Cocaine Self-Administration Alters the Morphology of Dendrites and Dendritic Spines in the Nucleus Accumbens and Neocortex. Synapse *266*, 257–266.

Rodriguez, A., Ehlenberger, D.B., Dickstein, D.L., Hof, P.R., and Wearne, S.L. (2008). Automated three-dimensional detection and shape classification of dendritic spines from fluorescence microscopy images. PLoS One *3*.

Rogers, J.L., and See, R.E. (2007). Selective inactivation of the ventral hippocampus attenuates cue-induced and cocaine-primed reinstatement of drug-seeking in rats. Neurobiol. Learn. Mem. *87*, 688–692.

Rothwell, P.E., Kourrich, S., and Thomas, M.J. (2011). Synaptic adaptations in the nucleus accumbens caused by experiences linked to relapse. Biol. Psychiatry *69*, 1124–1126.

Russo, S.J., and Nestler, E.J. (2013). The brain reward circuitry in mood disorders. Nat. Rev. Neurosci. *14*, 609–625.

Russo, S.J., Dietz, D.M., Dumitriu, D., Morrison, J.H., Malenka, R.C., and Nestler, E.J. (2010). The addicted synapse: mechanisms of synaptic and structural plasticity in nucleus accumbens. Trends Neurosci. *33*, 267–276.

Sanchis-segura, C., and Spanagel, R. (2006). Behavioural assessment of drug reinforcement and addictive features in rodents : an overview. Addict. Biol. 2–38.

Schoenbaum, G., Setlow, B., Saddoris, M.P., and Gallagher, M. (2003). Encoding predicted outcome and acquired value in orbitofrontal cortex during cue sampling depends upon input from basolateral amygdala. Neuron *39*, 855–867.

Schwarz, L. a., Miyamichi, K., Gao, X.J., Beier, K.T., Weissbourd, B., DeLoach, K.E., Ren, J., Ibanes, S., Malenka, R.C., Kremer, E.J., et al. (2015). Viral-genetic tracing of the input–output organization of a central noradrenaline circuit. Nature.

Su, H. -S, and Bentivoglio, M. (1990). Thalamic midline cell populations projecting to the nucleus accumbens, amygdala, and hippocampus in the rat. J. Comp. Neurol. *297*, 582–593.

Vogl, A.M., Brockmann, M.M., Giusti, S.A., MacCarrone, G., Vercelli, C.A., Bauder, C.A., Richter, J.S., Roselli, F., Hafner, A.S., Dedic, N., et al. (2015). Neddylation inhibition impairs spine development, destabilizes synapses and deteriorates cognition. Nat. Neurosci. *18*, 239–251.

Volkow, N.D., and Fowler, J.S. (2000). Addiction, a disease of compulsion and drive: involvement of the orbitofrontal cortex. Cereb. Cortex *10*, 318–325.

Wall, N., DeLaParra, M., Callaway, E., and Kreitzer, A. (2013). Differential innervation of direct- and indirect-pathway striatal projection neurons. Neuron *79*, 347–360.

Wall, N.R., Wickersham, I.R., Cetin, A., De La Parra, M., and Callaway, E.M. (2010). Monosynaptic circuit tracing in vivo through Cre-dependent targeting and complementation of modified rabies virus. Proc. Natl. Acad. Sci. U. S. A. *107*, 21848–21853.

Wickersham, I.R., Lyon, D.C., Barnard, R.J.O., Mori, T., Finke, S., Conzelmann, K.-K., Young, J. a T., and Callaway, E.M. (2007). Monosynaptic restriction of transsynaptic tracing from single, genetically targeted neurons. Neuron *53*, 639–647.

Winstanley, C.A., Bachtell, R.K., Theobald, D.E.H., Laali, S., Green, T.A., Kumar, A., Chakravarty, S., Self, D.W., and Nestler, E.J. (2009). Increased impulsivity during withdrawal from cocaine self-administration: Role for ??FosB in the orbitofrontal cortex. Cereb. Cortex *19*, 435–444.

Wunsch, A.M., Yager, L.M., Donckels, E.A., Le, C.T., Neumaier, J.F., and Ferguson, S.M. (2017). Chemogenetic inhibition reveals midline thalamic nuclei and thalamo-accumbens projections mediate cocaine-seeking in rats. Eur. J. Neurosci. *46*, 1850–1862.

Zhu, Y., Wienecke, C.F.R., Nachtrab, G., and Chen, X. (2016). A thalamic input to the nucleus accumbens mediates opiate dependence. Nature *530*.

APPENDIX A:

Circuit-based Frameworks of Depressive Behaviors: The Role of Reward Circuitry and Beyond

Daniel Knowland, Byung Kook Lim

Abstract

Major depressive disorder (MDD) is a common but serious neuropsychiatric affliction that comprises a diverse set of symptoms such as the inability to feel pleasure, lack of motivation, changes in appetite, and cognitive difficulties. Given the patient to patient symptomatic variability in MDD and differing severities of individual symptoms, it is likely that maladaptive changes in distinct brain areas may mediate discrete symptoms in MDD. The advent and recent surge of studies using viral-genetic approaches have allowed for circuit-specific dissection of networks underlying motivational behavior. In particular, areas such as the ventral tegmental area (VTA), nucleus accumbens (NAc), and ventral pallidum (VP) are thought to generally promote reward, with the medial prefrontal cortex (mPFC) providing top-down control of reward seeking. On the contrary, the lateral habenula (LHb) is considered to be the aversive center of the brain as it has been shown to encode negative valence. The behavioral symptoms of MDD may arise from a disruption in the reward circuitry, hyperactivity of aversive centers, or a combination of the two. Thus, gaining access to specific circuits within the brain and how separate motivational-relevant regions transmit and encode information between each other in the context of separate depression-related symptoms can provide critical knowledge towards symptom-specific treatment of MDD. Here, we review published literature emphasizing circuit- and cell type-specific dissection of depressive-like behaviors in animal models of depression with a particular focus on the chronic social defeat stress model of MDD.

Introduction

Major depressive disorder (MDD) affects about 10% of adults in the United States and twice as many suffer at least one depressive episode during their lifetime (Andrade et al., 2003; Ferrari et al., 2013). Despite this widespread prevalence and continued investment into identifying effective cures, long-term treatments are generally required for MDD and have variable effectiveness – some achieve complete remission while other patients exhibit little to no change in behavioral or cognitive symptoms (Berton and Nestler, 2006; Nestler, 1998). To date, it is unclear what molecular or genetic factors might confer positive or negative response to treatment.

Those experiencing MDD display a common but often variable set of symptoms including but not limited to anhedonia, psychomotor impairment, sleep impairment, loss of appetite, and retraction from social interaction (Nestler and Hyman, 2010; Russo and Charney, 2013). The DSM V criteria for MDD lists nine discrete symptoms including the aforementioned, with at least five required to be present daily for MDD diagnosis. This diversity in behavioral symptoms of depression suggests that different circuits, or discrete components of a single circuit, may underlie separate depressive-like phenotypes. This idea is a driving impetus for the many circuit-focused papers invading the field.

Some of the most common symptoms of MDD are characterized by decreases in appetite and motivation. As such, intense focus has been placed on understanding the aberrant signaling and changes of the reward and motivational circuitry in MDD. In particular, the mesolimbic dopaminergic circuitry comprising of the nucleus accumbens (NAc) and ventral tegmental area (VTA) have been extensively studied and will be emphasized in this review. In

line with this reasoning, polymorphisms in dopaminergic receptors (in particular, D_3 and D_4) and catechol-O-methyltransferase, an enzyme critical in degrading dopamine (DA), have been identified in patients with MDD (Cravchik and Goldman, 2000; Dunlop and Nemeroff, 2007; Lopez Leon et al., 2005; Szegedi et al., 2005). Concentrations of DA metabolites in the cerebro-spinal fluid of MDD patients have also been measured to be lower than those of healthy individuals (Mendels et al., 1972; Roy et al., 1989). While dopamine and the reward circuitry have been identified as putative targets for MDD, the wide and varied behavioral symptoms patients present with in MDD still represents a significant barrier in both treatment and developing a unifying animal model that adequately captures the spectrum of phenotypes present in humans.

To date, the most common and reliable animal model in depression research is chronic social defeat stress (CSDS), although many other variations such as chronic variable stress (CVS) and chronic mild stress (CMS) are widely used (Golden 2011). CSDS comprises of two distinct stages of defeat (Figure A.1). First, an experimental intruder animal is placed in the home cage of a resident, aggressive CD-1 male mouse and undergoes roughly 10 minutes of physical defeat. Immediately after physical defeat, the experimental animal is transferred to the opposite side of a clear, perforated divider placed in the resident cage. For 24 hours, the intruder maintains sensory contact with the resident that had just defeated him. This process is repeated for 10 consecutive days. Animals experiencing social defeat exhibit several physiological changes including retarded growth, sensitivity to other environmental stressors, increased anxiety, and heightened levels of glucocorticoid activity (Meerlo et al., 1996; Tornatzky and Miczek, 1993). Repeated exposure to social defeat induces a number of depressive-like behaviors that parallel those seen in humans providing nice face validity.

These include: helplessness/behavioral despair, as tested by reduced mobility in the forced swim test and tail suspension test; anhedonia, as tested by reduced preference for a sucrose solution in the sucrose preference test; and social dysfunction, as displayed by profound social avoidance in the social interaction test (Figure A.1) (Berton et al., 2006; Hollis et al., 2010). Most of these behavioral changes persist for at least 4 weeks and can be reversed by chronic, but not acute, antidepressant administration (Berton et al., 2006; Berton and Nestler, 2006; Rygula et al., 2006a; Rygula et al., 2006b; Tsankova et al., 2006), providing robust predictive validity as a model for depression in humans. Interestingly, a subset of animals subjected to CSDS appear unaffected by this protocol and do not display depressive-like behaviors. These animals are deemed to be resilient and are thought to represent an active coping mechanism in response to environmental stressors (Krishnan et al., 2007; Krishnan and Nestler, 2008; 2011). On the contrary, animals that undergo CSDS and show depression-related behaviors are called susceptible. Animals can be screened in an unbiased manner to differentiate resilience or susceptibility by a post-CSDS social interaction test (Krishnan et al., 2007). Since humans also display different levels of response and coping towards aversive external stimuli, comparing resilient and susceptible animals provides another level of investigation towards elucidating the circuits and molecular mechanisms underlying how heterogeneous responses to aversive events contribute to the development of depressive phenotypes. Due to its robust predictive and face validity, this review will focus heavily on studies utilizing the CSDS model of depression-related behaviors, but will also briefly touch on its shortcomings and other models.

Overcoming the enormous complexity of brain area-, cell type-, projection-, and molecular-specific adaptations over the course of healthy individuals descending into

depression represents a daunting undertaking. The advent of viral-genetic techniques such as viral-mediated circuit tracing and optogenetics in tandem with mouse lines driving Cre-recombinase in specific cell types have allowed for precise dissection and manipulation of neural circuits to begin to tackle this question in animal models of depression. In this review, we will summarize the existing literature of the motivational circuitries and their role in stress-induced depression with a particular emphasis on the CSDS model of depression and its effects on the NAc and VTA and their related circuitry, as well as the emerging role of the ventral pallidum (VP).

Circuit-specific roles of VTA dopaminergic neurons in depressive behaviors

Through multiple layers of results in past decades, the role of DA in reward processing and motivation-related behaviors has been well documented (Lammel et al., 2014). Since a hallmark of depression is loss of motivation and blunted ability to feel reward (anhedonia), it follows that the dopamine circuitry is likely involved in mediating depressive-like behaviors. Corroborating this theory, many studies have found that repeated aversive or traumatic experiences such as stress can induce several core symptoms of depression such as social dysfunction, anhedonia or helplessness that are driven by maladaptive function of mesolimbic DA signals (Berton et al., 2006; Chaudhury et al., 2013; Krishnan et al., 2007; Tye et al., 2013; Willner, 2005).

Previous studies indicate that phasic bursting and excitability of VTA DA neurons increases after social defeat stress *in vivo* and in *ex vivo* brain slice (Friedman et al., 2014; Razzoli et al., 2011). This increase is specific to animals susceptible to CSDS, as animals that underwent CSDS but did not display depressive-like phenotypes (resilient) did not have

heightened VTA DA activity (Cao et al., 2010; Chaudhury et al., 2013). Enhanced VTA DA activity that was induced by CSDS was normalized by chronic antidepressant treatment, suggesting that antidepressants may exert their behavioral effects through regulation of VTA DA neuronal activity (Cao et al., 2010). Studies have also shown that VTA DA neurons from susceptible animals also display increased I_h current (Cao et al., 2010). Furthermore, local infusion of I_h channel inhibitors ZD7288 or DK-AH 269 into the VTA reversed CSDS-induced social withdrawal. I_h currents may also represent an important target by which selective serotonin reuptake inhibitors (SSRIs), commonly prescribed antidepressant medications in humans, exert their behavioral effects. Chronic SSRI treatment (fluoxetine) significantly reduced I_h current in susceptible animals which correlated with a reduction in their depressive-like behavioral symptoms (Cao et al., 2010). Paradoxically, resilient animals have an even larger I_h current which correlates with an increase in potassium channel currents (Friedman et al., 2014). Artificially increasing level of I_h current by local infusion of lamotrigine, an I_h channel potentiator that has previously been used as a mood stabilizer, promoted a resilient phenotype in animals subjected to CSDS. Taken together, we see that both reducing and enhancing I_h current levels after stress has antidepressive effects. Curiously, this may be due to a tightly regulated range of I_h current in VTA DA neurons which contributes to the development of depression-related behavior. Any deviation from this, whether it be an increase or decrease, promotes normal behavior. Understanding the precise contribution of abnormal electrophysiological profiles due to aberrant I_h channel activity, and how careful titering of I_h current can lead to separate behavioral outcomes, remain important future questions.

Changes in protein expression levels or secretion of neurotrophic factors have also been thought to contribute to the development of depression-related behaviors. In particular, brain derived neurotrophic factor (BDNF) has been proposed as a molecular signature of susceptibility to CSDS. Susceptible, but not resilient, animals show increased protein levels of BDNF specifically in the NAc (Krishnan et al., 2007). A naturally occurring single nucleotide polymorphism (SNP) in the BDNF gene in humans impairs BDNF secretion. Mice that have a similar polymorphism, and thus have an impaired ability to secrete BDNF, are less susceptible to CSDS than control animals (Krishnan et al., 2007). While increased BDNF secretion in the NAc, but not VTA, is characteristic of susceptible animals, enhanced VTA activity is an essential prerequisite for heightened BDNF NAc levels. Optogenetic activation of VTA DA neurons during CSDS was found to significantly increase levels of BDNF in the NAc as well as exacerbate behavioral deficits (Berton et al., 2006; Eisch et al., 2003; Wook Koo et al., 2016). Blockade of BDNF-TrkB signaling in the NAc reversed this effect (Wook Koo et al., 2016). However, optogenetically driving VTA DA activity by itself is not sufficient to induce susceptibility or increases in NAc BDNF levels. CSDS-induced susceptibility and secretion of corticotropin-releasing factor secretion (CRF), a hormone secreted when animals undergo stressful experiences, were required for elevated BDNF levels (Walsh et al., 2014). Infusion of a CRF antagonist prevented VTA DA-induced increases in BDNF and promoted resilience to CSDS in both mice and hamsters (Cooper and Huhman, 2007; Walsh et al., 2014). Thus, while elevated BDNF levels in the NAc correlate with increased VTA DA firing in susceptible animals, neither is sufficient by itself to induce susceptibility in stress naïve mice. External environmental stressors such as CSDS likely promote the release of stress hormones

such as CRF which gate and promote the release of BDNF which ultimately induces susceptibility.

There is an increasing body of evidence propounding the idea that DA neurons within the VTA are anatomically distinct depending on their projection pattern and may have distinct functional roles (Lammel et al., 2008; Lammel et al., 2011). For example, cocaine administration induces alterations in AMPA/NMDA ratio in NAc-projecting VTA DA neurons, while cortex-projecting VTA DA neurons show no change. Conversely, cortex-projecting VTA DA neurons, but not NAc-projecting neurons, respond to aversive formalin injection into the paw (Lammel et al., 2011). Further, the authors showed that the medial and lateral shell of NAc exhibit differential responses to cocaine administration or aversive stimulation, further supporting the target specific roles of VTA DA neurons, even within subregions of the NAc (Lammel et al., 2011). As such, bulk manipulation of VTA DA neurons in animal models of depression may not be sufficient to fully capture the heterogeneity of these neurons.

Taking this heterogeneity into account, studies have used optogenetics to manipulate discrete components of the VTA DA circuitry in an attempt to parse out discrete contributions to depressive-like behaviors. Phasic channelrhodopsin (ChR2) mediated stimulation of NAc projecting VTA DA neurons (VTA-NAc) during a subthreshold social defeat paradigm that does not normally induce depressive-like behaviors is sufficient to generate social withdrawal and anhedonia (Chaudhury et al., 2013). Thus, aversive environmental stressors in parallel with increased VTA-NAc activity is sufficient to induce depression-related behaviors, but not VTA-NAc activity by itself. However, the same manipulation of VTA-medial prefrontal

cortex (mPFC) projecting DA neurons had no effect. It was also found that optogenetic inhibition of VTA-NAc DA neurons acutely reverses CSDS-induced social withdrawal and anhedonia, while inhibition of VTA-mPFC DA neurons reduces social interaction (Chaudhury et al., 2013). In line with these results, another study found that optogenetic stimulation of the mPFC elicits antidepressant-like effects after CSDS (Covington et al., 2010). These opposing effects of the VTA-NAc and VTA-mPFC circuits extend to the cellular level as well, as VTA-mPFC projecting DA neurons were measured to have reduced firing and no change in I_h current in susceptible animals (Chaudhury et al., 2013; Friedman et al., 2014). Conversely, VTA-NAc DA neurons from susceptible, but not resilient animals have significantly enhanced firing rates in slice and increased I_h current (Chaudhury et al., 2013; Razzoli et al., 2011). Collectively, these results suggest that VTA DA neurons have differential roles at the behavioral and cellular level in response to CSDS depending on their efferent target.

In addition to circuit-specific contributions to behavior, the type and duration of stress may also have profound effects on DA signaling in NAc. In mice exposed to chronic mild stress (CMS), a separate type of depressive-behavior induction protocol involving weeks of mild, unpredictable stressors, phasic VTA DA stimulation attenuated depression-related behavior in the tail-suspension test, forced swim test, and sucrose preference test, suggesting that increased VTA DA neuronal activity induces antidepressive effects (Tye et al., 2013). Silencing VTA DA neurons was also sufficient to drive depressive-like behaviors in the aforementioned assays (Tye et al., 2013). Moreover, separate studies in rats also exposed to CMS found a reduction in *in vivo* VTA DA neuronal firing rate (Chang and Grace, 2014; Moreines et al., 2017). Oppositely, in mice exposed to CSDS, phasic activation of VTA DA neurons induced persistent depressive-like symptoms, while inhibition attenuated these

behaviors (Chaudhury et al., 2013). It is thus possible that the type and length of external stressors used as an induction protocol could have a profound effect on the physiological changes observed in the brain. Interestingly, this suggests that while the outward behavioral phenotypes may be similar, the underlying etiology precipitating these behaviors may be separate further emphasizing the complexity of studying conditions such as MDD.

In addition to differences in the stress protocol (CMS vs. CSDS), other factors may in part explain this discrepancy. Artificial stimulation of VTA DA neurons does not recapitulate the natural neural activity pattern *in vivo*. It is known that burst firing *in vivo* promotes increased DA release in target areas compared to slow frequency tonic firing (Grace et al., 2007). In line with this, Chaudhury et al. (2013) revealed that the pro-depressive behavioral effects caused by VTA DA optogenetic stimulation was dependent on the stimulation protocol. Driving phasic firing of 5 pulses at 20 Hz every 10 seconds for 10 minutes induced depression-related behavior, however a tonic stimulation protocol of continuous 0.5 Hz stimulation did not have any effect. While Tye et al. (2013) also used a phasic stimulation protocol, VTA DA neurons were activated slightly differently at 5 pulses at 30 Hz every 5 seconds for 3 minutes. Thus, the difference in stimulation pattern of VTA DA neurons could have a distinct impact on the behavioral effects seen.

Moreover, recent studies have suggested that separate depression-related behaviors could be mediated by distinct circuits (Knowland et al., 2017). As such, the behavioral assays selected to assess depressive-like behaviors could have profound effects on the behavioral outcomes due to optogenetic manipulation. Tye et al. (2013) predominantly focused on behavioral despair as assessed by the tail suspension test (TST), and anhedonia as assessed by

the sucrose preference test (SPT). Chaudhury et al. (2013) used the social interaction test (SI) and the SPT. It remains possible that the disparate responses due to optogenetic stimulation could be due to using the TST or SI tests. The distinct activity pattern of VTA DA neurons might thus differentially mediate separate depressive-related behaviors. Moreover, since techniques like optogenetics provide precise temporal access to cell manipulation, whether ChR2-mediated stimulation or NpHR-mediated inhibition is given during the stress induction protocol (CMS or CSDS) or the depression-related behavioral assays (tail suspension test, social interaction test, etc.) could have differential functional consequences. While Tye et al. (2013) drove VTA DA activity for 30 minutes during the SPT, Chaudhury et al. (2013) optogenetically stimulated during subthreshold defeat, or during a 2.5 minute window prior to the SPT. Collectively, these subtle differences may have a significant effect on a condition as complex to model in animals as MDD, and could account for some of the discrepancies reported in these studies.

Taken together, the VTA DA circuit contribution towards depressive-like behaviors can depend on its output targets or type of environmental stress. Some studies have shown that GABAergic neurons within the VTA can promote aversion, yet their contributions towards depression or CSDS-induced depression related phenotypes is still unclear (Tan et al., 2012; van Zessen et al., 2012). Additionally, recent studies have reported that transcriptional changes in the VTA, in particular, Otx2, can bidirectionally affect susceptibility or resilience to CSDS (Pena et al., 2017). Further studies requiring cell type- and projection-specific manipulation, recordings, and molecular analyses are necessary to comprehensively understand the VTA contribution towards depression.

Roles of different NAc cell types in CSDS-induced depressive behaviors

As previously discussed, DA signaling in the NAc emanating from the VTA have been implicated in depressive behaviors. Many studies have underscored the importance of the NAc in MDD. In humans, deep brain stimulation of the NAc has been shown to alleviate anhedonic symptoms of depression (Schlaepfer et al., 2008). However, the NAc is a heterogenous structure comprising of different cell types, various dopamine receptors, and other neuromodulatory signaling (Francis and Lobo, 2017). These characteristics make it difficult to elucidate the precise role of the NAc circuitry in depressive behaviors.

D1-receptor expressing and D2-receptor expressing medium spiny neurons (D1-MSNs and D2-MSNs, respectively) comprise the predominant cell populations in the NAc. Emerging evidence shows that D1-MSNs and D2-MSNs in the NAc have distinct roles in stress-induced depressive behaviors. In mice susceptible to CSDS, D1-MSNs were measured to have increased intrinsic excitability and reduced mEPSC frequency, while D2-MSNs exhibit increased mEPSC frequency but no change in intrinsic excitability (Francis et al., 2015). Moreover, resilient animals displayed an upregulation of synaptic strength at large mushroom spines of D1-MSNs and a concomitant downregulation in D2-MSNs (Khibnik et al., 2016). In addition, excitatory inputs to D1-MSNs, not to D2-MSNs, showed long-term synaptic depression in mice with stress-induced anhedonia, a major symptom of depression. These alterations were mediated by alpha-melanocortin stimulating hormone (MSH) signaling (Lim et al., 2012).

Using optogenetics and chemogenetics to specifically manipulate D1- or D2-MSNs *in vivo*, Francis et al. (2015) demonstrated that driving an increase in D1-MSN activity rescues

social interaction and sucrose preference deficits in susceptible animals, while inhibition of these neurons had the opposite effect. On the other hand, stimulation of D2-MSNs was sufficient to produce social avoidance, but no change in sucrose preference, following subthreshold social defeat stress (Francis et al., 2015). As evidenced by these results, it appears that distinct cell types in the NAc are differentially involved in stress-induced depressive behaviors. To this point, a recent report using *in vivo* fiber photometry to monitor neuronal dynamics *in vivo* revealed that heightened activity in D1-MSN activity during social interaction before CSDS was predictive of resilience, but not D2-MSN activity (Muir et al., 2017).

Based on the distinct roles of NAc MSNs in stress-induced depression, it is not surprising that different molecular mechanisms have been proposed to underlie separate cell-type neural adaptations in the NAc in response to stress. Indeed, Lobo et al. (2013) showed that ΔFosB expression is enhanced in D1-MSNs of resilient mice and enhanced in D2-MSNs of susceptible mice in NAc. This corroborates an earlier study reporting increased numbers of ΔFosB-positive neurons in the NAc and mPFC after stress (Nikulina et al., 2008). Furthermore, using engineered zinc-finger proteins to target the *FosB* gene, induction of histone acetylation in D2-MSNs, or histone methylation in D1-MSNs, promoted a susceptible phenotype in mice undergoing CSDS. Conversely, histone methylation of D2-MSNs or histone acetylation in D1-MSNs induced a pro-resilience (Hamilton et al., 2017). These results provide interesting insight into the role of cell-type specific epigenetic and histone modifications and their effect on the development of depressive-like phenotypes.

Moreover, increased protein levels of ΔFosB in the NAc, but not other isoforms, FosB and Δ2ΔFosB, negatively correlated with the level of defeat animals exhibited (Vialou et al., 2015). Paradoxically, chronic fluoxetine treatment, an FDA-approved selective serotonin reuptake inhibitor commonly prescribed as an antidepressant, reversed CSDS-induced behavioral deficits yet ΔFosB protein levels were found to be further increased from control and susceptible levels in the NAc (Vialou et al., 2015). Thus, levels of ΔFosB may be tightly regulated in which increased levels induce susceptibility, yet a further increase can promote resilience or reverse depressive behaviors in susceptible animals, similar to what has been seen with increasing I_h current in the VTA (Friedman et al., 2014). Furthermore, Slc6a15, a molecule linked to MDD susceptibility in humans, was specifically reduced in D2-MSNs after CSDS (Chandra et al., 2017). Artificially enhancing Slc6a15 in D2-MSNs promoted susceptibility to subthreshold defeat stress (Chandra et al., 2017).

While accumulating data highlights the differential roles of D1-MSNs and D2-MSNs, recent reports paradoxically show that the anatomical projections of these neurons are quite similar (Knowland et al., 2017; Kupchik et al., 2015). Thus, interpretation of these cell-type differences likely go beyond efferent circuitry disparities. Separate downstream synaptic adaptations from D1- and D2-MSNs to VP have begun to be reported (Creed et al., 2016), yet how NAc D1-MSNs or D2-MSNs separately modulate downstream circuitry in response to stress has not yet been explored and will be required for future studies.

In addition to the canonical D1- and D2-MSN cell-type dichotomy in the NAc, neurons can also be discriminated by their expression of dynorphin (it is of note that these neurons are not an independent subpopulation, they co-express with predominantly D1-

MSNs, but to a lesser degree D2-MSNs), the endogenous ligand of the kappa opioid receptor (KOR, Al-Hasani et al., 2015). Activation of KORs are well known to elicit aversive behaviors in humans and mice, and present a tractable pharmacologic target for MDD (Laman-Maharg et al., 2017; Mucha and Herz, 1985; Pfeiffer et al., 1986).In regards to depression-related behaviors, infusion of a KOR antagonist in both mice and rats reduced immobility time in the forced swim test which correlated with a selective increase in expression of the immediate early gene, *cfos*, in the NAc (Carr et al., 2010; Mague and Pliakas, 2003; McLaughlin et al., 2003). Similarly, KOR antagonist infusion into the NAc, but not hippocampus, attenuated depressive-like behaviors in mice exposed to the learned helplessness model of depression (Newton et al., 2002). KOR activation and inhibition has also been shown to modulate dopamine release in the NAc. Microdialysis and fast scan cyclic voltammetry studies in the NAc in response to KOR antagonist administration increased DA release in the NAc, while supra-threshold concentrations of KOR agonist treatment decreased phasic dopamine release concordant with a reduction in VTA DA activity (Di Chiara and Imperato, 1988; Ebner et al., 2010; Shippenberg and Rea, 1997). How then might this paradoxical situation arise, in which KOR agonists induce pro-depressive like behavioral effects, yet elicits a reduction in VTA DA activity and DA release in the NAc, contrary to previous reports on increased VTA DA activity projecting to NAc in models of depression (Cao et al., 2010; Chaudhury et al., 2013)? Curiously, optogenetic activation of dynorphin neurons induces either aversion and preference dependent on their anatomical localization within the NAc (Al-Hasani et al., 2015). Thus, future studies investigating whether subpopulations of VTA DA neurons projecting to distinct prodynorphin-rich subregions of the NAc may be differentially affected during depression-related behaviors are required. It has

also been proposed that the timing of KOR antagonist administration, whether before, during, or after stressors are given to the animal, may be critical to specify its effects (Knoll and Carlezon, 2010).

Together, we see a convergence of putative cell-type specific factors capable of contributing to the expression or attenuation of depressive-like behaviors. Further identification of the interactions or overlap between these neurons using a Boolean viral intersectional strategy (Fenno et al., 2014) and the ideal temporal manipulation to target them for treatment remain important unanswered questions.

Roles of afferent connections to NAc in depressive behaviors

Medial prefrontal cortex (mPFC)

The nucleus accumbens is known to receive input from a broad array of brain areas. In addition to dopaminergic signaling from the VTA, afferents originating from the ventral hippocampus (vHPC), basolateral amygdala (BLA), and medial prefrontal cortex (mPFC) have received particular attention in both depression and addiction (Dumitriu et al., 2012; Khibnik et al., 2016; MacAskill et al., 2014; MacAskill et al., 2012). How these input-specific afferents generate diverse adaptations at D1- and D2-MSN synapses have been outlined in several motivational contexts. In humans, chronic deep brain stimulation (DBS) of the subgenual cingulate cortex (Cg25), the equivalent of the rodent vmPFC, restores and alleviates several symptoms of depression in treatment-resistant MDD patients (Dunlop and Mayberg, 2014; Mayberg et al., 2005). DBS in the vmPFC of rodents exposed to CSDS also reversed social withdrawal deficits as well as normalized aberrant structural and physiological changes in serotonergic dorsal raphe nuclei neurons (Veerakumar et al., 2014). Subsequent

rodent studies have reinforced these results and shown that electrical and optogenetic stimulation of the mPFC in rats alleviated depressive-like symptoms (Hamani et al., 2010). Furthermore, precise optogenetic manipulation of mPFC neurons projecting to NAc promoted resiliency in animals exposed to CSDS (Covington et al., 2010). Other studies using light delivery to manipulate precise circuits show that mPFC efferents to other brain areas including lateral habenula (LHb) and dorsal raphe nucleus (DRN) are also involved in several symptoms of depression (Warden et al., 2012). Interestingly, reduced dopaminergic activity in the mPFC correlates with reductions in social interaction in subthreshold defeat mice (Figure A.2) (Chaudhury et al., 2013).

The mPFC contribution to depression has also been thoroughly investigated at the epigenetic and molecular level. A comprehensive transcriptional profiling study identified Sdk1, amongst others, as a susceptible-specific transcriptional regulator. Sdk1 overexpression in the mPFC increased sociability in susceptible mice, while Sdk1 overexpression in the vHPC had the opposite effect (Bagot et al., 2016). This highlights the importance of brain region-specific manipulations and analyses, as the same protein may have drastically difference effects dependent on its regional localization. Epigenetic modifications in the mPFC have also been reported in depression. Inhibition of histone deacetylases in the mPFC induces anti-depressive-like effects after CSDS (Covington et al., 2015). Furthermore, the histone demethylase, *Phf8* is highly expressed in the mPFC. Knockout of *Phf8* confers no developmental effects, however mice exhibit a significant increase in resilience to CSDS (Walsh et al., 2017). Specific deletion of *Phf8* in mPFC induces a substantial upregulated of serotonin receptors (Htr1a, Htr1b, and Htr2a) in the area, suggesting that histone modifications are crucial regulators of depression. Interestingly, 5-Htr1b has been suggested

to regulate the response to selective serotonin reuptake inhibitors and has been shown to be downregulated in the NAc in susceptible animals (Bagot et al., 2017). This downregulation was reversed after treatment with ketamine, a promising treatment for MDD (Bagot et al., 2017; Zanos et al., 2016). Further studies investigating subregional differences within the mPFC, and whether projection-specific epigenetic or transcriptional changes occur are required as technologies advance.

Ventral hippocampus (vHPC)

An abundance of evidence has also implicated the vHPC as another good candidate for differentially regulating NAc D1- and D2-MSNs. Interestingly, unlike mPFC-NAc afferents, attenuating synaptic strength of vHPC-NAc via an artificial long term depression induces resiliency to CSDS, while enhancement of these inputs induces a susceptible phenotype to stress (Figure A.2) (Bagot et al., 2015). Indeed, synaptic transmission from vHPC to NAc is increased in mice susceptible to CSDS whereas that from mPFC to NAc is decreased; supporting the notion of pathway specific neural adaptations in response to CSDS. Moreover, chronic optogenetic stimulation within the vHPC induced distinct changes in the expression of ΔFosB (Lobo et al., 2013). As previously mentioned, ΔFosB expression in the NAc D1-MSNs and D2-MSNs has separate roles in depressive behaviors, suggesting that these different cell types may receive different information from the vHPC in response to stress.

Studies have also reported transcriptional changes within the vHPC that underlie susceptibility to depression. *Dkkl1*, *Neurod2*, and *Sdk1* were all identified as genes that were upregulated in the vHPC following CSDS. Overexpression of these molecules specifically in the vHPC all induced susceptibility (Bagot et al., 2016). Moreover, chronic imipramine

treatment, a tricyclic antidepressant, induced a significant upregulation in *CTLA4*, a gene previously implicated in cohorts of Korean and Chinese MDD patients (Bagot et al., 2017; Jun et al., 2001; Liu et al., 2011). Circuit specific manipulations, in particular how NAc-projecting vHPC neurons differentially express these genes compared to other vHPC neurons, will be interesting to elucidate whether the efferent targets of neurons within a single brain region can affect gene expression in response to aversive environmental events.

Basolateral amygdala (BLA)

The BLA also sends strong projections to the NAc. While optogenetic stimulation of amygdala inputs to NAc in susceptible animals acutely reversed social withdrawal behavior, synaptic changes as tested by paired pulse ratio (PPR) were not as significant as those seen from vHPC and mPFC afferents (Figure A.2) (Bagot et al., 2015). Additionally, optogenetically inducing LTD at BLA-NAc synapses had no effect on behavior in contrast to vHPC afferents. Correspondingly, expression of the immediate early genes *Arc* and *Egr1* showed no significant change in the BLA of depressed animals while a significant reduction in *Arc* was measured in susceptible, but not resilient animals in NAc-projecting mPFC neurons (Bagot et al., 2015). Other studies using extracellular *in vivo* recordings show that activity of the mPFC-to-BLA circuit is predictive of stress vulnerability (Kumar et al., 2014). Collectively, it appears that the NAc, mPFC, vHPC, and BLA circuits are all inextricably linked and it is likely that epigenetic, transcriptional, and cellular changes in one region induces adaptations in other regions that ultimately manifest as MDD. Studies analyzing how these separate regions integrate changes from other areas will be necessary in the future to comprehensively describe the etiology of depression.

Thalamic inputs

More recent NAc afferent studies have expanded focus to thalamic areas (Zhu et al., 2016). Christoffel et al. (2015) reported significantly increased excitatory synaptic strength of intralaminar thalamic (ILT) neurons projecting to the NAc in susceptible, but not resilient mice (Figure A.2). Artificial reduction of the ILT-NAc pathway induced a reversal in social withdrawal behavior, and caused structural changes in NAc MSNs as well as measured by spine density (Christoffel et al., 2015).

Together, the broad and varied input circuitry to the NAc beget diverse and separate roles for specific inputs. As evidenced here, different inputs to the same brain area may have opposing roles. Thus, it is increasingly imperative to consider specific afferents, and specific cell types within a single brain area to fully capture the heterogenous roles in a condition as complex and nuanced as MDD.

Roles of LHb in depressive behaviors

The lateral habenula (LHb), a relatively small epithalamic structure, has received considerable preclinical and clinical attention in treating MDD in recent years. The LHb is broadly believed to signal aversion, with increases in activity resulting in behavioral avoidance in many animal studies (Proulx et al., 2014). The LHb also extensively connects with monoaminergic centers of the brain including the DRN containing serotonergic neurons and the previously mentioned VTA DA neurons, which have been heavily linked to development of MDD (Beier et al., 2015; Watabe-Uchida et al., 2012; Weissbourd et al., 2014).

These connections make the LHb anatomically poised to encode monoaminergic tone into motivational output. Indeed, previous reports have shown that inputs to the LHb from the entopeduncular nucleus (EP), the rodent correlate of the human globus pallidus interna, mediate aversion and negative affect associated with cocaine withdrawal (Meye et al., 2016; Shabel et al., 2014). While dopamine has no effect on EP-to-LHb synaptic transmission, serotonin suppressed both excitatory input to the LHb and the intrinsic excitability of LHb neurons (Shabel et al., 2012). Alteration of glutamate and GABA co-release at the EP-to-LHb synapse has been reported in the chronic learned helplessness (cLH) model of depression as well. In line with the hypothesis that increased activity in LHb encodes aversion, cLH animals exhibited reduced ratios of inhibitory/excitatory response at the EP-to-LHb synapse primarily driven by reduced GABAergic transmission. Furthermore, chronic citalopram (a commonly prescribed SSRI antidepressant) administration not only alleviated behavioral symptoms of cLH animals, but also increased GABA/AMPA ratios providing a possible mechanism for antidepressant action in the LHb (Shabel et al., 2014).

Other reports have corroborated these results and found that increased activity in VTA-projecting LHb neurons correlates with the severity of helplessness behavior exhibited by animals subjected to cLH (Li et al., 2011). This potentiation of excitatory activity in the LHb was reported to be due to an increase in presynaptic release probability. Furthermore, injection of the GABA agonist muscimol into LHb induced antidepressant-like effects in cLH rats (Winter et al., 2011). These effects do not appear limited to the cLH model of depressive-like symptoms, as chemogenetic inhibition of the LHb with DREADDs increased social approach behavior in animals that underwent CSDS (Sachs et al., 2015).

The plethora of preclinical work has underscored the LHb as a potential therapeutic target in humans. Promising preclinical work in rodents using DBS of the LHb has yielded significant reversal of depressive-like behaviors (Li et al., 2011). This has translated into promising nascent studies using LHb DBS in humans in treatment resistant depression. DBS resulted in complete remission of depressive-like symptoms in one patient, with relapses closely corresponding with malfunctions in the DBS pacer, and an ongoing second patient showing 50% improvement on a depressive symptom scale (Kiening and Sartorius, 2013; Sartorius et al., 2010). Collectively, the work generated from animal models and human clinical studies highlight the LHb as a critical mediator of depressive-like behaviors that merits further study.

Roles of distinct ventral pallidal circuits in CSDS-induced depressive behaviors

The ventral pallidum (VP) is known to receive dense inputs from both D1- and D2-MSNs in the NAc and transmits this information to downstream targets such as the LHb, VTA, and lateral hypothalamus (LH) (Kupchik et al., 2015; Root et al., 2015). Studies have also underscored the dopaminergic, glutamatergic, and GABAergic VTA neurons as major efferent targets of the VP (Beier et al., 2015; Faget et al., 2016). Thus, it follows that the VP is proposed to be an important convergent point at the interface of the motivational and reward circuitry implicated in drug addiction and depression. Its varied outputs and close connections with aversive centers such as the LHb, and reward-promoting centers such as the VTA, make it potentially well situated to encode diverse types of valence information (Root et al., 2015). Indeed, a recent study revealed differential cocaine-induced synaptic alterations in VTA-

projecting VP neurons receiving input from either D1- or D2-MSNs (Creed et al., 2016). This synapse requires further investigation in the context of depression.

Additional studies have shown selective decreases in VP serotonin receptor binding in patients with MDD, and that the VP is critical for the antidepressant effects of ketamine (Murrough et al., 2011; Yamanaka et al., 2014). However, it remains largely unknown how the VP circuitry contributes to depression, and whether specific cell types within the VP are responsible for these effects, much like what has been described in the NAc (Chandra et al., 2017; Francis et al., 2015).

Recent studies have identified parvalbumin-positive (PV) neurons in the VP as key regulators of phenotypes induced by CSDS (Knowland et al., 2017). Chronic silencing of VP PV neuronal activity during the induction phase of CSDS promotes a pro-resilient phenotype in mice. VP PV neurons were found to send largely non-collateralized projections to the lateral habenula (LHb) or ventral tegmental area (VTA), but not both and exhibited different electrophysiological adaptations in response to CSDS. VP PV neurons that project to the VTA receive increased excitatory input in susceptible, but not animals resilient to CSDS (Figure A.2) (Knowland et al., 2017). Conversely, neurons projecting to the LHb from susceptible animals exhibited significant increases in intrinsic excitability, an effect not seen in resilient animals. Furthering their relevance towards depression, these cellular adaptations were normalized back to control levels when susceptible animals were given two weeks of chronic fluoxetine treatment (Knowland et al., 2017).

Interestingly, LHb-projecting VP PV neurons were found to be predominantly glutamatergic. Thus, increased activity in this population of neurons found in susceptible

animals would ultimately drive increased LHb cellular activity, in line with what other studies have seen in animal models of depression (Proulx et al., 2014). On the other hand, the neurotransmitter identity of VTA-projecting VP PV neurons depended on their cellular target within the VTA. GABAergic VTA neurons received exclusively GABAergic input from VP PV neurons while DA VTA neurons received mixed excitatory and inhibitory input, with a slight bias toward glutamatergic innervation. Given that VTA-projecting VP PV neurons exhibited increased firing in animals susceptible to CSDS, it may be that increased GABAergic innervation onto local VTA GABAergic neurons results in net disinhibition of VTA DA neurons. Net disinhibition would increase VTA DA activity and be in line with previous studies describing hyperactivity of VTA DA neurons in the depressive state (Cao et al., 2010; Chaudhury et al., 2013). Furthermore, since glutamatergic VP neurons are biased towards VTA DA neurons, this may provide another, more direct mechanism by which susceptible animals exhibit enhanced VTA DA activity. Collectively, hyperactivity within the VP may lie upstream of aberrant VTA DA activity that has been highlighted as a hallmark of animals susceptible to CSDS, however more studies are required to support this hypothesis.

It was also found that selective chemogenetic or optogenetic silencing of LHb-projecting VP PV neurons attenuated behavioral despair in the tail suspension test, with no effect on VTA-projecting VP PV manipulation. Conversely, silencing of VTA-projecting VP PV neurons in susceptible animals reversed social withdrawal induced by CSDS (Knowland et al., 2017). Together, this suggests that separate circuits that originate from the same brain area and even same cell type can mediate discrete behavioral facets of depression and can exhibit separate cellular adaptations as well. Further studies are required to differentiate whether VP-to-VTA DA neurons or VP-to-VTA GABAergic neurons are selectively

necessary or sufficient to engage a depressive circuit, or if coordinated activity between these two downstream areas is more important.

In contrast, another study in rats reported a reduction in VTA DA firing after CMS was given (Chang and Grace, 2014), paralleling other studies using the CMS model of stress-elicited depression-related behaviors (Tye et al., 2013). This CMS-induced reduction in VTA DA firing was dependent on VP activity, as blockade of glutamatergic inputs to the VP via local infusion of kynurenic acid reversed this effect (Chang and Grace, 2014). These inputs likely originated from the BLA, as attenuation of BLA activity recapitulated the effect on VTA DA neurons. While the direction of stress-induced changes in VTA DA activity remains to be parsed out on a model by model basis, these studies highlight the intimate relationship of the VP-VTA circuitry and its putative relevance towards MDD.

These studies begin to shed light on how the VP integrates with other major players in the depressive circuitry such as the NAc and VTA and how concerted activity between these areas may contribute to the diverse behavioral phenotypes that manifest in MDD. However there remains a dearth of studies examining the role of the VP in the context of depression. While a few human imaging studies also support this idea (Murrough et al., 2011; Yamanaka et al., 2014), further efforts to elucidate the underlying mechanisms must be undertaken to provide more useful insight for relevant and effective human clinical studies.

Monoamines

Alterations in monoaminergic tone have long been believed to be a critical etiology in MDD (Chaudhury et al., 2015; Heninger et al., 1996). Indeed, many available, approved therapeutic treatments such as serotonin and norepinephrine reuptake inhibitors (SSRIs) target

these chemical pathways. DBS stimulation in the vmPFC in rodents reversed social deficits induced by CSDS while also reversing CSDS-induced serotonergic neuronal alterations (Veerakumar et al., 2014). Many animal studies have highlighted antidepressant serotonergic effects on the EP-LHb pathway (Li et al., 2011; Shabel et al., 2014; Shabel et al., 2012). Others have found significant effects of fluoxetine on neural activity in the VP which receives dense input from the major serotonergic nuclei in the brain, the dorsal raphe nucleus (DRN) (Knowland et al., 2017). Moreover, reports have delineated differential effects of fluoxetine, ketamine, and imipramine on gene expression in the mPFC, NAc, amygdala, and vHPC (Bagot et al., 2017; Vialou et al., 2015). Social defeat in rats resulted in a significant increase in *cfos* reactivity in serotonergic neurons in the DRN, suggesting that they play a critical role mediated social defeat-induced depressive-like behaviors (Paul et al., 2011). Tryptophan hydroxylase 2 knockin mice which display a 60-80% reduction in brain serotonin levels were more susceptible to CSDS and resistant to antidepressant treatment (Sachs et al., 2015).

Since aberrations in VTA DA neuronal activity have been heavily studied in MDD and the DRN is one of the largest input structures to these neurons, the $DRN^{serotonin}$ to $VTA^{dopamine}$ pathway remains an interesting, yet largely unexplored circuit. Norepinephrine (noradrenaline) may also contribute to the expression of depression-related behaviors, as chronic stimulation of norepinephrine terminals in the VTA originating from the locus coeruleus (LC) after CSDS promoted recovery of social withdrawal deficits. Similarly, chronic treatment of the □2-noradrenergic receptor antagonist idazoxan which increases LC firing recapitulates the optogenetic antidepressant effects (Isingrini et al., 2016)

How interconnected or separate are monoaminergic pathways involved in the expression of depressive-like behaviors? Few studies have attempted to examine the concerted relative contributions of serotonin and dopamine towards discrete depressive-like behaviors. This is in spite of the fact that one of the main inputs to the VTA is the DRN (Beier et al., 2015; Faget et al., 2016; Watabe-Uchida et al., 2012) and alterations of this circuitry have been shown to mediate antidepressant efficacy (Adachi et al., 2017; Neumaier et al., 1996). Understanding how serotonergic inputs to the VTA can affect animals' response to stress, especially in the context of depression, and how this input may modulate different downstream targets such as the LHb or dopaminergic signaling in the NAc or mPFC remain important questions to answer in the future.

Beyond monoamines, as previously described in detail in this review, other studies have honed in on aberrant dopamine signaling in the VTA-NAc and VTA-mPFC circuit or NAc dynorphinergic activity as a critical driver of depressive-like behaviors (Chaudhury et al., 2013; Knoll and Carlezon, 2010; Tye et al., 2013). Additional studies have highlighted the antidepressant effects of increased oxytocin in CSDS (Lukas et al., 2011), further revealing the complex etiology and path towards an effective treatment for MDD.

Modelling depression-related behaviors in females

MDD and related affective disorders are nearly twice as prevalent in females than males (Kessler et al., 1993, 2005). In spite of this significant disparity, male-centric preclinical animal studies of MDD predominate the literature. In particular, CSDS relies upon male on male intruder-resident aggressive behavior which is absent in female C57BL6 mice.

Thus, significant efforts to develop and adopt new models of MDD, or adapt existing models, with sufficient predictive and face validity are currently underway.

California mice, as opposed to the widely used C57BL6 laboratory strain, are territorial creatures that will actively attack intruders encroaching on their home. This unbiased aggression allows for social defeat in both males and females. Curiously, CSDS in California mice induces social avoidance only in females (Trainor et al., 2011) and results in an increase in the number of tyrosine hydroxylase, a marker for putative dopaminergic neurons, positive neurons in the VTA (Greenberg et al., 2015). In line with studies in male C57BL6 mice, social defeat stress in both male and female California mice also elicited increases in dopamine in the NAc and that stress-induced social withdrawal ins dependent on D1 receptors in the NAc (Campi et al., 2014). While useful, a significant drawback using California mice is the substantial lack of genetic lines expressing Cre-recombinase. Thus, circuit-based studies using cell type-specific expression of viral opsins remain severely limited at this point in time.

Bypassing the need to use California mice, a recent study successfully adapted CSDS in C57BL6 female animals. Instead of the classical two part physical/sensory stage CSDS paradigm, females observe the physical defeat of a conspecific male intruder by a male CD1 aggressor. Aptly named vicarious defeat stress (VDS), females only observe physical defeat but never actually experience it. 10 consecutive days of VDS induces the typical phenotypes of social avoidance, anhedonia, and increased serum corticosterone levels normally found in CSDS (Iñiguez et al., 2017). Although the induction protocol is slightly different than regular

CSDS and different circuits may be involved, VDS offers a close correlate by which investigators can utilize the myriad viral-genetic approaches in C57BL6 female mice.

As previously mentioned, there also exist models such as CMS or learned helplessness that are capable of inducing depressive-like phenotypes in both males and females. Despite this, many studies still choose to focus strictly on male subjects (Chang and Grace, 2014; Li et al., 2013; Moreines et al., 2017; Tye et al., 2013). This may be, in large part, due to the fact that studies which incorporate both sexes find significant sex-dependent molecular and physiological differences (Brancato et al., 2017; Hodes et al., 2015; Labonté et al., 2017). Ironically, this also underscores the pressing need to not only adopt sex-inclusive models of depression, but to compare both sexes in a study.

An adaptation of CMS, the subchronic variable stress model (SCVS) which relies upon roughly a week of daily variable unpredictable stressors, induces depressive-like behaviors only in females, which may mirror the increased susceptibility of females to MDD in humans (Hodes et al., 2015). Using SCVS, researchers found measured a more pronounced upregulation of DNA methyltransferase 3a (*Dnmt3a*) in the NAc in females than in males (Hodes et al., 2015). Interestingly, NAc-specific overexpression of *Dnmt3a* in females promoted resilience, while the same treatment in males promoted susceptibility (Hodes et al., 2015). Other studies have utilized to SCVS to uncover sex-specific synaptic and micro-RNA profile changes in the NAc as well (Brancato et al., 2017; Pfau et al., 2016). Females undergoing SCVS exhibited an increase in expression of the vesicular glutamate transporter-2, and a reduction in vesicular glutamate transporter-1 in the NAc (Brancato et al., 2017).

Beyond the NAc, region specific RNA-seq analysis after CVS (similar to SCVS but for 3 weeks and elicits depression-related behaviors in both sexes) also found a selective downregulation of *Dusp6* in females in mPFC. Correspondingly, viral downregulation of mPFC *Dusp6* also promoted anhedonia and increased latency to eat in the novelty-suppressed feeding test as well (Labonté et al., 2017). Contrarily, *Emx1* was found to be selectively upregulated in males post CVS and viral overexpression promoted susceptibility to depression-related behaviors (Labonté et al., 2017).

Indeed, several useful models capable of inducing depression-related behaviors in strictly males, females, or both are being developed; each with their advantages and drawbacks. Careful consideration of the construct, face, and predictive validities of each in the context of interpreting results remain critical to effectively driving the field forward and to properly model the sex differences that exist in human MDD patients.

Conclusions and future directions

The development of viral-mediated gene delivery tools, transgenic mice approaches, and the increased accessibility of RNA sequencing (RNA-seq) in single cells have created exciting avenues for in depth analysis of the mesolimbic circuitry including the NAc, VP, and VTA. Even with several decades of research on reward circuitry, the molecular diversity of these brain circuitry has not been fully elucidated. As we have seen, discrete cell types (i.e. dopaminergic neurons) within a single brain region might display considerable functional heterogeneity depending on its efferent target. Thus, uncovering separate molecular markers that can discriminate between these two populations will make development of precise therapeutics that can pharmacologically target them more tractable. Single cell molecular

profiling techniques such as Drop-seq, which utilizes cell-specific DNA barcodes to sequence individual cells, allows for unbiased screening and identification of potentially novel subpopulations of neurons not previously identified that could have functional relevance in depression-related behaviors (Macosko et al., 2015). Further refinement of other existing techniques utilizing fluorescence-activated cell sorting (FACS) combined with single cell profiling techniques would allow for researchers to virally label cell-type and projection-specific populations and obtain sequencing data for these separate populations as well (Tirosh et al., 2016). Combining the available anatomical circuit information with the precise molecular identity of neurons will be beneficial to provide a fundamental framework to understand the neural basis of MDD as well as reward-related behaviors and their disorders.

Given these recent advances, why then is there such a disconnect between bench discoveries to bedside treatments? Clearly, no obvious answer exists except for that MDD is a multi-faceted, complex condition; but we can offer a supplementary explanation.

Provided that most manipulations either directly or indirectly target activity within the reward and/or motivational circuitry, it is fair to wonder if these experiments are simply temporary alleviations of depression-related behaviors by virtue of acutely increasing reward, but ultimately don't address the underlying etiology. Acute optogenetic-induced reversals of depression-related behavior may simply be epiphenomena. How do we separate temporary induced aversion from exacerbation of the core cause of depression, or is it simply a debate of semantics? It is telling that the vast majority of studies using optogenetic manipulations or overexpression of certain genes after CMS or CSDS look predominantly at a single timepoint tested right after the CMS or CSDS protocol, even though certain CSDS-induced symptoms

are reported to persist 40 days after stress cessation (Krishnan et al., 2007). Most manipulations report a reduction in social avoidance and anhedonic behavior during manipulation; however, no long-term follow up is provided. Do depression-related behaviors that are temporarily attenuated during manipulation re-emerge one day, a week, or even immediately after cessation? While manipulating reward or motivation-related brain areas may be necessary or sufficient to induce acute reward that can temporarily 'override' depressive-like behaviors in animals, the ultimate goal towards the development of better treatments or a cure, so to speak, for MDD based on animal research is not just a temporary fix but understanding and reversing the core etiology. Thus, adjusting the standard for studies to use long-term follow up as a critical study end-point is imperative for the future.

In sum, the wide patient to patient variability of behavioral symptoms of depression compel researchers to understand how separate circuits or cell-types in the brain can underlie specific depressive-like phenotypes. Future studies that take a systematic approach to integrate separate pathways and how they differentially regulate behavioral symptoms of depression will be critical to uncover the etiology of MDD and drive the discovery of more effective therapeutics.

Appendix A, Circuit-based Frameworks of Depressive Behaviors: The Role of Reward Circuitry and Beyond, is a reprint of Knowland D, Lim BK. *The Neural Basis of Depressive Behaviors: The Role of Reward Circuitry and Beyond*. Pharmacology Biochemistry and Behavior (2018) DOI: 10.1016/j.pbb.2017.12.010. The dissertation author was the primary researcher and author of this review paper.

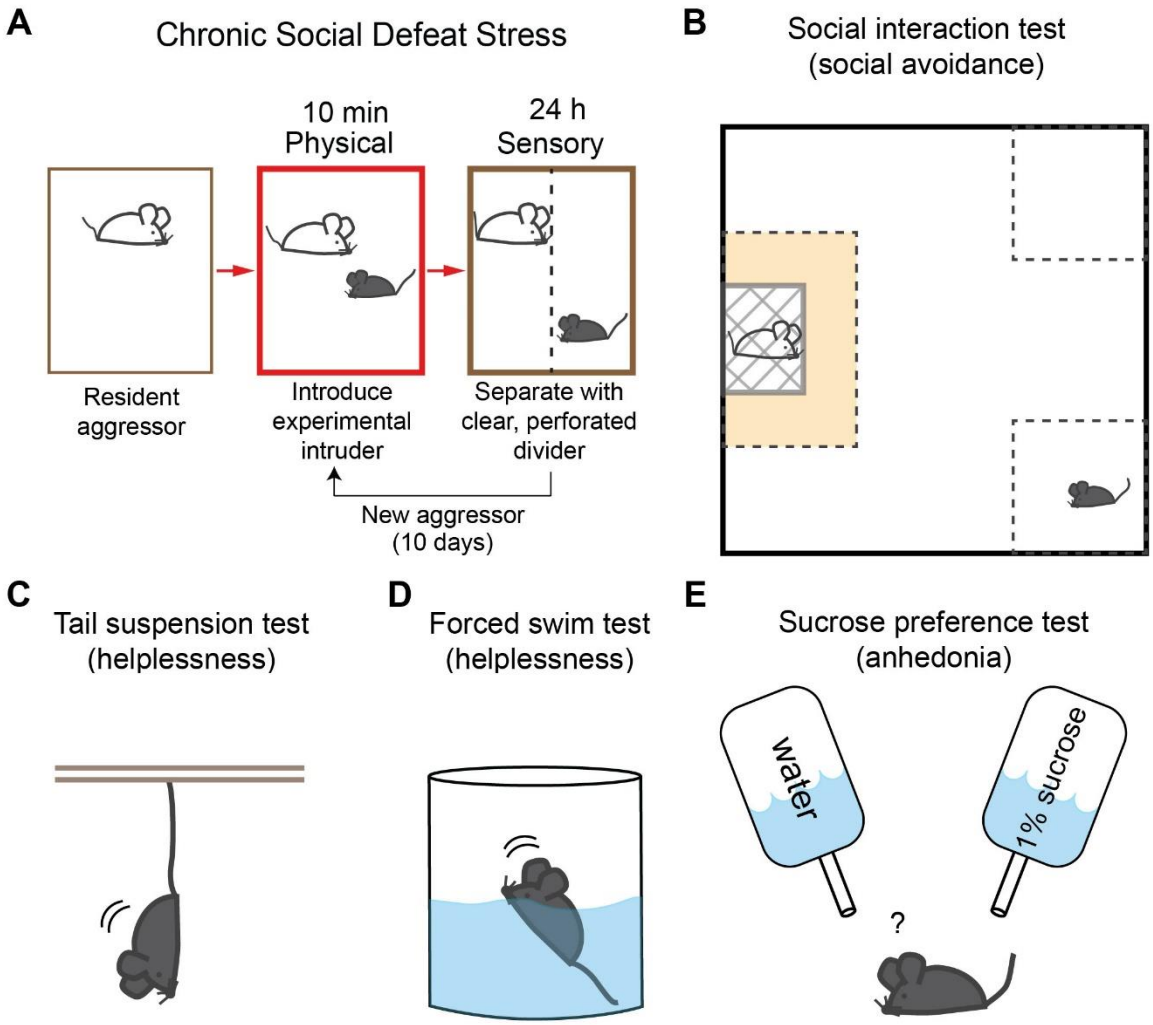

Figure A.1: Schematic diagram of chronic social defeat stress (CSDS) (A), and commonly used behavioral tests for different depressive behaviors, social interaction (B), helplessness (C, D), and anhedonia (E).

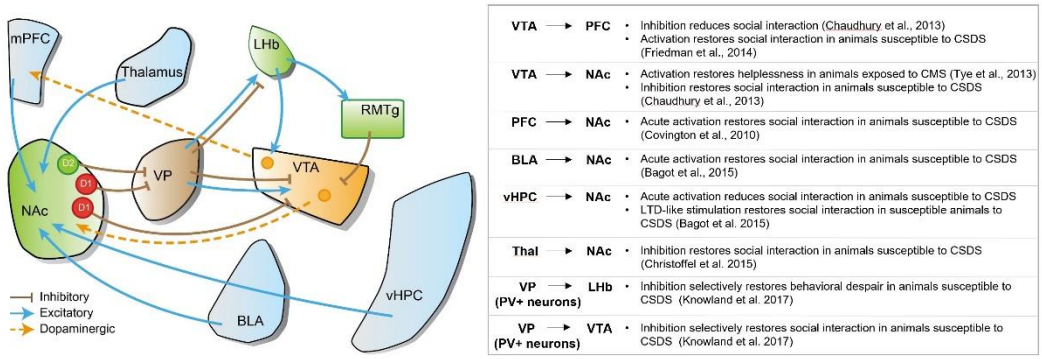

Figure A.2: Optogenetic manipulations of neural circuits in animal models of depression. . Schematic diagram of the reward circuitry and its connections. Summary of accumulated optogenetic evidence of NAc afferent projections and dopaminergic outputs in animal models of depression.

References

Adachi M, Autry AE, Mahgoub M, Suzuki K and Monteggia LM (2017) TrkB Signaling in Dorsal Raphe Nucleus is Essential for Antidepressant Efficacy and Normal Aggression Behavior. Neuropsychopharmacology 42:886-894.

Al-Hasani, R., McCall, J.G., Shin, G., Gomez, A.M., Schmitz, G.P., Bernardi, J.M., Pyo, C.O., Park, S. Il, Marcinkiewcz, C.M., Crowley, N.A., et al. (2015). Distinct Subpopulations of Nucleus Accumbens Dynorphin Neurons Drive Aversion and Reward. Neuron 87, 1063–1077.

Andrade L, Caraveo-Anduaga JJ, Berglund P, Bijl RV, De Graaf R, Vollebergh W, Dragomirecka E, Kohn R, Keller M, Kessler RC, Kawakami N, Kilic C, Offord D, Ustun TB and Wittchen HU (2003) The epidemiology of major depressive episodes: results from the International Consortium of Psychiatric Epidemiology (ICPE) Surveys. Int J Methods Psychiatr Res 12:3-21.

Bagot RC, Cates HM, Purushothaman I, Lorsch ZS, Walker DM, Wang J, Huang X, Schluter OM, Maze I, Pena CJ, Heller EA, Issler O, Wang M, Song WM, Stein JL, Liu X, Doyle MA, Scobie KN, Sun HS, Neve RL, Geschwind D, Dong Y, Shen L, Zhang B and Nestler EJ (2016) Circuit-wide Transcriptional Profiling Reveals Brain Region-Specific Gene Networks Regulating Depression Susceptibility. Neuron 90:969-983.

Bagot RC, Cates HM, Purushothaman I, Vialou V, Heller EA, Yieh L, LaBonte B, Pena CJ, Shen L, Wittenberg GM and Nestler EJ (2017) Ketamine and Imipramine Reverse Transcriptional Signatures of Susceptibility and Induce Resilience-Specific Gene Expression Profiles. Biol Psychiatry 81:285-295.

Bagot RC, Parise EM, Pena CJ, Zhang HX, Maze I, Chaudhury D, Persaud B, Cachope R, Bolanos-Guzman CA, Cheer JF, Deisseroth K, Han MH and Nestler EJ (2015) Ventral hippocampal afferents to the nucleus accumbens regulate susceptibility to depression. Nat Commun 6:7062.

Beier KT, Steinberg EE, DeLoach KE, Xie S, Miyamichi K, Schwarz L, Gao XJ, Kremer EJ, Malenka RC and Luo L (2015) Circuit Architecture of VTA Dopamine Neurons Revealed by Systematic Input-Output Mapping. Cell 162:622-634.

Berton O, McClung CA, Dileone RJ, Krishnan V, Renthal W, Russo SJ, Graham D, Tsankova NM, Bolanos CA, Rios M, Monteggia LM, Self DW and Nestler EJ (2006) Essential role of BDNF in the mesolimbic dopamine pathway in social defeat stress. Science 311:864-868.

Berton O and Nestler EJ (2006) New approaches to antidepressant drug discovery: beyond monoamines. Nat Rev Neurosci 7:137-151.

Brancato, A., Bregman, D., Ahn, H.F., Pfau, M.L., Menard, C., Cannizzaro, C., Russo, S.J., and Hodes, G.E. (2017). Sub-chronic variable stress induces sex-specific effects on glutamatergic synapses in the nucleus accumbens. Neuroscience 350, 180–189.

Campi, K.L., Greenberg, G.D., Kapoor, A., Ziegler, T.E., and Trainor, B.C. (2014). Sex differences in effects of dopamine D1 receptors on social withdrawal. Neuropharmacology 77, 208–216.

Cao JL, Covington HE, 3rd, Friedman AK, Wilkinson MB, Walsh JJ, Cooper DC, Nestler EJ and Han MH (2010) Mesolimbic dopamine neurons in the brain reward circuit mediate susceptibility to social defeat and antidepressant action. J Neurosci 30:16453-16458.

Carr, G. V, Bangasser, D.A., Bethea, T., Young, M., Valentino, R.J., and Lucki, I. (2010). Antidepressant-Like Effects of κ-Opioid Receptor Antagonists in Wistar Kyoto Rats. Neuropsychopharmacology 35, 752–763.

Chandra R, Francis TC, Nam H, Riggs LM, Engeln M, Rudzinskas S, Konkalmatt P, Russo SJ, Turecki G, Iniguez SD and Lobo MK (2017) Reduced Slc6a15 in Nucleus Accumbens D2-Neurons Underlies Stress Susceptibility. J Neurosci 37:6527-6538.

Chang, C.H., and Grace, A.A. (2014). Amygdala-ventral pallidum pathway decreases dopamine activity after chronic mild stress in rats. Biol. Psychiatry 76, 223–230.

Chaudhury D, Liu H and Han MH (2015) Neuronal correlates of depression. Cell Mol Life Sci 72:4825-4848.

Chaudhury D, Walsh JJ, Friedman AK, Juarez B, Ku SM, Koo JW, Ferguson D, Tsai HC, Pomeranz L, Christoffel DJ, Nectow AR, Ekstrand M, Domingos A, Mazei-Robison MS, Mouzon E, Lobo MK, Neve RL, Friedman JM, Russo SJ, Deisseroth K, Nestler EJ and Han MH (2013) Rapid regulation of depression-related behaviours by control of midbrain dopamine neurons. Nature 493:532-536.

Christoffel DJ, Golden SA, Walsh JJ, Guise KG, Heshmati M, Friedman AK, Dey A, Smith M, Rebusi N, Pfau M, Ables JL, Aleyasin H, Khibnik LA, Hodes GE, Ben-Dor GA, Deisseroth K, Shapiro ML, Malenka RC, Ibanez-Tallon I, Han MH and Russo SJ (2015) Excitatory transmission at thalamo-striatal synapses mediates susceptibility to social stress. Nat Neurosci 18:962-964.

Cooper, M.A., and Huhman, K.L. (2007). Corticotropin-releasing factor receptors in the dorsal raphe nucleus modulate social behavior in Syrian hamsters. Psychopharmacology (Berl). 194, 297–307.

Covington HE, 3rd, Lobo MK, Maze I, Vialou V, Hyman JM, Zaman S, LaPlant Q, Mouzon E, Ghose S, Tamminga CA, Neve RL, Deisseroth K and Nestler EJ (2010)

Antidepressant effect of optogenetic stimulation of the medial prefrontal cortex. J Neurosci 30:16082-16090.

Covington HE, 3rd, Maze I, Vialou V and Nestler EJ (2015) Antidepressant action of HDAC inhibition in the prefrontal cortex. Neuroscience 298:329-335.

Cravchik A and Goldman D (2000) Neurochemical individuality: genetic diversity among human dopamine and serotonin receptors and transporters. Arch Gen Psychiatry 57:1105-1114.

Creed M, Ntamati NR, Chandra R, Lobo MK and Luscher C (2016) Convergence of Reinforcing and Anhedonic Cocaine Effects in the Ventral Pallidum. Neuron 92:214-226.

Di Chiara, G., and Imperato, A. (1988). Opposite effects of mu and kappa opiate agonists on dopamine release in the nucleus accumbens and in the dorsal caudate of freely moving rats. J Pharmacol Exp Ther 244, 1067–1080.

Dumitriu D, Laplant Q, Grossman YS, Dias C, Janssen WG, Russo SJ, Morrison JH and Nestler EJ (2012) Subregional, dendritic compartment, and spine subtype specificity in cocaine regulation of dendritic spines in the nucleus accumbens. J Neurosci 32:6957-6966.

Dunlop BW and Mayberg HS (2014) Neuroimaging-based biomarkers for treatment selection in major depressive disorder. Dialogues Clin Neurosci 16:479-490.

Dunlop BW and Nemeroff CB (2007) The role of dopamine in the pathophysiology of depression. Arch Gen Psychiatry 64:327-337.

Ebner, S.R., Roitman, M.F., Potter, D.N., Rachlin, A.B., and Chartoff, E.H. (2010). Depressive-like effects of the kappa opioid receptor agonist salvinorin A are associated with decreased phasic dopamine release in the nucleus accumbens. Psychopharmacology (Berl). 209, 241–252.

Eisch AJ, Bolanos CA, de Wit J, Simonak RD, Pudiak CM, Barrot M, Verhaagen J and Nestler EJ (2003) Brain-derived neurotrophic factor in the ventral midbrain-nucleus accumbens pathway: a role in depression. Biol Psychiatry 54:994-1005.

Faget L, Osakada F, Duan J, Ressler R, Johnson AB, Proudfoot JA, Yoo JH, Callaway EM and Hnasko TS (2016) Afferent Inputs to Neurotransmitter-Defined Cell Types in the Ventral Tegmental Area. Cell Rep 15:2796-2808.

Fenno, L.E., Mattis, J., Ramakrishnan, C., Hyun, M., Lee, S.Y., He, M., Tucciarone, J., Selimbeyoglu, A., Berndt, A., Grosenick, L., et al. (2014). Targeting cells with single vectors using multiple-feature Boolean logic. Nat. Methods 11, 763–772.

Ferrari AJ, Charlson FJ, Norman RE, Flaxman AD, Patten SB, Vos T and Whiteford HA (2013) The epidemiological modelling of major depressive disorder: application for the Global Burden of Disease Study 2010. PLoS One 8:e69637.

Francis TC, Chandra R, Friend DM, Finkel E, Dayrit G, Miranda J, Brooks JM, Iniguez SD, O'Donnell P, Kravitz A and Lobo MK (2015) Nucleus accumbens medium spiny neuron subtypes mediate depression-related outcomes to social defeat stress. Biol Psychiatry 77:212-222.

Francis TC and Lobo MK (2017) Emerging Role for Nucleus Accumbens Medium Spiny Neuron Subtypes in Depression. Biol Psychiatry 81:645-653.

Friedman AK, Walsh JJ, Juarez B, Ku SM, Chaudhury D, Wang J, Li X, Dietz DM, Pan N, Vialou VF, Neve RL, Yue Z and Han MH (2014) Enhancing depression mechanisms in midbrain dopamine neurons achieves homeostatic resilience. Science 344:313-319.

Grace, A.A., Floresco, S.B., Goto, Y., and Lodge, D.J. (2007). Regulation of firing of dopaminergic neurons and control of goal-directed behaviors. Trends Neurosci. 30, 220–227.

Greenberg, G.D., Steinman, M.Q., Doig, I.E., Hao, R., and Trainor, B.C. (2015). Effects of social defeat on dopamine neurons in the ventral tegmental area in male and female California mice. Eur. J. Neurosci. 1–14.

Hamani C, Diwan M, Macedo CE, Brandao ML, Shumake J, Gonzalez-Lima F, Raymond R, Lozano AM, Fletcher PJ and Nobrega JN (2010) Antidepressant-like effects of medial prefrontal cortex deep brain stimulation in rats. Biol Psychiatry 67:117-124.

Hamilton PJ, Burek DJ, Lombroso SI, Neve RL, Robison AJ, Nestler EJ and Heller EA (2017) Cell-Type-Specific Epigenetic Editing at the Fosb Gene Controls Susceptibility to Social Defeat Stress. Neuropsychopharmacology.

Heninger GR, Delgado PL and Charney DS (1996) The revised monoamine theory of depression: a modulatory role for monoamines, based on new findings from monoamine depletion experiments in humans. Pharmacopsychiatry 29:2-11.

Hodes, G.E., Pfau, M.L., Purushothaman, I., Ahn, H.F., Golden, S.A., Christoffel, D.J., Magida, J., Brancato, A., Takahashi, A., Flanigan, M.E., et al. (2015). Sex Differences in Nucleus Accumbens Transcriptome Profiles Associated with Susceptibility versus Resilience to Subchronic Variable Stress. J. Neurosci. 35, 16362–16376.

Hollis F, Wang H, Dietz D, Gunjan A and Kabbaj M (2010) The effects of repeated social defeat on long-term depressive-like behavior and short-term histone modifications in the hippocampus in male Sprague-Dawley rats. Psychopharmacology (Berl) 211:69-77.

Iñiguez, S.D., Flores-Ramirez, F.J., Riggs, L.M., Alipio, J.B., Garcia, I., Hernandez, M.A., Sanchez, D.O., Lobo, M.K., Serrano, P.A., Braren, S.H., et al. (2017). Vicarious Social Defeat Stress Induces Depression-related Outcomes in Female Mice. Biol. Psychiatry 1–9.

Isingrini, E., Perret, L., Rainer, Q., Amilhon, B., Guma, E., Tanti, A., Martin, G., Robinson, J., Moquin, L., Marti, F., et al. (2016). Resilience to chronic stress is mediated by noradrenergic regulation of dopamine neurons. Nat. Neurosci. 19.

Jun TY, Pae CU, Chae JH, Bahk WM and Kim KS (2001) Polymorphism of CTLA-4 gene for major depression in the Korean population. Psychiatry Clin Neurosci 55:533-537.

Kessler, R.C., McGonagle, K.A., Swartz, M., Blazer, D.G., and Nelson, C.B. (1993). Sex and depression in the National Comorbidity Survey I: Lifetime prevalence, chronicity and recurrence. J. Affect. Disord. 29, 85–96.

Kessler, R.C., Chiu, W.T., Demler, O., and Walters, E.E. (2005). Prevalence, Severity, and Comorbidity of. Arch Gen Psychiatry 62, 617–627.

Khibnik LA, Beaumont M, Doyle M, Heshmati M, Slesinger PA, Nestler EJ and Russo SJ (2016) Stress and Cocaine Trigger Divergent and Cell Type-Specific Regulation of Synaptic Transmission at Single Spines in Nucleus Accumbens. Biol Psychiatry 79:898-905.

Kiening K and Sartorius A (2013) A new translational target for deep brain stimulation to treat depression. EMBO Mol Med 5:1151-1153.

Knoll, A.T., and Carlezon, W.A. (2010). Dynorphin, stress, and depression. Brain Res. 1314, 56–73.

Knowland D, Lilascharoen V, Pacia CP, Shin S, Wang EH and Lim BK (2017) Distinct Ventral Pallidal Neural Populations Mediate Separate Symptoms of Depression. Cell 170:284-297 e218.

Krishnan V, Han MH, Graham DL, Berton O, Renthal W, Russo SJ, Laplant Q, Graham A, Lutter M, Lagace DC, Ghose S, Reister R, Tannous P, Green TA, Neve RL, Chakravarty S, Kumar A, Eisch AJ, Self DW, Lee FS, Tamminga CA, Cooper DC, Gershenfeld HK and Nestler EJ (2007) Molecular adaptations underlying susceptibility and resistance to social defeat in brain reward regions. Cell 131:391-404.

Krishnan V and Nestler EJ (2008) The molecular neurobiology of depression. Nature 455:894-902.

Krishnan V and Nestler EJ (2011) Animal models of depression: molecular perspectives. Curr Top Behav Neurosci 7:121-147.

Kumar S, Hultman R, Hughes D, Michel N, Katz BM and Dzirasa K (2014) Prefrontal cortex reactivity underlies trait vulnerability to chronic social defeat stress. Nat Commun 5:4537.

Kupchik YM, Brown RM, Heinsbroek JA, Lobo MK, Schwartz DJ and Kalivas PW (2015) Coding the direct/indirect pathways by D1 and D2 receptors is not valid for accumbens projections. Nat Neurosci 18:1230-1232.

Labonté, B., Engmann, O., Purushothaman, I., Menard, C., Wang, J., Tan, C., Scarpa, J.R., Moy, G., Loh, Y.-H.E., Cahill, M., et al. (2017). Sex-specific transcriptional signatures in human depression. Nat. Med. 23, 1102–1111.

Laman-Maharg, A.R., Copeland, T., Sanchez, E.O., Campi, K.L., and Trainor, B.C. (2017). The long-term effects of stress and kappa opioid receptor activation on conditioned place aversion in male and female California mice. Behav. Brain Res. 332, 299–307.

Lammel S, Hetzel A, Hackel O, Jones I, Liss B and Roeper J (2008) Unique properties of mesoprefrontal neurons within a dual mesocorticolimbic dopamine system. Neuron 57:760-773.

Lammel S, Ion DI, Roeper J and Malenka RC (2011) Projection-specific modulation of dopamine neuron synapses by aversive and rewarding stimuli. Neuron 70:855-862.

Lammel S, Lim BK and Malenka RC (2014) Reward and aversion in a heterogeneous midbrain dopamine system. Neuropharmacology 76 Pt B:351-359.

Li B, Piriz J, Mirrione M, Chung C, Proulx CD, Schulz D, Henn F and Malinow R (2011) Synaptic potentiation onto habenula neurons in the learned helplessness model of depression. Nature 470:535-539.

Li, K., Zhou, T., Liao, L., Yang, Z., Wong, C., Henn, F., Malinow, R., Yates, J.R., and Hu, H. (2013). βCaMKII in lateral habenula mediates core symptoms of depression. Science (80-.). 341, 1016–1020.

Lim BK, Huang KW, Grueter BA, Rothwell PE and Malenka RC (2012) Anhedonia requires MC4R-mediated synaptic adaptations in nucleus accumbens. Nature 487:183-189.

Liu J, Li J, Li T, Wang T, Li Y, Zeng Z, Li Z, Chen P, Hu Z, Zheng L, Ji J, Lin H, Feng G and Shi Y (2011) CTLA-4 confers a risk of recurrent schizophrenia, major depressive disorder and bipolar disorder in the Chinese Han population. Brain Behav Immun 25:429-433.

Lobo MK, Zaman S, Damez-Werno DM, Koo JW, Bagot RC, DiNieri JA, Nugent A, Finkel E, Chaudhury D, Chandra R, Riberio E, Rabkin J, Mouzon E, Cachope R, Cheer JF,

Han MH, Dietz DM, Self DW, Hurd YL, Vialou V and Nestler EJ (2013) DeltaFosB induction in striatal medium spiny neuron subtypes in response to chronic pharmacological, emotional, and optogenetic stimuli. J Neurosci 33:18381-18395.

Lopez Leon S, Croes EA, Sayed-Tabatabaei FA, Claes S, Van Broeckhoven C and van Duijn CM (2005) The dopamine D4 receptor gene 48-base-pair-repeat polymorphism and mood disorders: a meta-analysis. Biol Psychiatry 57:999-1003.

Lukas, M., Toth, I., Reber, S.O., Slattery, D.A., Veenema, A.H., and Neumann, I.D. (2011). The Neuropeptide Oxytocin Facilitates Pro-Social Behavior and Prevents Social Avoidance in Rats and Mice. Neuropsychopharmacology 36, 2159–2168.

MacAskill AF, Cassel JM and Carter AG (2014) Cocaine exposure reorganizes cell type- and input-specific connectivity in the nucleus accumbens. Nat Neurosci 17:1198-1207.

MacAskill AF, Little JP, Cassel JM and Carter AG (2012) Subcellular connectivity underlies pathway-specific signaling in the nucleus accumbens. Nat Neurosci 15:1624-1626.

Macosko EZ, Basu A, Satija R, Nemesh J, Shekhar K, Goldman M, Tirosh I, Bialas AR, Kamitaki N, Martersteck EM, Trombetta JJ, Weitz DA, Sanes JR, Shalek AK, Regev A and McCarroll SA (2015) Highly Parallel Genome-wide Expression Profiling of Individual Cells Using Nanoliter Droplets. Cell 161:1202-1214.

Mague, S.D., Pliakas, A.M., Todtenkopf, M.S., Tomasiewicz, H.C., Zhang, Y., Stevens, W.C., Jones, R.M., Portoghese, P.S. and Carlezon, W.A. (2003). Antidepressant-like effects of κ-opioid receptor antagonists in the forced swim test in rats. Journal of Pharmacology and Experimental Therapeutics 305(1), 323-330.

Mayberg HS, Lozano AM, Voon V, McNeely HE, Seminowicz D, Hamani C, Schwalb JM and Kennedy SH (2005) Deep brain stimulation for treatment-resistant depression. Neuron 45:651-660.

McLaughlin, J.P., Marton-Popovici, M., and Chavkin, C. (2003). Kappa opioid receptor antagonism and prodynorphin gene disruption block stress-induced behavioral responses. J. Neurosci. 23, 5674–5683.

Meerlo P, Overkamp GJ, Daan S, Van Den Hoofdakker RH and Koolhaas JM (1996) Changes in Behaviour and Body Weight Following a Single or Double Social Defeat in Rats. Stress 1:21-32.

Mendels J, Weinstein N and Cochrane C (1972) The relationship between depression and anxiety. Arch Gen Psychiatry 27:649-653.

Meye FJ, Soiza-Reilly M, Smit T, Diana MA, Schwarz MK and Mameli M (2016) Shifted pallidal co-release of GABA and glutamate in habenula drives cocaine withdrawal and relapse. Nat Neurosci 19:1019-1024.

Muir J, Lorsch ZS, Ramakrishnan C, Deisseroth K, Nestler EJ, Calipari ES and Bagot RC (2017) In Vivo Fiber Photometry Reveals Signature of Future Stress Susceptibility in Nucleus Accumbens. Neuropsychopharmacology.

Moreines, J.L., Owrutsky, Z.L., and Grace, A.A. (2017). Involvement of Infralimbic Prefrontal Cortex but not Lateral Habenula in Dopamine Attenuation After Chronic Mild Stress. Neuropsychopharmacology 42, 904–913.

Mucha, R.F., and Herz, A. (1985). Motivational properties of kappa and mu opioid receptor agonists studied with place and taste preference conditioning. Psychopharmacology (Berl). 86, 274–280.

Murrough JW, Henry S, Hu J, Gallezot JD, Planeta-Wilson B, Neumaier JF and Neumeister A (2011) Reduced ventral striatal/ventral pallidal serotonin1B receptor binding potential in major depressive disorder. Psychopharmacology (Berl) 213:547-553.

Nestler EJ (1998) Antidepressant treatments in the 21st century. Biol Psychiatry 44:526-533.

Nestler EJ and Hyman SE (2010) Animal models of neuropsychiatric disorders. Nat Neurosci 13:1161-1169.

Neumaier JF, Root DC and Hamblin MW (1996) Chronic fluoxetine reduces serotonin transporter mRNA and 5-HT1B mRNA in a sequential manner in the rat dorsal raphe nucleus. Neuropsychopharmacology 15:515-522.

Newton, S.S., Thome, J., Wallace, T.L., Shirayama, Y., Schlesinger, L., Sakai, N., Chen, J., Neve, R., Nestler, E.J., and Duman, R.S. (2002). Inhibition of cAMP response element-binding protein or dynorphin in the nucleus accumbens produces an antidepressant-like effect. J. Neurosci. 22, 10883–10890.

Nikulina EM, Arrillaga-Romany I, Miczek KA and Hammer RP, Jr. (2008) Long-lasting alteration in mesocorticolimbic structures after repeated social defeat stress in rats: time course of mu-opioid receptor mRNA and FosB/DeltaFosB immunoreactivity. Eur J Neurosci 27:2272-2284.

Paul, E.D., Hale, M.W., Lukkes, J.L., Valentine, M.J., Sarchet, D.M., and Lowry, C.A. (2011). Repeated social defeat increases reactive emotional coping behavior and alters functional responses in serotonergic neurons in the rat dorsal raphe nucleus. Physiol. Behav. 104, 272–282.

Pena CJ, Kronman HG, Walker DM, Cates HM, Bagot RC, Purushothaman I, Issler O, Loh YE, Leong T, Kiraly DD, Goodman E, Neve RL, Shen L and Nestler EJ (2017) Early life stress confers lifelong stress susceptibility in mice via ventral tegmental area OTX2. Science 356:1185-1188.

Pfau, M.L., Purushothaman, I., Feng, J., Golden, S.A., Aleyasin, H., Lorsch, Z.S., Cates, H.M., Flanigan, M.E., Menard, C., Heshmati, M., et al. (2016). Integrative Analysis of Sex-Specific microRNA Networks Following Stress in Mouse Nucleus Accumbens. Front. Mol. Neurosci. 9.

Pfeiffer, A., Knepel, W., Braun, S., Meyer, H.D., Lohmann, H., and Brantl, V. (1986). Effects of a kappa-opioid agonist on adrenocorticotropic and diuretic function in man. Horm Metab Res 18, 842–848.

Proulx CD, Hikosaka O and Malinow R (2014) Reward processing by the lateral habenula in normal and depressive behaviors. Nat Neurosci 17:1146-1152.

Razzoli M, Andreoli M, Michielin F, Quarta D and Sokal DM (2011) Increased phasic activity of VTA dopamine neurons in mice 3 weeks after repeated social defeat. Behav Brain Res 218:253-257.

Root DH, Melendez RI, Zaborszky L and Napier TC (2015) The ventral pallidum: Subregion-specific functional anatomy and roles in motivated behaviors. Prog Neurobiol 130:29-70.

Roy A, De Jong J and Linnoila M (1989) Cerebrospinal fluid monoamine metabolites and suicidal behavior in depressed patients. A 5-year follow-up study. Arch Gen Psychiatry 46:609-612.

Russo SJ and Charney DS (2013) Next generation antidepressants. Proc Natl Acad Sci U S A 110:4441-4442.

Rygula R, Abumaria N, Domenici E, Hiemke C and Fuchs E (2006a) Effects of fluoxetine on behavioral deficits evoked by chronic social stress in rats. Behav Brain Res 174:188-192.

Rygula R, Abumaria N, Flugge G, Hiemke C, Fuchs E, Ruther E and Havemann-Reinecke U (2006b) Citalopram counteracts depressive-like symptoms evoked by chronic social stress in rats. Behav Pharmacol 17:19-29.

Sachs BD, Ni JR and Caron MG (2015) Brain 5-HT deficiency increases stress vulnerability and impairs antidepressant responses following psychosocial stress. Proc Natl Acad Sci U S A 112:2557-2562.

Sartorius A, Kiening KL, Kirsch P, von Gall CC, Haberkorn U, Unterberg AW, Henn FA and Meyer-Lindenberg A (2010) Remission of major depression under deep brain stimulation of the lateral habenula in a therapy-refractory patient. Biol Psychiatry 67:e9-e11.

Schlaepfer TE, Cohen MX, Frick C, Kosel M, Brodesser D, Axmacher N, Joe AY, Kreft M, Lenartz D and Sturm V (2008) Deep brain stimulation to reward circuitry alleviates anhedonia in refractory major depression. Neuropsychopharmacology 33:368-377.

Shabel SJ, Proulx CD, Piriz J and Malinow R (2014) Mood regulation. GABA/glutamate co-release controls habenula output and is modified by antidepressant treatment. Science 345:1494-1498.

Shabel SJ, Proulx CD, Trias A, Murphy RT and Malinow R (2012) Input to the lateral habenula from the basal ganglia is excitatory, aversive, and suppressed by serotonin. Neuron 74:475-481.

Shippenberg, T.S., and Rea, W. (1997). Sensitization to the behavioral effects of cocaine: modulation by dynorphin and kappa-opioid receptor agonists. Pharmacol Biochem Behav 57, 449–455.

Szegedi A, Rujescu D, Tadic A, Muller MJ, Kohnen R, Stassen HH and Dahmen N (2005) The catechol-O-methyltransferase Val108/158Met polymorphism affects short-term treatment response to mirtazapine, but not to paroxetine in major depression. Pharmacogenomics J 5:49-53.

Tan KR, Yvon C, Turiault M, Mirzabekov JJ, Doehner J, Labouebe G, Deisseroth K, Tye KM and Luscher C (2012) GABA neurons of the VTA drive conditioned place aversion. Neuron 73:1173-1183.

Tirosh, I., Izar, B., Prakadan, S.M., Wadsworth, M.H., Treacy, D., Trombetta, J.J., Rotem, A., Rodman, C., Lian, C., Murphy, G., et al. (2016). Dissecting the multicellular ecosystem of metastatic melanoma by single-cell RNA-seq. Science (80-.). 352, 189–196.

Tornatzky W and Miczek KA (1993) Long-term impairment of autonomic circadian rhythms after brief intermittent social stress. Physiol Behav 53:983-993.

Trainor, B.C., Pride, M.C., Landeros, R.V., Knoblauch, N.W., Takahashi, E.Y., Silva, A.L., and Crean, K.K. (2011). Sex differences in social interaction behavior following social defeat stress in the monogamous California mouse (peromyscus californicus). PLoS One 6.

Tsankova NM, Berton O, Renthal W, Kumar A, Neve RL and Nestler EJ (2006) Sustained hippocampal chromatin regulation in a mouse model of depression and antidepressant action. Nat Neurosci 9:519-525.

Tye KM, Mirzabekov JJ, Warden MR, Ferenczi EA, Tsai HC, Finkelstein J, Kim SY, Adhikari A, Thompson KR, Andalman AS, Gunaydin LA, Witten IB and Deisseroth K (2013) Dopamine neurons modulate neural encoding and expression of depression-related behaviour. Nature 493:537-541.

van Zessen R, Phillips JL, Budygin EA and Stuber GD (2012) Activation of VTA GABA neurons disrupts reward consumption. Neuron 73:1184-1194.

Veerakumar, A., Challis, C., Gupta, P., Da, J., Upadhyay, A., Beck, S.G., and Berton, O. (2014). Antidepressant-like effects of cortical deep brain stimulation coincide with pro-neuroplastic adaptations of serotonin systems. Biol. Psychiatry 76, 203–212.

Vialou V, Thibault M, Kaska S, Cooper S, Gajewski P, Eagle A, Mazei-Robison M, Nestler EJ and Robison AJ (2015) Differential induction of FosB isoforms throughout the brain by fluoxetine and chronic stress. Neuropharmacology 99:28-37.

Walsh, J.J., Friedman, A.K., Sun, H., Heller, E.A., Ku, S.M., Juarez, B., Burnham, V.L., Mazei-robison, M.S., Ferguson, D., Golden, S.A., et al. (2014). Stress and CRF gate neural activation of BDNF in the mesolimbic reward pathway. Nat. Publ. Gr. 17, 27–29.

Walsh RM, Shen EY, Bagot RC, Anselmo A, Jiang Y, Javidfar B, Wojtkiewicz GJ, Cloutier J, Chen JW, Sadreyev R, Nestler EJ, Akbarian S and Hochedlinger K (2017) Phf8 loss confers resistance to depression-like and anxiety-like behaviors in mice. Nat Commun 8:15142.

Warden MR, Selimbeyoglu A, Mirzabekov JJ, Lo M, Thompson KR, Kim SY, Adhikari A, Tye KM, Frank LM and Deisseroth K (2012) A prefrontal cortex-brainstem neuronal projection that controls response to behavioural challenge. Nature 492:428-432.

Watabe-Uchida M, Zhu L, Ogawa SK, Vamanrao A and Uchida N (2012) Whole-brain mapping of direct inputs to midbrain dopamine neurons. Neuron 74:858-873.

Weissbourd B, Ren J, DeLoach KE, Guenthner CJ, Miyamichi K and Luo L (2014) Presynaptic partners of dorsal raphe serotonergic and GABAergic neurons. Neuron 83:645-662.

Willner P (2005) Chronic mild stress (CMS) revisited: consistency and behavioural-neurobiological concordance in the effects of CMS. Neuropsychobiology 52:90-110.

Winter C, Vollmayr B, Djodari-Irani A, Klein J and Sartorius A (2011) Pharmacological inhibition of the lateral habenula improves depressive-like behavior in an animal model of treatment resistant depression. Behav Brain Res 216:463-465.

Wook Koo J, Labonte B, Engmann O, Calipari ES, Juarez B, Lorsch Z, Walsh JJ, Friedman AK, Yorgason JT, Han MH and Nestler EJ (2016) Essential Role of Mesolimbic Brain-Derived Neurotrophic Factor in Chronic Social Stress-Induced Depressive Behaviors. Biol Psychiatry 80:469-478.

Yamanaka H, Yokoyama C, Mizuma H, Kurai S, Finnema SJ, Halldin C, Doi H and Onoe H (2014) A possible mechanism of the nucleus accumbens and ventral pallidum 5-HT1B receptors underlying the antidepressant action of ketamine: a PET study with macaques. Transl Psychiatry 4:e342.

Zanos P, Moaddel R, Morris PJ, Georgiou P, Fischell J, Elmer GI, Alkondon M, Yuan P, Pribut HJ, Singh NS, Dossou KS, Fang Y, Huang XP, Mayo CL, Wainer IW, Albuquerque EX, Thompson SM, Thomas CJ, Zarate CA, Jr. and Gould TD (2016) NMDAR inhibition-independent antidepressant actions of ketamine metabolites. Nature 533:481-486.

Zhu Y, Wienecke CF, Nachtrab G and Chen X (2016) A thalamic input to the nucleus accumbens mediates opiate dependence. Nature 530:219-222.